WORKSHOP ON PHYSICS OF MESOSPHERE-STRATOSPHERE-TROPOSPHERE INTERACTIONS WITH SPECIAL EMPHASIS ON MST RADAR TECHNIQUES

(13 - 24 November 2000)

THE INSTRUMENTAL PRINCIPLES OF MST RADARS AND INCOHERENT SCATTER RADARS AND THE CONFIGURATION OF RADAR SYSTEM HARDWARE

Prof. Röttger Jürgen

Max-Planck Institut Für Aeronomie
Katlenburg-Lindau
GERMANY

THE INSTRUMENTAL PRINCIPLES
OF MST RADARS AND INCOHERENT SCATTER RADARS
AND THE CONFIGURATION OF RADAR SYSTEM HARDWARE

Jürgen Röttger

EISCAT Scientific Association
P.O. Box 812, S-981 28 Kiruna, Sweden
(on leave from Max-Planck-Institut für Aeronomie, W.Germany)

ABSTRACT

The principle of pulse modulation used in case of coherent scatter radars (MST radars) and incoherent scatter radars (IS radars) is first discussed. Coherent detection and the corresponding system configuration is delineated. Antenna requirements and design are outlined and the phase-coherent transmitter/receiver system is described. Transmit/receive duplexers, transmitters, receivers, quadrature detectors are explained. The radar controller, integrator, decoder and correlator design as well as the data transfer and the control and monitoring by the host computer is delineated. Typical operation parameters of some well-known radars are finally summarised.

1.   INTRODUCTION TO PRINCIPLES OF THE ATMOSPHERIC RADAR TECHNIQUE

This tutorial lecture note aims to give a general summary and overview on the MST radar and the incoherent scatter radar technique. With the MST radars the mesosphere, stratosphere and the troposphere are investigated, whereas with incoherent scatter (IS) radars the ionosphere is investigated. It is not intended to present here a review for experts working in this field, but rather to give an overview to newcomers to allow a basic introduction for those who are joining this research field. For more specific technical descriptions of the radar technique in general and the atmospheric radar technique in particular, the reader is referred to other books and articles, such as those by SKOLNIK (1970), HARDY (1972), WILSON and MILLER (1972), BATTAN (1973), GOSSARD and STRAUCH (1983), DOVIAK and ŽRNIC (1984). Very specified descriptions of MST radar techniques can be found in Handbooks for MAP (BOWHILL and EDWARDS, 1983, 1984, 1986), an explicit and useful explanation of the MST and incoherent scatter MU radar was published by FUKAO et al. (1985a,b), and a review of UHF and VHF radar techniques for atmospheric research and wind profiler applications was recently prepared by RÖTTGER and LARSEN (1989). Good overviews on the incoherent scatter radar technique are given by EVANS (1969), BARON (1977) and HAGFORS (1977). Since important features of the MST and IS radar hardware result from certain principles of the basic radar technique, the scattering mechanisms and the data acquisition procedures, these will be briefly outlined in the course of this lecture note, which, however, mainly aims towards the description of radar instrumentation. Further tutorial introductions to the applications of MST and IS radars in atmospheric and ionospheric research can be found in the other articles published in this volume of the Handbook for MAP.

We will describe here the very basic technical principles, which are profound in all radar applications but are usually adjusted according to specific requirements of certain scientific experiments and operational realizations. Some of those are outlined in the following chapters and for more details than given in this tutorial or the in mentioned reviews the reader is referred to the relevant literature summarized in the reference list at the end of this paper.

C01

1.1. Basics of Pulsed Doppler Radars

Usually the MST radars as well as the incoherent scatter radars apply the conventional pulse modulation technique, i.e. a short radar pulse is transmitted as shown in the sketch of Fig. 1, and the backscattered radar echo from a range r (or altitude z) is received after the time t. Sampling the received echoes as function of time then allows to evaluate the echoes from different ranges r $=ct/2$, where c is the propagation velocity of the radar signal, namely the speed of light for the radars operating in the VHF and UHF bands.
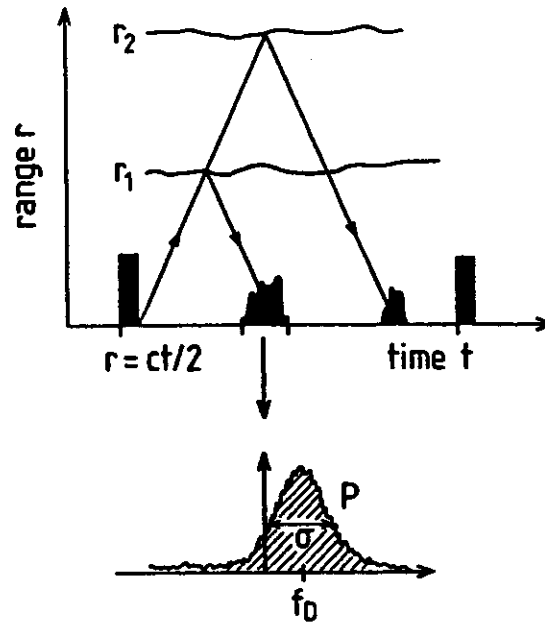

Figure 1. Principle of a pulsed Doppler radar:
A transmitted radar pulse is scattered by some refractive index irregularity at the ranges r. The backscattered radar signal is received after the time of flight t from the ranges r = $ct/2$, where c is the speed of light. Usually the power or Doppler spectrum (as shown in the lower insert) is computed for signals received in certain range gates and the basic parameters total power P, Doppler shift f_D and the spectrum width σ are deduced. In addition further useful parameters can be determined from the particular shapes of Doppler spectra.

The procedure of pulse radar is described in some more detail in Fig. 2. Let a pulsed electromagnetic wave be transmitted at the time T_1. The pulse duration of this radar signal shall be δt_t. For simplification the pulse shape is assumed to be rectangular, but in real applications it may be a smoothed trapezoid or triangle or Gaussian shaped. In a nondispersive propagation medium (at the high frequencies used in the MST and IS radar application the refractive index is very close to one such that dispersion does not have to be considered) the pulse travels with the speed of light c and reaches the range r_a after the time t_1 = r_a/c. A target at r_a can scatter or reflect the radar signal in some directions. A small fraction returns to the location of the transmitter, where this radar echo will be received after the time t_1' = $2t_1$ = $2r_a/c$. This yields the basic relation r = $ct/2$, which allows determination of the range of any radar target by measuring the round-trip time t. This relation holds for monostatic radars (transmitter and receiver are at almost the same location). For bistatic radars (with the receiver separated horizontally from the transmitter by a distance comparable to or larger than the ranges to the target) a modified

r

r_b

r_{max}

$r_a + \frac{\Delta r}{2}$

r_a

$r_a - \frac{\Delta r}{2}$

r_{min}

0

T_1 Δt_t t_1 t_1' $t_1'+\Delta t_t$ $T_2 = T_1 + K \cdot \Delta t_t$ t_2' t
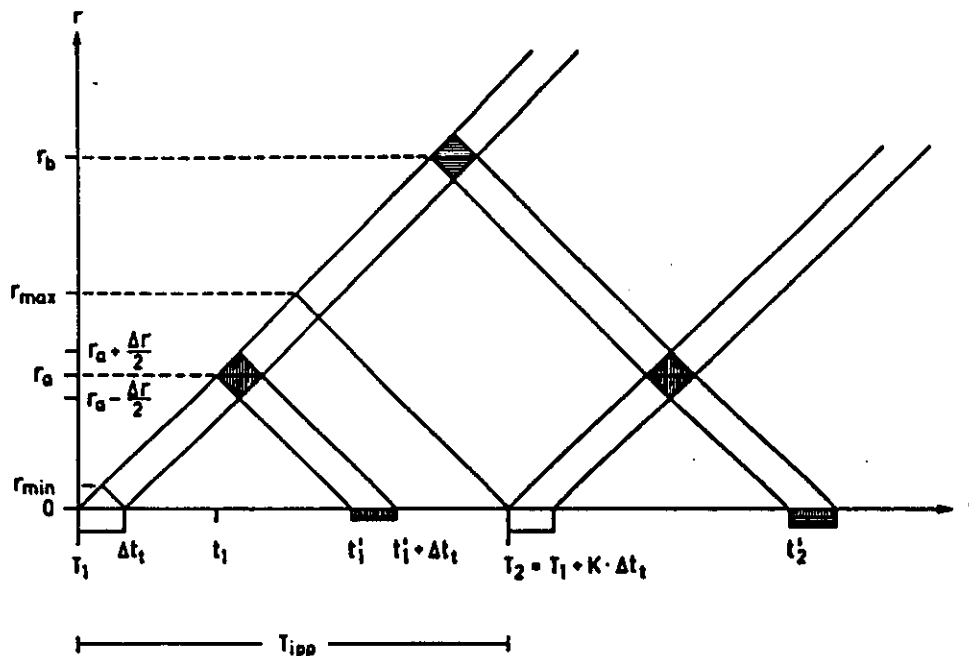
|——————— T_{ipp} ———————|

Figure 2. Range-time diagram explaining the main features
of pulse transmission and scattering from a volume target
at the range r and the reception after a time t (see text
for the explanation of the other parameters).

expression has to be applied. Bistatic or multistatic operation will not be discussed in detail here, but is just mentioned for completeness (see Evans, 1969, for more details).

Since the transmitted pulse has a finite duration δt_t, its trailing edge will reach the range r_a at a time $t_1+\delta t_t$, and reach the receiver at $2t_1+\delta t_t = t_1'+\delta t_t$. If the radar target is a thin reflecting surface (called discrete, single or hard target scattering), the shape of the received pulse is the replica of the transmitted pulse. Now assume that many scatterers fill all ranges along the radar beam (called soft target or volume scattering). It is then obvious from Fig. 2 that echoes from the range between $r_a-\delta r/2$ and r_a reach the receiver simultaneously at t_1', and those from r_a to $r_a+\delta r/2$ are received at $t_1'+\delta t_t$. The pulse of duration δt_t, thus, at one time illuminates a volume at r_a extended along a range $\delta r = c \cdot \delta t_t/2$. This is the range gate or range cell from which the radar echoes are received. Fig. 2 shows that most of the echo power results from the range r_a, and minimum power is received from $r_a \pm \delta r/2$. Thus, the resulting range weighting function of the single range gate centered around r_a is a triangle.

Because of the finite receiver bandwidth (usually matched to the bandwidth of the transmitted pulse) the receiver gate has a finite width in time. The receiver pulse response (given by about the inverse of the receiver bandwidth) distorts the received pulse by smoothing its leading and trailing edges and thus delaying it by about the receiver response time. The transmitter pulse length δt_t, to which the receiver response time is matched, determines the range resolution δr. The instrumental distortions of the radar pulse are not depicted in Fig. 2 to maintain the clearness of survey, but they eventually have to be considered in the final analysis of the radar data.

In radar applications short pulses are normally transmitted periodically, i.e. the n-th pulse follows the (n-1)-th pulse after a specified time. For convenience this time period is set here to be a multiple (K>1) of δt_t. This time (T_n-T_{n-1}) is called the interpulse period T_{ipp}, IPP, T_i or just T. Its

inverse is called the pulse repetition frequency $f_{prf} = 1/T_{ipp}$. The off-on-ratio of the transmitter $T_{ipp}/\delta t_t - 1$ determines approximately the range from which radar echoes can be unambiguously received (in units of range resolution). It is more customary, however, to use the ratio $d = \delta t_t/T_{ipp}$, which is called duty cycle or duty factor. The average transmitter power P_a, to be averaged over (more than) one interpulse period, is the product of the duty cycle and the transmitter pulse peak power P_p, i.e. $P_a = d \cdot P_p$. In Table 1 the basic technical terms used in radar applications are summarised.

TABLE 1

DEFINITION OF TECHNICAL TERMS
USED IN ATMOSPHERIC RADAR EXPERIMENTS:
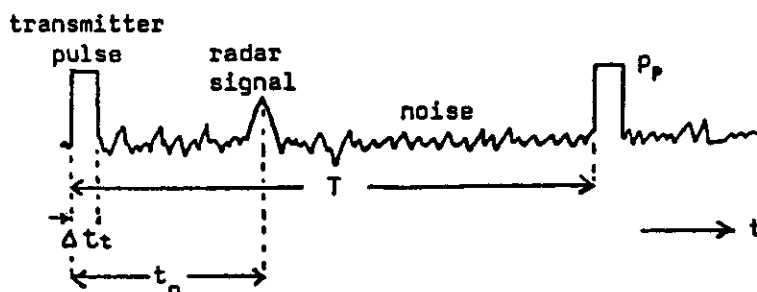
T	= interpulse period (IPP), also T_{ipp}
1/T	= pulse repetition frequency (PRF)
δt_t	= transmitter pulse length (duration)
P_p	= transmitter peak power
$\delta t_t/T$	= d = duty cycle
dP_p	= average transmitter power
$r = ct_o/2$	= one-way distance to the radar target

Assume that the radar echo power is due to volume scatter and that isotropic scatterers totally fill the radar beam. Then the received radar echo power P_s is given by the radar equation:

$$P_s = \frac{A \, P_p \, \delta r \, \eta}{8\pi r^2} \, , \qquad (1)$$

where A is the effective antenna area and η is the radar reflectivity.

If the radar echo is due to reflection from a large surface of a refractive index discontinuity, which is stratified perpendicular to the radar wave propagation, the received radar echo power P_r is given by:

$$P_r = \frac{P_p \, A^2 \, |\varsigma|^2}{4\Omega_o^2 r^2} \, , \qquad (2)$$

where ς is the amplitude reflection coefficient of the surface. For MST radar applications the reflection coefficient can be very small, resulting in partial reflection. In many cases of radar observations scattering takes place, and particularly in ionosphere observations with IS radars the only mechanism is (incoherent) scattering. The partial reflection mechanism is difficult to be distinguished from anisotropic scatter, which both have a pronounced aspect sensitivity (dependence of echo power on beam direction) observed with the long wavelength MST radars. We refer to detailed explanations of these effects, which are for instance outlined in other articles of this book (e.g., HOCKING, 1989).

$C04$

As compared to radar echoes from single hard targets (e.g. airplanes), where the echo power is proportional to r^{-4}, P_s and P_r are proportional to r^{-2}. This is simply explained by the fact that the volume or the partially reflecting surface or layer of the atmosphere, which is illuminated by the radar beam, is not constant but increases with the square of the range. We particularly have to note the direct dependency of the received signal power on the transmitted peak power P_P and the antenna area A, which means that both these quantities should be optimised. For the reason that the sensitivity of the radars is directly determined by these two parameters, transmitter power and antenna aperture, the quantity "power-aperture product P·A" is used often as the main indicator of the radar capability or sensitivity and it allows a better comparison of measurements done at different radars. Also the term signal-to-noise ratio (SNR), which is the ratio of signal power $P_{s,r}$ and noise power P_n, is used frequently to determine the echo signal strength although this can be misleading because the noise level varies particularly with frequency and antenna look angle, with receiver front-end sensitivity and with loss rates of the antenna and feed systems.

Because in normal radar operations the pulse repetition frequency is kept constant, i.e. the transmitted pulse train is periodic, range-aliasing may occur. This ambiguity is depicted in Fig. 2. At time t_2' an echo of the pulse at T_2 is received from range r_a, and an echo of the pulse at T_1 is received from range r_b. Of course higher order range-aliasing can occur from ranges $r_n = c(t+(n-1)T_{ipp})/2$. Because these echoes return from separate scatter volumes, the echo signals are uncorrelated but still their power accumulates in the same receiver range gate. If no special arrangements (e.g. pulse-coding, frequency changes or non-periodic T_{ipp}) are being made, the maximum unambiguous range is $r_{max} = c \cdot T_{ipp}/2$. The minimum range r_{min} obviously is given by the pulse duration δt_t plus some instrumentally entailed transition time between transmission and reception.

Assume that a bulk motion carries the scatterers or reflectors in the volume at range r. Because of the Doppler effect, the rate of change of phase $\emptyset$ of the returned signal is then $d\emptyset/dt = 4\pi/\Lambda_o \cdot dr/dt$, where Λ_o is the radar wavelength. When V' is the (radial) velocity in direction of the radar signal path, $V' = dr/dt$. The phase change $d\emptyset/dt$ is the angular Doppler frequency $\Omega_D = 2\pi f_D$, which yields $f_D = -2V'/\Lambda_o$. Since the radar signal is pulsed at a frequency f_{prf}, i.e. the radar echo is sampled at a rate T_{ipp}, this yields the maximum Doppler frequency to be resolved by pulse-to-pulse analysis (Nyquist frequency): $f_{Dmax} = f_{prf}/2 = 1/2T_{ipp}$. This corresponds to a maximum radial velocity $V'_{max} = \Lambda_o f_{Dmax}/2$ and $V'_{max} = \Lambda_o c/8r_{max}$. V'_{max}, as defined here, is much larger than any realistic velocity observed in the lower and middle atmosphere.

In cases of large Doppler shift and/or large spectrum widths, i.e. the inverse of the signal correlation time, which are observed for incoherent scatter echoes from the ionospheric E- and F-region, the maximum frequency cannot be resolved by the pulse-to-pulse technique and other means have to be applied. The difference of "coherent signals" observed in MST radar applications and "incoherent signals" observed in IS radar applications is sketched in Fig. 3. For short signal correlation times (shorter than the interpulse period) all samples for the autocorrelation function and the spectrum analysis have to be taken during a single interpulse period (incoherent signal). For long correlation times (longer than the interpulse period) these samples need to be taken during several interpulse periods (coherent signals), which is called "pulse-to-pulse" technique. Details of the corresponding instrumental configurations are discussed in the following Chapter 1.2 and of the data acquisition in Chapter 5.
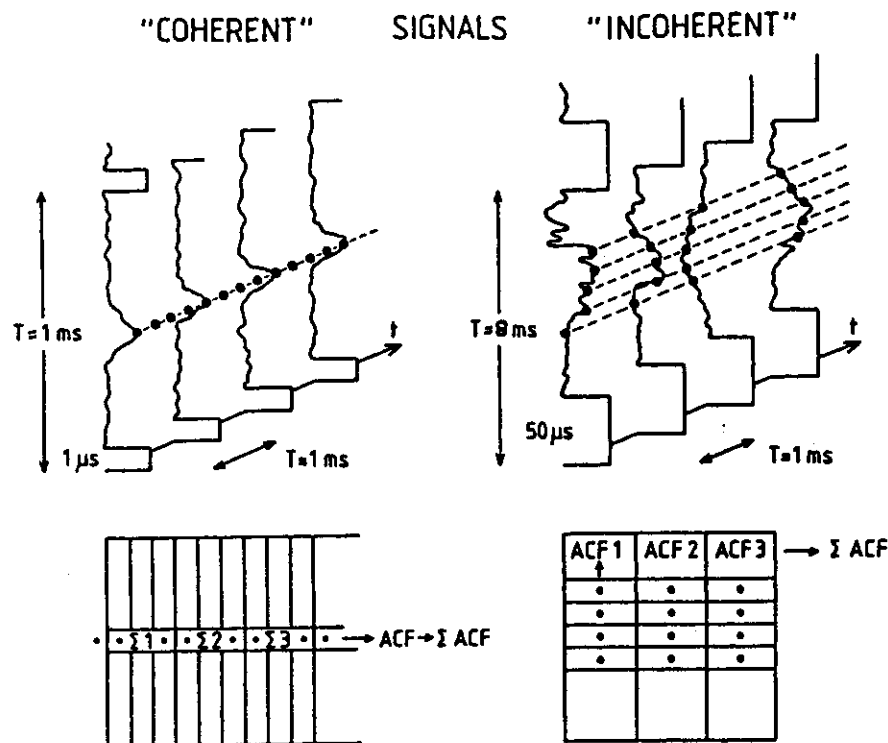
COS

"COHERENT"   SIGNALS   "INCOHERENT"

Figure 3. Range-time-amplitude diagrams for coherent (underspread) and
incoherent (overspread) signals. The dots mark the sample points, which
are used to compute autocorrelation functions ACF. The tables symbolize
that for coherent signals coherent integrations ($\Sigma1,\Sigma2,\ldots$) are performed
for fixed range gates over several interpulse periods, then the ACFs are
computed which are finally accumulated (ΣACF). This is called "pulse-to-
pulse technique". For incoherent signals the ACFs are computed within
every interpulse period (ACF1, ACF2,...) and are accumulated (ΣACF).

1.2. An Overview of Particular Radar Systems

Radars operating in the extended frequency range from MF (medium frequency)
to UHF (ultra-high frequency) are used to investigate the structure and dynamics
of the troposphere, stratosphere, mesosphere and thermosphere/ionosphere. In
Table 2 different kinds of radars and their basic technical parameters are
summarized. The MF radars, making use of partial reflection from electron den-
sity irregularities, are particularly applied to measure electron density pro-
files of the ionospheric D-region and lower E-region as well as the horizontal
wind velocity in this altitude range, comprising the mesosphere and lower ther-
mosphere. The HF radars (conventionally known as ionosondes) and the ionospheric
irregularity scatter radars (somewhat ambiguously also called "coherent radars")
are used to study total reflections from the ionosphere and scattering from E-
and F-region plasma irregularities. The meteor radars make use of echoes retur-
ned from meteor trails to measure wind velocities in the upper mesosphere and
lower thermosphere. The mesosphere-stratosphere-troposphere (MST/ST) radars,
detecting echoes from turbulence-induced inhomogeneities of the radio refractive
index, are applied to investigate winds, waves, turbulence and stability in the
indicated altitude regions. Incoherent scatter (also called Thomson scatter)
radars, making use of scatter from free electrons, are applied to study the
ionosphere and thermosphere. IS radar echoes from the D-region also have long
coherence times like MST radar echoes. We concentrate here on the basic prin-
ciples and applications of the incoherent scatter (IS) and the MST radars, but
we note that many principles apply also to the other kinds of radars.

6

TABLE 2

RADAR METHODS FOR INVESTIGATIONS OF THE LOWER AND MIDDLE ATMOSPHERE
AND THE THERMOSPHERE/IONOSPHERE

Typical operation parameters (approximate)

Radar Method	Frequency Range	Wavelength Λ in m	Average Power in kW	Antenna Dimension in m	Height Region
MF Radar	MF-HF	150-50	0.01-1	1-10	M,L
HF Radar*	HF	300-10	0.01-5	0.5-1	Th/Io
Coherent Radar*	HF-VHF	30-1	0.1-1	5-50	Th/Io
Meteor Radar	HF-VHF	10-6	0.1-10	2-10	M,LT
MST Radar	VHF	6-7	1-100	5-50	M,S,T
Incoherent Scatter Radar	VHF-UHF	1.4-0.25	100-300	100-300	M,LT
ST Radar	VHF-SHF	6-0.1	1-500	10-500	S,T

MF = 0.3-3.0 MHz	M = Mesosphere
HF = 3.0-30 MHz	S = Stratosphere
VHF = 30-300 MHz	T = Troposphere
UHF = 300-3000 MHz	LT = Lower Thermosphere
SHF = 3-30 GHz	Th/Io = Thermosphere/Ionosphere
* = Ionosonde	+ = Irregularity Scatter

The MST radars operate in the lower VHF band around 50 MHz, corresponding to wavelengths around 6 m. Since quasi-vertical antenna beam directions are used, ranges are roughly equal to altitudes. For MST radar observations of the lower and middle atmosphere the range limits r_{max} are between 10-20 km and 100 km. This yields typical pulse repetition frequencies between 10 kHz and 1 kHz. Altitude resolutions from about 1 km down to at least 100 m are required to resolve typical vertical scales in the troposphere, stratosphere and the mesosphere. This corresponds to pulse lengths of about 1-10 µs. Thus, typical duty cycles are between about 10^{-1} and 10^{-3}. Longer coded pulses are frequently used, which is discussed in Chapter 4.5.

MST radars make use of scattering and reflection from variations of humidity, temperature and electron density, induced by turbulence in the lower and middle atmosphere. Essentially, MST radars can observe: the 3-dimensional wind vector, atmospheric reflectivity and stability, and morphology of turbulence and waves. The continuous measurements with MST radars offer very good quality and quantity middle atmosphere observations of wind velocities. MST radars operate at frequencies around 50 MHz, and therefore are also called VHF radars (VHF = very high frequency band between 30 MHz and 300 MHz). Higher frequency radars mostly cover only the troposphere and stratosphere. Typical peak powers of VHF radars are between 1 kW and 1 MW. Range resolutions down to about 100 m and time resolutions down to some ten second are possible. The antenna arrays with typi-

resolutions down to some ten second are possible. The antenna arrays with typical dimensions of 1000 m² to some 10000 m² point close to the zenith direction. Coherent detection, digital control and data acquisition are mandatory as is described in Chapter 4.

There are basically two methods which are applied by MST radars, in particular to measure velocities, as is sketched in Fig. 4. One method uses a narrow radar beam pointed into various directions and measures the Doppler shift of echoes scattered from irregularities. This method is usually called the "Doppler method" and for this reason these radars are also called "Doppler radars". The other method uses three or more spaced antennas and the received echoes are cross-correlated to determine the drift speed of irregularities and is called "spaced antenna or SA method". Since the irregularities are usually moving with the wind velocity, both methods are capable to measure the wind velocity. Although both methods are basing on the same physical mechanism, in praxis the technical implementation may favour one or the other of these methods. The spaced antenna method can also be applied in the spatial domain radar interferometer mode, which is advantageous for studying the structure of the scattering/-reflecting irregularities. In all these applications a phase-coherent radar system is applied, it is even required for the Doppler and the interferometer method.
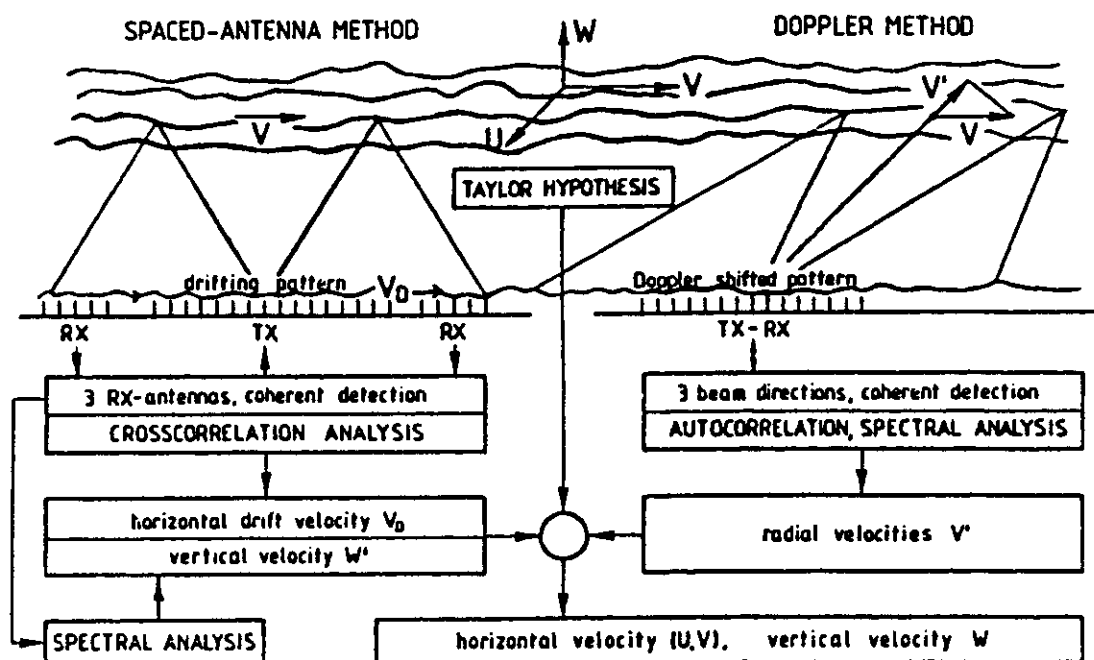
3-DIM VELOCITY MEASUREMENTS WITH VHF-RADAR

Figure 4. The two principle methods of three-dimensional velocity measurements with monostatic mesosphere-stratosphere-troposphere (MST) radars. These methods are the Doppler method using oblique beams to deduce the horizontal and vertical velocity from the measured radial velocity, and the spaced antenna method apply-ing drifting pattern measurements to deduce the horizontal wind velocity.

8

r² ∂𝒳

The smaller versions of this Doppler radar category, the stratosphere-troposphere (ST) radars operate according to the same principle like the MST radars, but frequently operate on higher frequencies in the UHF band with smaller powers and antenna apertures of several ten square meters only. They are not capable to detect echoes from the mesosphere since either their power-aperture product is too small, yielding too low a sensitivity, or their frequency is so high that their wavelength is in the inertial subrange of refractive index variations such that the scatter echoes are not detectable. These radars apply the Doppler method to measure velocities and are mostly very capable to investigate the lower atmosphere (particularly the troposphere and the boundary layer) with a very good height resolution of some 10 meters or better.

The state of the art of the ST radars and their suitable applicability to measure continuously the wind profiles in the troposphere and the lower stratosphere has attracted wide attention in the meteorological community. As a consequence such ST radars are included into meteorological research networks and particular instrumentation is being designed to allow long-term routine operations of these so-called wind profilers. Since this is a development by industrial companies, we will not discuss these particular designs in the context of this tutorial. A short summary of system specifications of wind profilers, however, can be found in Tables 6 and 7 in Chapter 6.
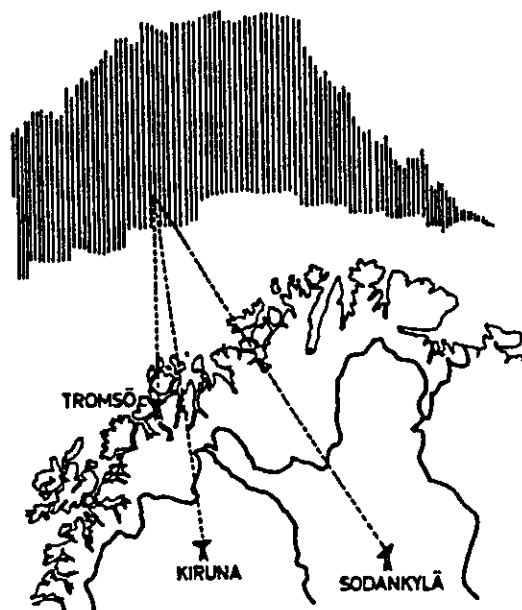

Figure 5.   The principle of tri-static incoherent scatter
           (IS) radar measurements of the auroral ionosphere by the EISCAT
           UHF system with transmitter and receiver in Tromsö, Norway,
           and remote receivers in Kiruna, Sweden, and Sodankylä, Finland.

The incoherent scatter radars operate at VHF and UHF frequencies with a much larger power-aperture product than the MST or ST radars. Mostly these radars have large dish antennas or phased arrays occasionally with diameters of several ten to hundred meters. Their peak powers are usually larger than 1 MW, their duty cycle can be up to 12 percent and their fastest interpulse period is mostly not smaller than 1 ms. Pulses as long as 1 ms are used, but frequently amplitude- or phase-coded. Typical altitude resolutions are 0.3 -50 km and time resolutions of some minute to several 10 minutes are achieved. These differences result from the fact that because of the very small volume reflectivity of in-

C'09

coherent scatter, the signal-to-noise ratios are mostly well below unity, whereas the SNR is usually much larger than 1 in the MST radar case. The incoherent scatter radars particularly measure electron density, electron temperature, ion temperature and ion velocity in the ionosphere. Fig. 5 shows the tri-static incoherent scatter UHF-radar system of the EISCAT Scientific Association which is operated in northern Scandinavia to study the auroral ionosphere. The tri-static radar configuration is most useful to measure the three-dimensional velocity with the best achievable accuracy. All the IS radars were also used for studies of the stratosphere and the troposphere, although some instrumental constraints had to be considered such as ground clutter, receiver recovery and dynamic range limitations.

A list of these radars is found in Table 9 at the end of this article.

1.3. The Principle of Phase-Coherent Radar Systems

Incoherent or Thomson scatter is caused by fluctuations in the radio refractive index at the radar Bragg wavelength resulting from thermal motions of free electrons in the presence of ions in the ionosphere. Due to these random motions the incoherent scatter signal is widened in frequency and it needs to be sampled fast enough to resolve the complete Doppler spectrum. In the lower ionosphere collisions between ions and neutrals impose the fluctuations of the neutral atmosphere on the plasma and consequently on the electrons. Since these fluctuations, although they can be strong in amplitude, do not contain such high frequency components as the thermal motions, the incoherent scatter signal displays a narrower spectrum, i.e. a longer coherence time in the lower ionosphere. Eventually, the structure of the plasma in the mesosphere (D-region) will be completely governed by the fluctuations due to neutral air turbulence. Instead of incoherent scatter this latter process is called coherent or turbulence scatter. Usually the signal spectrum due to turbulence scatter is much narrower than that of incoherent scatter. In addition to the widening of these signal spectra, they are shifted in frequency if there is a bulk radial velocity of the scattering medium. We would like to explain here that both these scattering processes are being studied with phase-coherent radar systems.

Knowing that fluctuating velocities and radial velocities with quasi-vertical MST radar beams do not exceed several 10 ms^{-1}, the Doppler frequency will barely exceed 10 Hz for MST radars operating at VHF and will be just an order of magnitude larger for UHF. Applying $f_{prf} > 1$ kHz, the MST/ST radar echo will be oversampled, i.e. its phase and amplitude does vary little from pulse to pulse as it was sketched in Fig. 3. This is called a coherent radar echo, in contrast to an incoherent radar echo, which, because of the much shorter correlation or coherence time of the ionospheric scatter medium, randomly changes phase and amplitude from one pulse to the next. Also the velocities in the ionosphere measured with incoherent scatter radars is usually much larger than the velocities in the middle and lower atmosphere, which additionally causes a more rapid change of the phase of the incoherent scatter signals. One does make efficient use of the characteristic coherency of MST radar echoes to improve the data acquisition procedures, which will be discussed in Chapter 4. These differences of the signal coherence times also determine the principle way of the data acquisition structure and instrumentation.

The differences between "coherent signals" detected by the MST/ST radars, used to study the lower and middle atmosphere, and "incoherent signals" detected by the incoherent scatter radars, used to study the ionosphere, is elucidated by the schematics of Figs. 6a and 6b. Since the coherence time, i.e. the inverse of the width of the Doppler spectrum, generally increases from the lower to the middle and to the upper atmosphere (ionosphere) due the increasing variations of
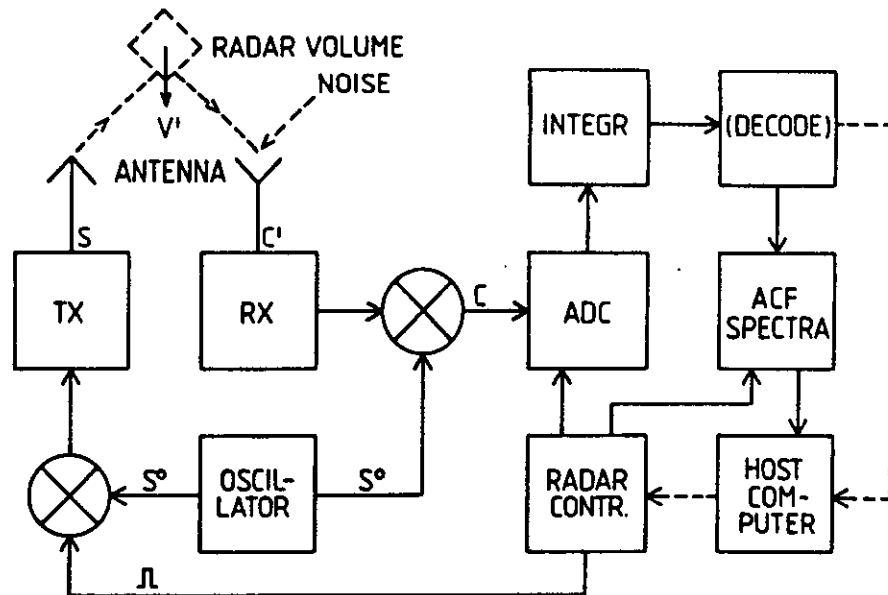
MST-RADAR

Figure 6a. Block diagram showing the basic configuration of an
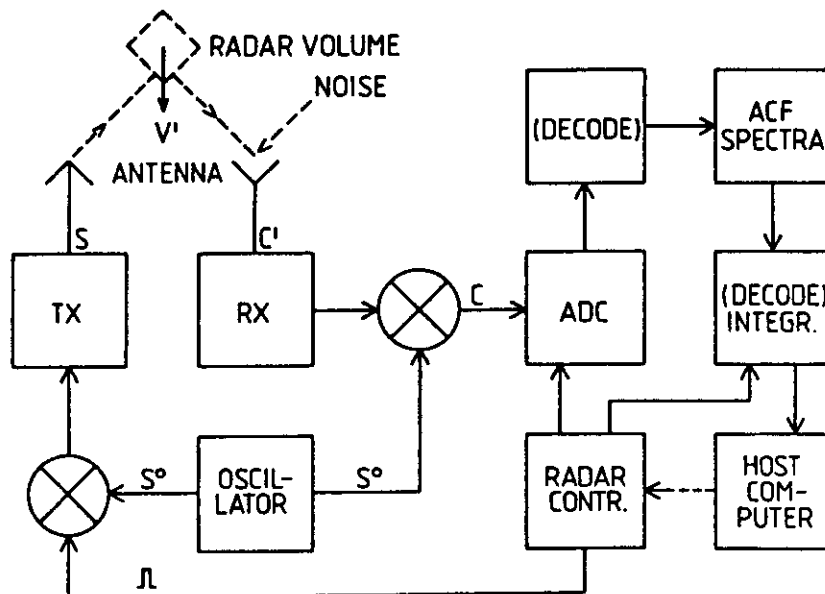MST radar system (data acquisition for coherent signals).

IS-RADAR

Figure 6b. Block diagram showing the basic configuration of an
incoherent scatter radar system (data acquisition for incohe-
rent signals).

the scattering medium. Whereas in the lower atmosphere the coherence time (determined principally by turbulent fluctuations) is generally much longer than a typical interpulse period of an MST/VHF radar of say 1 ms, it is generally much shorter (given by thermal fluctuations) than an interpulse period of incoherent scatter radars. This means that coherent integration and the autocorrelation functions (ACFs) or Doppler spectra are computed on the pulse-to-pulse basis for coherent signals ("pulse-to-pulse technique"). On the other hand, the ACFs have to be immediately computed without coherent integration for each single interpulse period using single long or coded pulses in the case of incoherent signals. The ACFs (from which the spectra are computed) are then postintegrated. The definition of a coherent signal, which we use here, is consequently that the coherence time is much longer than the interpulse period. The incoherent signal is defined by a coherence time which is much shorter than the interpulse period. At some places in the early ionosphere literature the terms under-spread and over-spread signals are used instead of coherent and incoherent signals, respectively. Both kinds of signals anyhow result from the scattering process being coherent in the former and incoherent in the latter case, and both are studied with phase-coherent radar instrumentation.

We notice that the instrumental technique as well as the data acquisition and analysis of the MST radars as well as the IS radars are basically similar, they are well developed, elaborated and fairly mature, although further refinement is always going on. We now will briefly outline the two only striking differences of the instrumental design of these two main radar categories, which result from the coherent and incoherent signal properties and later will discuss particular parts of the instrumental hardware and their principles.

In order to allow the measurement of all signal parameters, particularly the Doppler spectrum, all MST radars and IS radars are phase-coherent. This means that the receiver (RX) and the transmitter (TX) are controlled by or phase-locked to the same main oscillator (see Figs. 6a and 6b). The transmitter radiates through the antenna the electromagnetic signal S, which propagates to the radar volume in the atmosphere or the ionosphere. From there a small fraction of the electromagnetic energy is backscattered to the antenna (which can be a separate or the same antenna, provided that a transmit/receive duplexer can be used). External noise, received by the same antenna and internal receiver noise adds to the atmospheric/ionospheric echo and the total signal plus noise C' is amplified in the receiver and mixed to base band by the same oscillator signal S^0, which is used to control the transmitter. The resulting base band signal C is converted to a digital series in the analog-to-digital converter (ADC), which is controlled by a series of sample pulses from the radar controller. The radar controller also generates the transmitter modulation and other control pulses.

Following the ADC, the data acquisition procedures are different for MST- and IS-radars as delineated in the Figs. 6a and 6b. This difference results from the different coherence times as described earlier. Because of the long coherence times of echoes from the mesosphere, stratosphere and troposphere, the digital data are usually coherently added in the integrator of an MST radar (Fig. 6a), followed by a decoding procedure if the transmitter pulses are coded (see Chapter 4 for details). These raw, but pre-integrated and/or decoded, data are either directly dumped into the host computer or analyzed in terms of autocorrelation functions or Doppler (Fourier) spectra. The host computer is used to store the raw data together with other operating system parameters and the time, on file or tape, perform an on-line quicklook analysis or some further preprocessing such as computation or post-integration of ACFs or spectra. The host computer also supervises the entire system by loading and starting the radar controller etc. as well as checking the system performance and issuing interrupts in case of system malfunctions. In the case of an incoherent scatter radar

(Fig. 6b) first a decoding has to be performed, then usually ACFs are computed on-line which are post-integrated and then dumped into the host computer. In particular pulse coding schemes also an additional decoding procedure has to be applied after the ACF computation. Otherwise the instrumental design of an IS radar is principally similar to an MST radar.

2. RADAR ANTENNAS

The radiation pattern of MST- and IS-radar antennas has to be carefully designed in order to optimize the wanted atmospheric/ionospheric scatter signal as compared to interfering external influences. These are summarized in the sketch of Fig. 7. It is evident that all the unwanted components, - ground clutter, sea clutter, airplane or satellite echoes, radio interference and scatter received through antenna sidelobes - , have to be properly eliminated or minimized. To achieve a high sensitivity and a reasonable angular resolution the antenna gain should be large and thus the antenna beam width small. The cosmic noise level picked up by the antenna is unavoidable in the low VHF band. In the high VHF and in the UHF band the noise level is not given by the sky noise but by the system noise. This can be minimized by optimum design of the receiver front-end amplifier and adapted data processing.

The antennas of MST- and IS-radars usually consist of an ensemble of single elements which are phase-coherently combined to a large antenna array or are large dish antennas. Usually the dimensions of MST radar antennas are more than several ten radar wavelengths, their gain is mostly exceeding 20 dB, corresponding to a beam width of less than 10 degree. The IS radar antennas usually have antenna gains larger than 40 dB in order to detect the weak incoherent scatter signals. The beam directions can be mechanically or electrically positioned
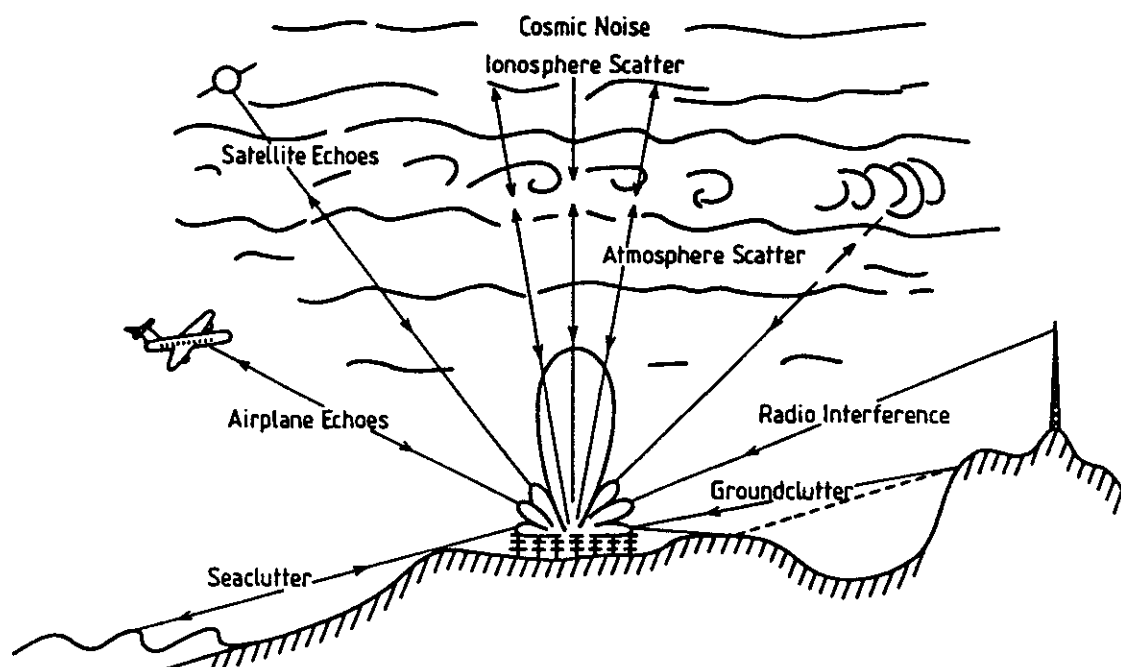

Figure 7. Schematic view of an atmospheric radar in an interference and clutter environment. The radar antenna is depicted here to consist of a phased array of Yagis, but could principally be any other kind of antenna system.
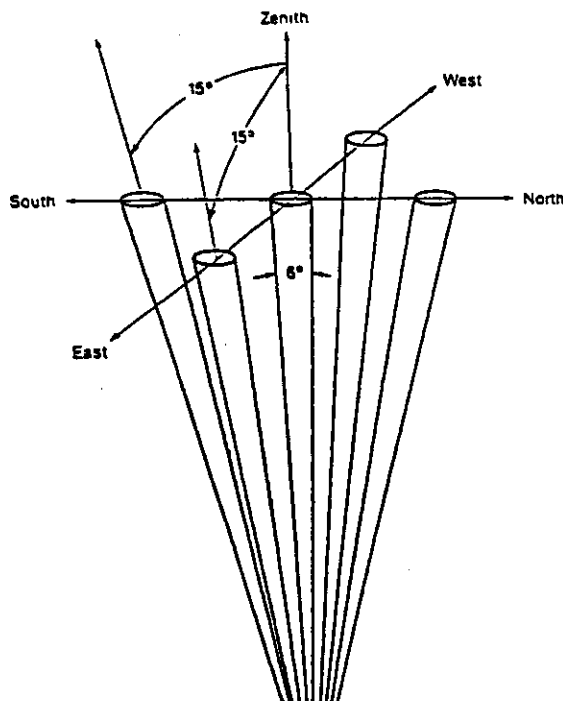
13

$C^{\prime}13$

Figure 8. Near-zenith pointing antenna beams of a 403 MHz phased array antenna of an ST radar (after FRISCH et al., 1986).

(e.g., Fig. 8) in order to observe spatial variations of the scatter process and to measure three-dimensional velocity components. The principle of measurements of the velocity components is explained by the schematics of Fig. 9. At a zenith angle δ in the direction of the wave vector $\underline{k}$ the radial velocity $v = u' + w'$ is measured, which consists of the projections w' of the vertical velocity w and the projection u' of the horizontal velocity u. The combination of the velocities measured in the directions δ and $-\delta$ yields the horizontal and the vertical velocity component. Depending on the requirements to measure all velocity components and their divergence as well as vorticity, more beam directions are necessary. Multi-static radars (e.g., Fig. 5) can also be used to measure the velocity components. The discussion of these possibilities and requirements is out of the scope of this lecture note but can be found elsewhere (see RÖTTGER and LARSEN, 1989, who discuss the applications of MST radars and give further references).
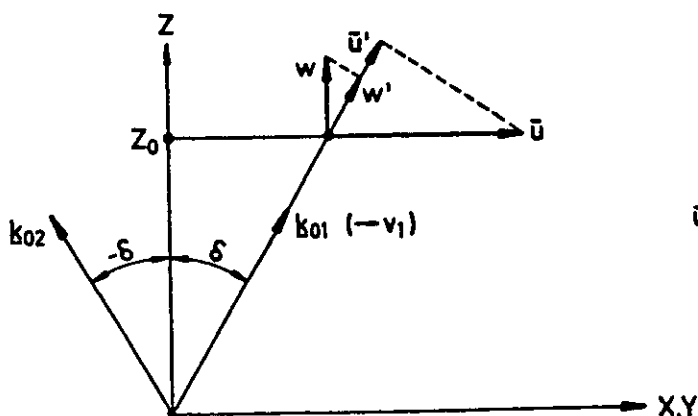
$$\bar{u} = \frac{v_1 - v_2}{2 \sin \delta} \quad , \quad w = \frac{v_1 + v_2}{2 \cos \delta}$$

Figure 9. Principle geometry of two antenna beam directions $\underline{k}_{01}$ and $\underline{k}_{02}$ at zenith angles δ and $-\delta$ for the deduction of the horizontal velocity component u and the vertical velocity component w. The measured radial velocity components v_1 and v_2 consist of the projections u' and w' of the u and w wind velocity components, respectively.

C 14

We now will briefly describe the basic antenna theory in order to allow an understanding of the antenna functions and the design optimization and then will describe some typical antenna systems used in MST radar applications.

2.1. Some Basic Antenna Parameters

The main parameter determining the antenna gain and the corresponding beam width is the size or the area of the antenna, which is also called the antenna aperture. The antenna aperture can be either regarded as a continuous radiator if it is illuminated by an independent feed system, or it can consist of several sub-elements which are electrically fed from a common transmitter source. Both approaches can be basically treated by a similar formalism, which we will explain for the simple case of a line of antenna dipole elements. Assume that N individual antenna elements with equal spacing d are horizontally lined up to form a multi-element array (see Fig. 10). In the array far-field $(r > (Nd)^2/\Lambda_o)$ the antenna polar diagram is

$$E(\delta) = \sum_{n=1}^{N} E_n(\delta)\exp(i(\frac{2\pi(n-1)d}{\Lambda_o} \sin\delta + \phi_n)),$$ (3)

where $E_n(\delta)$ is the pattern of an individual element and ϕ_n is a relative phase placed on this element. Thus, the polar diagram is just the Fourier transform of the spatial aperture distribution. If all the elements have similar $E_n(\delta)$ and ϕ_n, the polar diagram is a function $\sin Nx/\sin x$ with $x = \pi \cdot d \cdot \sin\delta/\Lambda_o$. If $d < \Lambda_o$, there is only one main lobe at $\delta = 0°$ (for $\phi = 0$). If $d > \Lambda_o$, grating lobes at $\delta_G = \arcsin(\Lambda_o/d)$ occur, for $E_n(\delta) = $ const with amplitudes similar to the main lobe. The width of the main lobe is $\delta_B = \arcsin(\Lambda_o/Nd)$. In radar applications also the two-way beam width $\delta_B/\sqrt{2}$ is used. If δ_B is small, it is directly proportional to the ratio of the wavelength Λ_o to the aperture dimension Nd. The radiation pattern has minima (nulls in theory) at $\delta_n = \pm n\delta_B$, where $n = 1,2,...,$ N/2, and sidelobes occur at $\delta_s = \delta_n \pm \delta_B/2$. If equal weighting W_n is applied to each of the single elements (e.g., $E_n'(\delta) = W_n \cdot E_n(\delta)$, with $W_n = $ const for all n), the first sidelobe closest to the main lobe is suppressed by 13.2 dB plus the fall-off of the individual element pattern $E_n(\delta)$ at δ_{s1}.
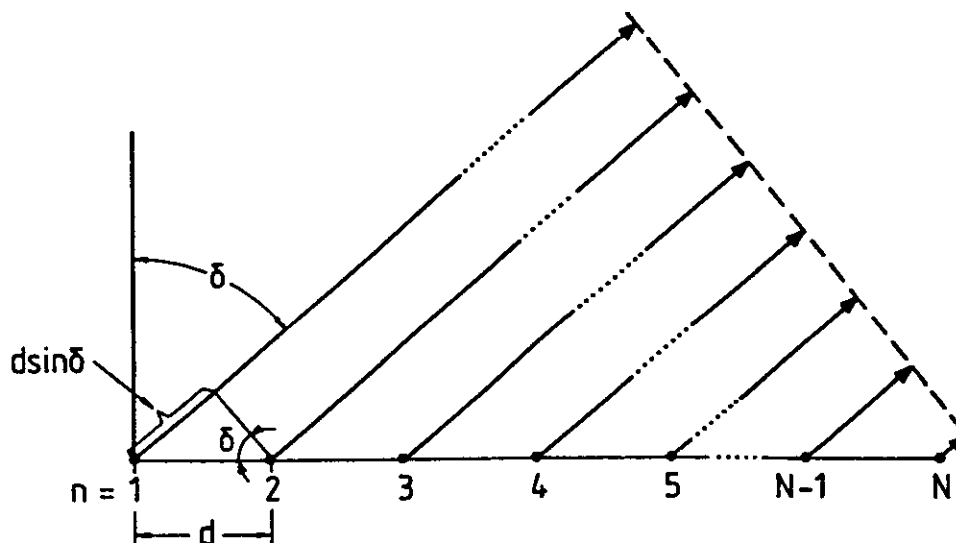

Figure 10. Schematic drawing of wave vectors of a plain wave radiated under a zenith angle δ from N isotropic antenna elements with spacing d.

The antenna pattern, particularly the desired variation of the direction δ_0 of the main lobe, can be changed by applying a linearly progressing phase ϕ_n from element to element, which has to be $\phi_n = 2\pi d(n-1)\sin\delta_0/\lambda_0$. This beam steering should be within reasonable limits of the individual element pattern $E_n(\delta)$ to avoid undesirable degrading of the antenna radiation. Furthermore the effective area of an antenna, which is fixed on the ground, is reduced with larger zenith angles because the illumination changes by $\sin\delta$.

To obtain improved sidelobe suppressions, a tapering of the antenna array can be applied by either changing the weighting function W_n (electrical weighting, i.e. feeding the outer elements of an array with less power than the inner elements), or by using unequal element spacings d_n (spatial weighting, i.e. applying larger spacings for the outer elements of an antenna array). The price one has to pay for the improvement of sidelobe suppression by tapering is always a broadening of the main lobe and lowering of the antenna gain G. Using a triangular weighting, for instance, improves the one-way suppression of the first sidelobe to -26 dB, but widens the main lobe by a factor of 1.44 and reduces the gain by 25%, as compared to uniform weighting. The respective values for a $\cos^2$-weighting, which is a good approximation to a Gaussian weighting, are -32 dB, 1.64 and 33%.

These one-dimensional considerations can be extended easily to a realistic two-dimensional radar antenna array by using, instead of d, the projections d' of all element positions onto n axis elongated in the azimuth direction a. The total antenna pattern then can be calculated by (3) for any a and δ. For a real radar antenna we also have to consider that the radiation can be into only one half-sphere. For an array system this means that reflections from the ground, a screen or reflector elements have to be included in the calculations. The antenna gain G is defined as the ratio of the maximum radiation intensity (in the main beam) to the average radiation intensity (averaged over all δ and a). For an antenna array with reasonable sidelobe suppression it is proportional to the antenna area and is given approximately by the inverse of the two orthogonal beam widths δ_B' and δ_B'' (in radians):

$$G = \frac{4\pi A}{\lambda_0^2} \approx \frac{4\pi}{\delta_B'\delta_B''} . \tag{4}$$

The effective area A or aperture of the antenna is the product of the physical area of the antenna and the efficiency of its illumination, which for instance may be reduced by tapering. It is noted that A does not include the losses of the antenna elements and its feed system.

The considerations of antenna arrays, consisting of several discrete elements, can generally be extended also to antennas with continuous aperture illumination, such as dish antennas. The aperture A of a phased array or a dish antenna is used to calculate the power-aperture product P·A, which defines the sensitivity of an MST radar. Note that P is the effective average power, which is radiated by the antenna, i.e. it is smaller than the output power of the transmitter due to losses in the antenna and feed lines.

This very brief outline is useful for estimating some basic values needed to plan and design a radar antenna system. The minimum requirement for investigations of the troposphere and stratosphere is a power aperture product P·A = 10^8 Wm², where P = P_a is the average transmitter power. We assume that the radar sensitivity is a function of A^k, where $1 < k < 2$ depending on the reflected contribution (see equation (2)). It means that in practice one should favour an extension of the antenna area against an increase of the transmitter power. For a commonly achievable transmitter power P = 10^3W, P·A = 10^8 Wm² yields the

dimension of a circular antenna array to be about $Nd \approx 36$ m, and $A \approx 1000$ m^2. For $n_o = 6$ m we can obtain a half-power beamwidth $\delta_B \approx 9°$, and a gain $G \approx 27$ dB. This estimate assumes that the array is optimally filled with elements. A single dipole element over a proper reflector screen has an effective area of about 15 m^2 (at $n_o = 6$ m). Thus, about 64 dipoles are needed to fill the array. For a square array with 8x8 elements the resulting spacing is d ≈ 0.75 n_o, and a grating lobe will not occur. The first nulls are at $\delta_n = \pm 9°$, and the first sidelobes at $\delta_s = \pm 13.5°$. To use such an array to measure reliable velocities, the antenna beam has at least to be steered to a zenith angle $\delta_o = 9°$ to place a null into zenith direction (minimizes influences of aspect sensitivity). Even then a sidelobe at $-4.5°$ is a problem.

When designing a radar antenna for atmospheric research one has to trade between the choices to optimize the effective aperture or to optimize the side-lobe suppressions. An optimization of the aperture increases the sensitivity, but does not minimize the side lobes. Suppression of sidelobes by tapering attenuates undesirable signals which spoil the estimates of reflectivity and velocity, but it reduces the antenna gain. Principally, any sidelobe effects or their minimization, however, are equivalent to a broadening of the antenna beam. This is generally a minor shortcoming as compared to the tedious procedures to remove sidelobe effects from the signal during the data analysis procedure. As an example of a well optimised MST radar antenna pattern we show in Fig. 11 the antenna diagram in two vertical planes of the mobile SOUSY VHF Radar (from CZECHOWSKY et al., 1984). Note the suppression of near-zenith sidelobes by 25 dB as compared to the main lobe and the grating lobe at 40°.

The radar echo signal is given by the product of the antenna pattern with the spatially varying reflectivity structure of the atmosphere. Thus, knowing the antenna pattern, it should be in principle possible to find the wanted signal parameters which however is generally an ambiguous and time-consuming inversion procedure. For vertically pointing main beams the sidelobe effects are efficiently suppressed if there is anisotropic scattering with maximum aspect sensitivity in zenith direction (e.g., for the 50 MHz MST radars). It follows that sidelobes in such cases are a minor problem for investigations with verti-cal beams. However, they can be crucial for methods applying off-zenith beams with 50 MHz MST radars. If a sidelobe is pointing towards the zenith a larger power may be received from the vertical than from off-vertical directions when there is an aspect sensitivity due to horizontally stratified scatterers or partially reflecting layers.
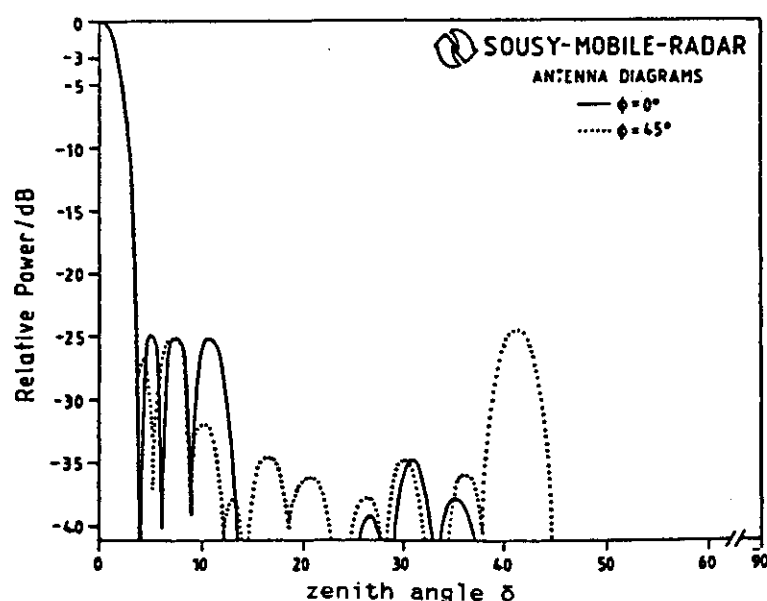

Figure 11. Computed radiation pattern of the mobile SOUSY VHF radar (53.5 MHz) phased array, consisting of 576 Yagi antennas. This antenna system is located on Andoya, Norway. (From Czechowsky et al., 1984).

Also sidelobes at low elevation angles have to be considered since these can cause strong echoes from the non-atmospheric targets in the surroundings of the radar antenna (particularly the ground clutter seen in Fig. 7). The superposition of ground reflected (hatched line in Fig. 7) and direct radiation does very effectively reduce the radiation at grazing angles ($\delta > 85-90°$) since the antenna elements of a phased array are horizontally polarized and the ground-reflected wave then suffers a phase reversal during reflection. This even can suppress low sidelobes of the array pattern which may be regarded as crucial if one would not take into account ground reflections. The location of an MST radar antenna array at a flat ground (extending out to several 100 m) may be sufficient, but a shallow valley generally should be preferred to further suppressing the low angle radiation effects. However, high extending targets, such as radio towers or mountains in the close vicinity, will still cause considerable clutter echoes, even when optimising the antenna array for low angle radiation suppression. For IS radar antennas the criteria of low angle radiation suppression are not so stringent, because ground clutter barely comprises a problem since the ionospheric target regions are usually at much larger ranges. However, for IS radars in auroral regions care has to be taken to suppress coherent echoes from ionospheric irregularities.

2.2. Antenna Types and Feed Systems

MST radars generally operate with quasi-vertical beams, i.e. the zenith angles are smaller than about 20°-30°. As shown in Fig. 8 usually zenith angles of 15° are chosen. IS radars mostly apply a variety f beam directions, also those very close to the horizon. For MST radar operation linear polarization is sufficient, but circular polarization is needed for incoherent scatter radars since the polarization can change due dispersion in the ionosphere. Essentially four different types of antenna systems are in use: dish antennas, dipole arrays, coaxial-collinear arrays (COCO) and Yagi arrays. In Fig. 12 we show as an example the 32-m dish antenna of the EISCAT incoherent scatter radar 933-MHz receiving station in Sweden, which can be pointed in all directions by mechanical steering. In Fig. 13 the 200m x 200m MST radar antenna of the Poker Flat Radar in Alaska is shown which has only a few fixed pointing directions to the vertical and at 15° off-vertical.
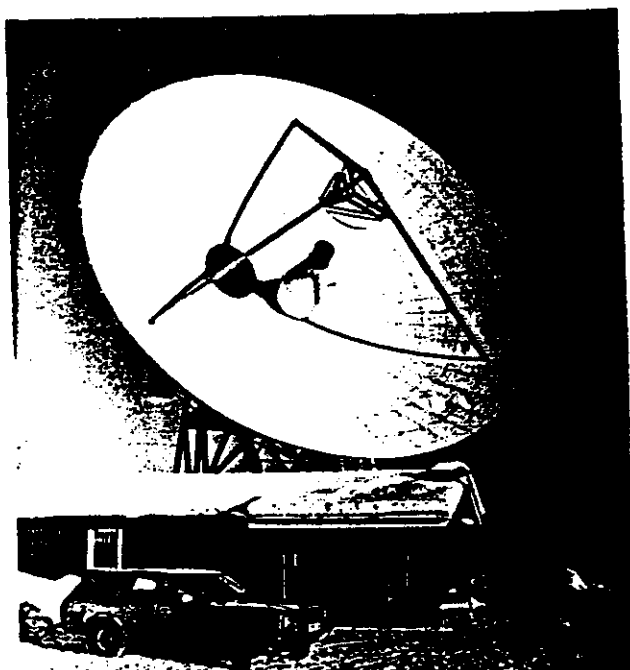

Figure 12. The 32-m receiving antenna dish of the incoherent scatter radar of the EISCAT UHF (933 MHz) radar system in Kiruna, Sweden.
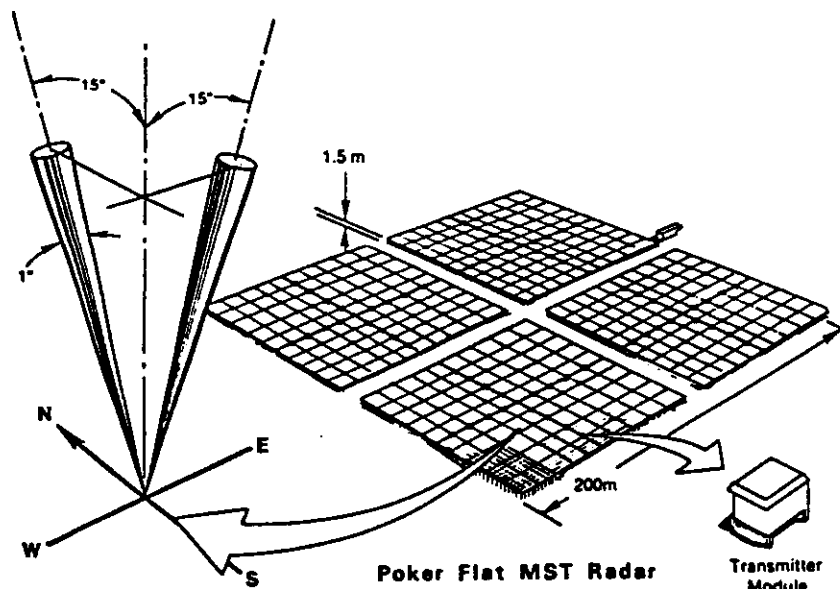
18

Figure 13. The 200m x 200m coaxial-collinear antenna array of
the Poker Flat MST radar in Alaska, operating on 50 MHz with
two off-vertical beam directions (from BALSLEY et al., 1980).

Dish or cylinder antennas are rarely used for MST radar applications be-
cause of their large dimensions, but they are quite frequently applied in IS
radar facilities. Only one or a few elements are applied as primary feed anten-
nas of the dish antennas. The beam steering is done either by moving the posi-
tion of the feed antenna (e.g., at the Arecibo Observatory (WOODMAN, 1980)) or
the entire dish (e.g., at the other UHF IS radars, see Table 9 at the end of
this article). This has the advantage that no complicated power distributions
and phasing network has to be used to feed the antenna. The EISCAT VHF radar
uses a long line feed to illuminate a 120m x 40m dish and allows mechanical
steering in one plane and side-steering by phasing in the other plane (HAGFORS
et al., 1982). Because of the limited size of the primary feed antennas of dish
antennas, the low-angle sidelobe suppression is usually not sufficient, which
results in strong clutter echoes, particularly when such antennas are also used
for MST radar applications.

Usually the antenna systems of MST radars are phased array antennas con-
sisting of many single elements as can be seen for instance in the lay-out of
the antenna system of the MU radar in Japan which consists of 475 crossed Yagi
antennas (Fig. 14). In the case of the MU radar modules of four antenna elements
are fed by single phase-coherent transmitters, which allows very fast electronic
beam steering. In many other cases the individual elements or modules are fed
from a single transmitter through a cascading network of cables, hybrids and
phase shifters. A relatively simple antenna array is the COCO antenna (coaxial-
collinear), which is built in form of an array (see Fig.15) by using coaxial
cable as radiating elements (e.g., BALSLEY et al., 1980). It has the advantage
that the feeding of elements in one line is just done by interchanging the inner
and outer conductor of a coaxial cable every half wavelength. The earliest
application of the COCO antenna can be found at the Jicamarca VHF radar in Peru
(see Fig. 16). The outer conductors of the aligned coaxial tube or coaxial cable
act as collinear dipoles. The feeding is done from the center of a line, which
may typically consist of 16-48 dipoles. Positioning several of these strings or
rows in parallel at spacing d < Λo , and feeding these by a suitable matching
network results in a COCO array (see Fig. 15). The radiation and the loss in a
coaxial string comprise some natural tapering, having the intrinsic advantage of

19
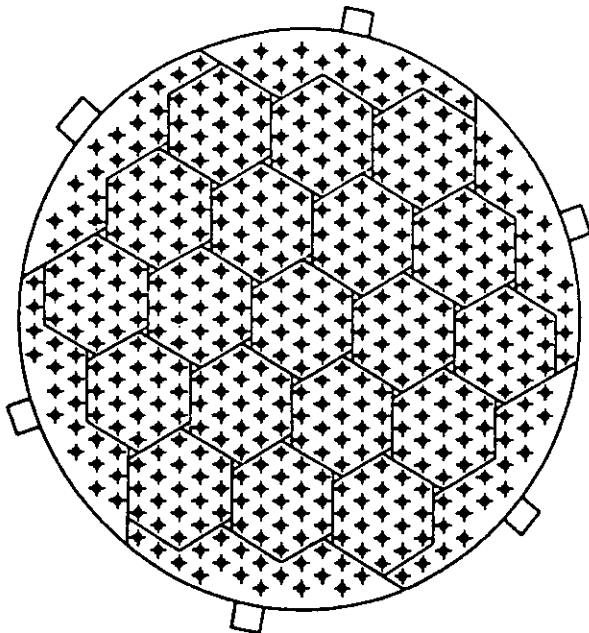
Figure 14. The lay-out of the 475 crossed Yagi-antenna elements of the 46.5-MHz MU radar in Japan (after FUKAO et al., 1985a,b).
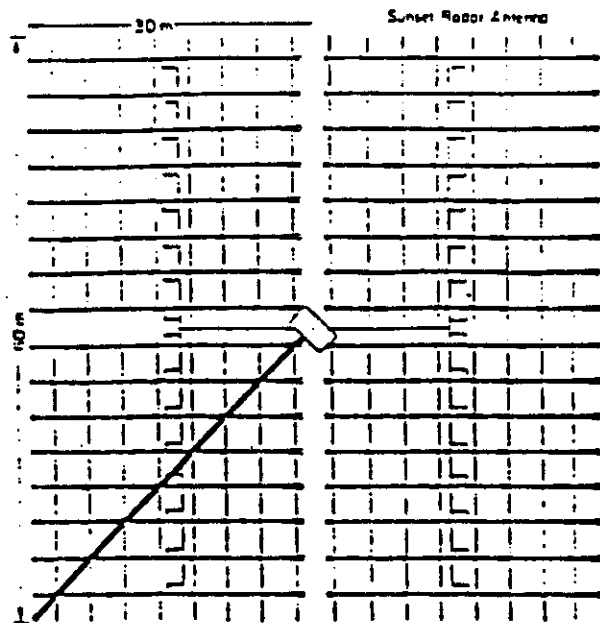
Figure 15. The coaxial-collinear antenna lay-out of the 50-MHz Sunset ST radar in Colorado, USA (from Green et al., 1975).
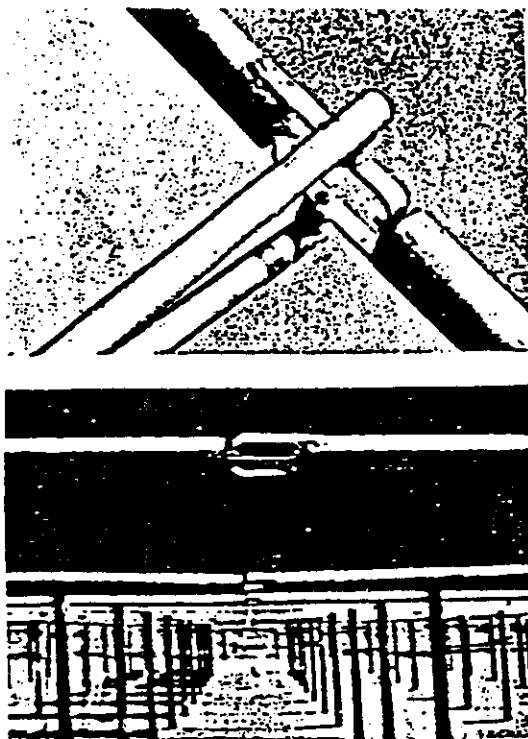
Figure 16. Part of the phased-array antenna of the 50-MHz Jicamarca radar in Peru and a close view of the interchange of inner and outer connector of the coaxial-collinear dipole tubes (from OCHS, 1965).

Figure 17. Yagi antennas and power dividers of the SOUSY-VHF-Radar in West Germany.

20

C 20

suppressing sidelobes in the plane of the string but the disadvantage of degra-
ding the antennna efficiency. Because of the phase relation along a string is
fixed, a beam steering parallel to the COCO string is not possible. Beam steer-
ing perpendicular to the string rows is achieved by inserting appropriate phase
delays in the cables feeding the parallel rows. The COCO dipoles have to be
lined up a quarter wavelength over reflector wires or screens. This antenna type
is relatively inexpensive, because coaxial cable is used for antenna elements
and the matching network is simple. The successive phasing from one collinear
element to the next, however, degrades the bandwidth of this antenna type.
Instead of coaxial cable as radiator, halve-wave dipoles can also be used which
are fed in a properly adjusted phase to form a collinear antenna. The applica-
tion of collinear dipole lines limits the steerability of an array, and for this
reason frequently three antenna arrays are used with three different fixed beam
directions (e.g., GREEN et al., 1975; BALSLEY et al., 1980).

Single dipole or Yagi antenna elements (see Fig. 17) are often set up to
form a phased array (see Fig. 14 and Fig. 18). They are fed by a cascading
network of open wire or coaxial cable systems, when a single transmitter is ap-
plied. The cascading is most appropriately done in 2^n branchings (n = 1.2,...),
as for instance shown in Fig. 19. By these means one can also feed parts of the
antenna array with 1/2, 1/4,... power to provide tapering without dissipating
power (see for instance Fig. 20). The branching is best done in couplers, power
dividers or 3dB-hybrids, which prevent RF-power, reflected from a mismatch to
return to the transmitter or other antenna elements rather than being dissipated
in the resistor port of the hybrid. These hybrid installations also minimize
effects due to mutual coupling between the single antenna elements. The coupling
can be critical if phase control is applied to steer the antenna beam. The phase
shifting, as shown in Fig. 21, is usually inserted close to the final elements,
which may also be connected to form modules of 4 or more elements. For continu-
ous beam steering phase shifting has to be done continuously, which mostly is a
sensible and difficult procedure particularly when narrow antenna beams are
used. The phasing is more easily done by inserting discrete phase delays in
steps of $2\pi/16$ with a binary phase shifter, which is shown in Fig. 22. The
switching can be achieved by only four relays, allowing phase delays of 22.5°,
45°, 90° and 180° to be inserted in all possible combinations, which are suffi-
cient for commonly applied beam width of several degrees. Another way of phase
shifting can be done with hybrids as is shown in the schematics of the later
Fig. 32.

/1 /2 /3 /4 /5 /6 /7 /8

/9 /10 /11 /12 /13 /14 /15 /16

/17 /18 /19 /20 /21 /22 /23 /24

/25 /26 /27 /28 /29 /30 /31 /32

/33 /34 /35 /36 /37 /38 /39 /40

/41 /42 /43 /44 /45 /46 /47 /48

/49 /50 /51 /52 /53 /54 /55 /56

/57 /58 /59 /60 /61 /62 /63 /64

64 (8×8) ELEMENT YAGI ARRAY
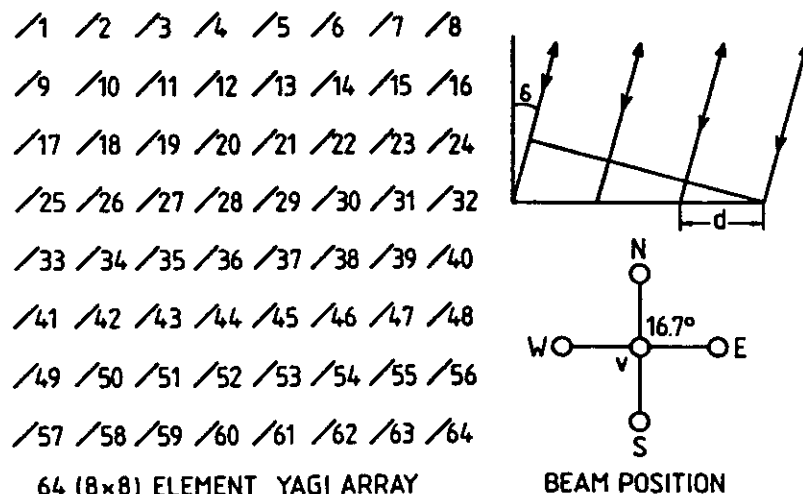
BEAM POSITION

Figure 18. Lay-out of one 64-Yagi-antenna module of the 52-MHz
Chung-Li VHF radar in Taiwan (after BROSNAHAN et al., 1984).

21
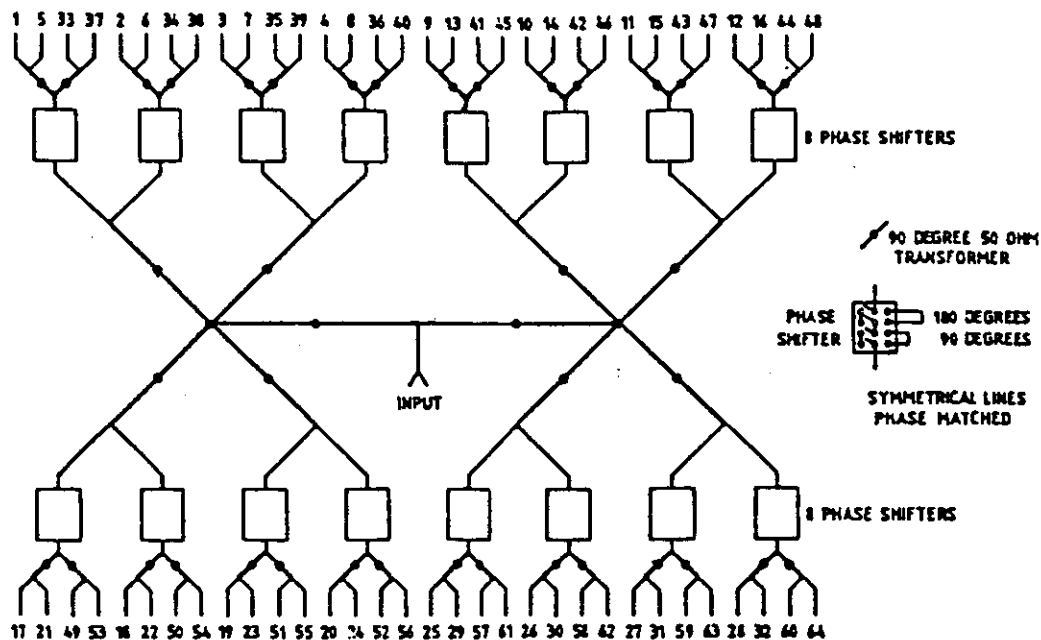
Figure 19. Power divider and beam-steering phase delay (0°, 90°, 180° and 270°) of the Chung-Li VHF radar, allowing five beam positions: vertical (δ = 0°) and north, east, south and west at δ = 16.7° zenith angle (from BROSNAHAN et al., 1984).
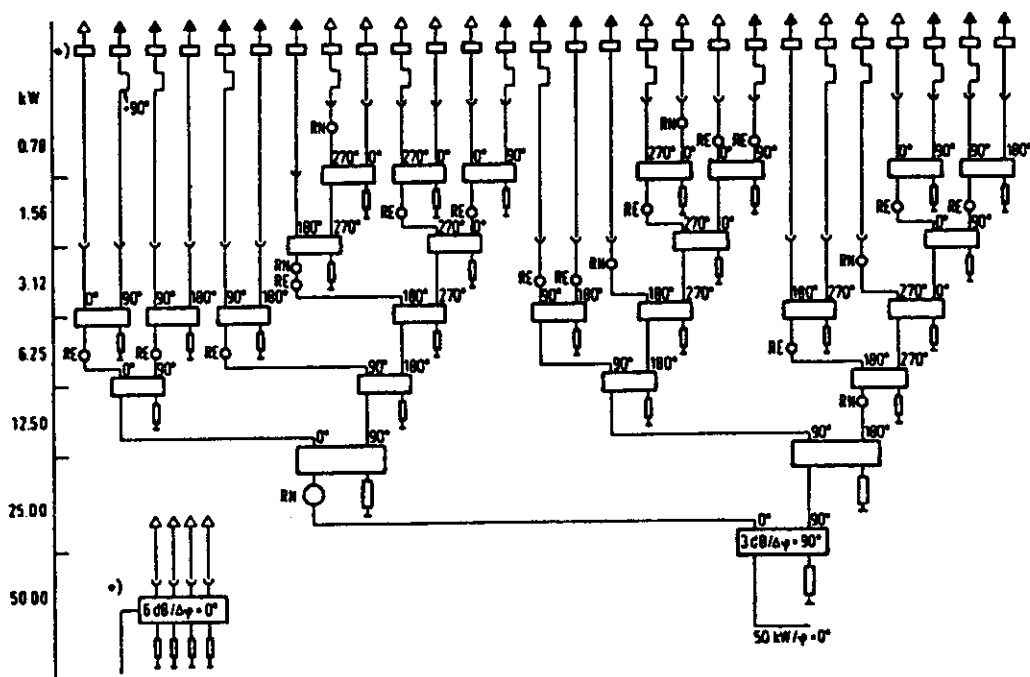
Figure 20. One quarter of the power divider system of the mobile SOUSY VHF radar antenna, allowing for tapering of the antenna elements by staggered power dividing hybrids (from CZECHOWSKY et al., 1984).

Figure 21. Schematics of a typical antenna feed distribution system using hybrids for power division. The two output ports of a hybrid are phase shifted by 90° with respect to each other. This has to be compensated by the phase shifters, which are also used to insert certain phase shifts for beam steering. The power, which is reflected from the antennas due to an impedance mismatch, is attenuated in the resistor port of the hybrids and does not return through the transmitter-receiver port.

Binary Phase Shifter
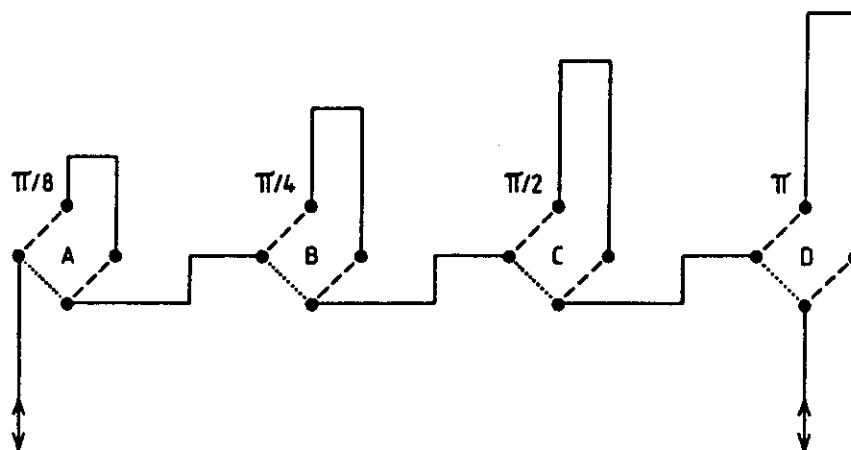
Figure 22. Principle of a binary phase shifter, allowing all the combinations of phases:

Phase shift:		$\pi/8$	$2\pi/8$	$3\pi/8$	$4\pi/8$	$5\pi/8$	$6\pi/8$	$7\pi/8$	π
Phase delay	A:	1	0	1	0	1	0	1	0
(1=on)	B:	0	1	1	0	0	1	1	0
(0=off)	C:	0	0	0	1	1	1	1	0
	D:	0	0	0	0	0	0	0	1

The phases between π and $15/8\pi$ are achieved by keeping the phase delay D in the on-position.

The advantage of Yagi against dipole antenna elements is that no ground screen is needed because of the Yagi reflector. The multi-element structure of a single Yagi allows for a higher gain (improving the filling factor of an array) and a negligible coupling (<-25 dB) between adjacent Yagi antennas in an array. Mostly Yagi antennas can be constructed in such a way that the bandwidth is several Megahertz. The bandwidth limiting factors in a Yagi system essentially are the phase shifters. The losses of a Yagi system are also considerably lower than those of a COCO antenna. However, such a Yagi system is obviously more expensive than a COCO system. The feeding of an array system can be from one transmitter, but also sub-modules can be fed separately by several phase-controlled transmitters (FUKAO et al., 1980). The transmitter phase control can even be used to steer the antenna beam. This, however, needs a similar phase control of the receiver channels.

3.   TRANSMIT-RECEIVE SYSTEM

Separate antenna arrays can be used for the transmission and for the reception mode as shown in the graph of Fig. 23. Such an antenna combination was first used with the SOUSY-VHF-Radar for MST measurements with the beam-swinging as well as the spaced-antenna mode, which was added at a later time. For a newly designed radar a combination of the two measurement modes using one antenna for transmission and reception is useful as shown in Fig. 24. While separate antenna arrays allow for sufficient decoupling of the receiver from the transmitter, a fast and highly insulating transmit-receive duplexer (ATR = antenna-transmit-receive switch or duplexer in Fig. 24) has to quickly switch the antenna from the transmitter to the receiver and vice versa, if only one antenna is used. The principle of a duplexer is outlined in Fig. 25. During the transmission phase the pin-diodes are short-circuited and the power at the hybrid output ports is reflected back into the hybrid from where it exits through the antenna port to the antenna. The small leakage through the diodes is combined in phase in the
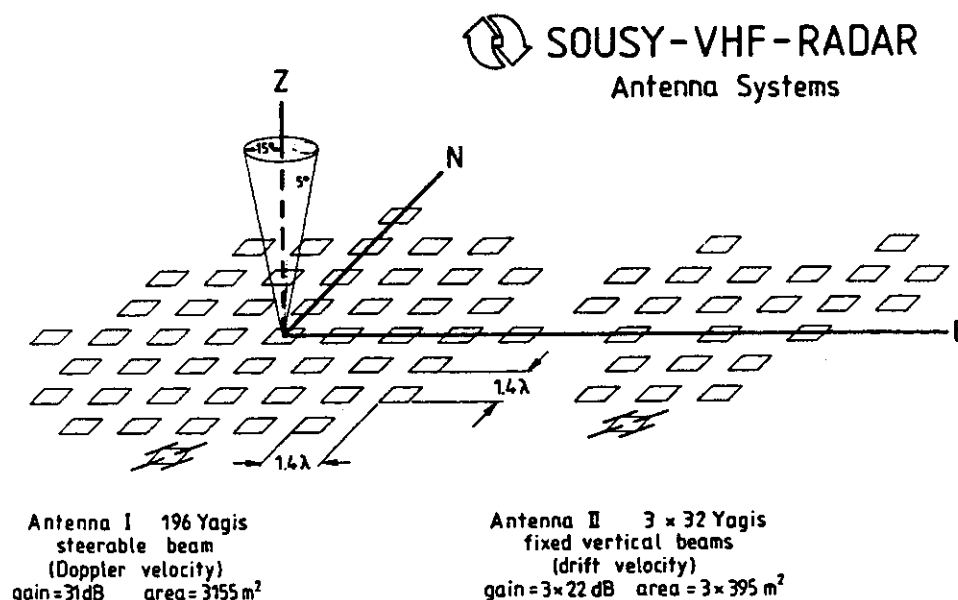
Figure 23.   Antenna systems of the SOUSY-VHF-Radar in W.Germany consisting of phased arrays of Yagi-antenna elements. The complete system is designed for beam steering in the Doppler mode with antenna I and in the spaced antenna mode with antenna I and antenna II. For the latter purpose the antenna I is pointed vertical and the separated three subunits of 32 Yagis of antenna II, which are forming a vertical beam also, are used for reception.

24

METEOROLOGICAL SAD-VHF-RADAR SYSTEM
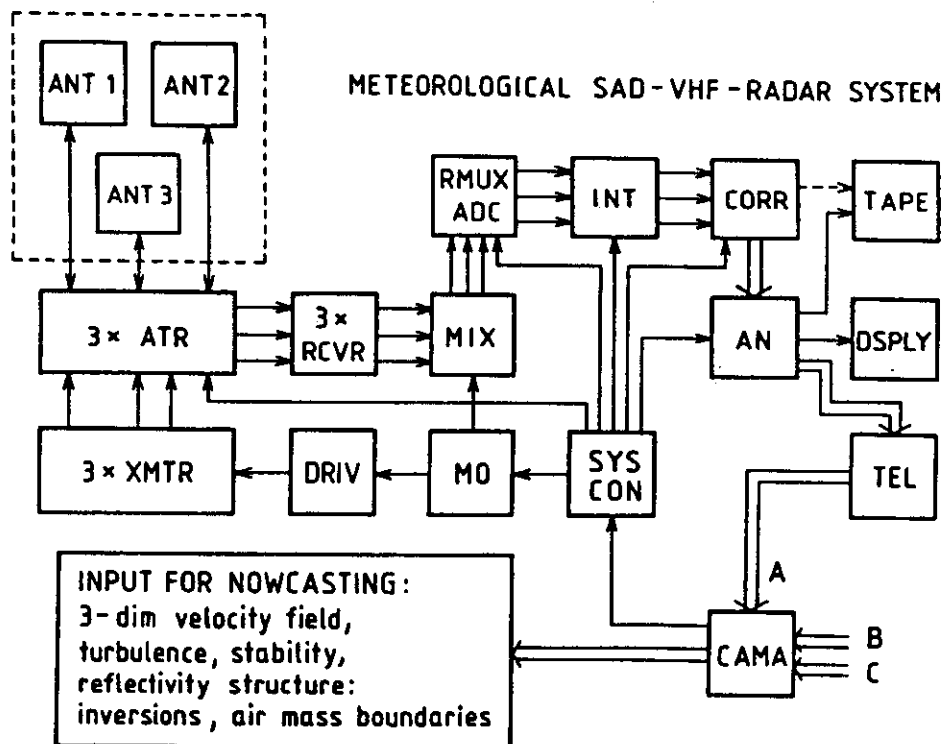
Figure 24. Radar system using three separate receiver-transmitter-antenna
modules, which can be operated phase-synchronized to allow beam steering as
well as spaced antenna measurements with the same full antenna array. The
system is laid out for range multiplexing (RMUX), on-line integration (INT),
correlation computation (CORR) and on-line analysis (AN), as well as data
telemetry (TEL) and remote control (CAMA). The latter additions of remote
control and data transfer are usually needed when such a radar system would
be used in operational applications as a wind profiler.
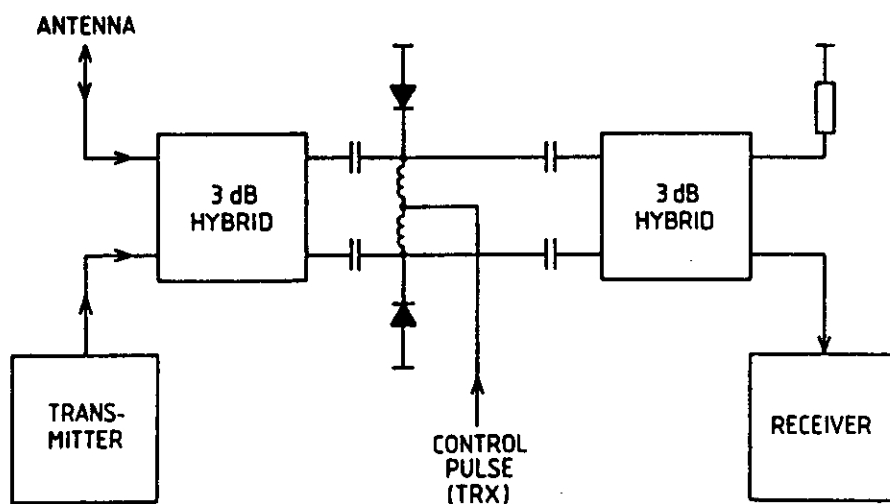
Figure 25. Transmit-receive duplexer (also called T/R switch)
using 3-dB hybrids and pin-diode switching.

receiver hybrid and exits through the resistor port. In the reception case the diodes are open and the split power from the antenna is combined in-phase in the receiver hybrid to pass through the receiver port to the receiver input. Any noise, which is still generated in the transmitter during the reception phase is combined into the resistor port of the receiver hybrid. The response and re-covery time of the duplexer should be in the order of the range sampling time, i.e. typically less than 10 µs. To insulate a peak transmitter pulse amplitude of 10^5W to a fraction of Watt, which will not affect the receiver, the decoupling attenuation has to be better than 60 dB. These specified values can be obtained with the described pin-diode hybrid switch. Other kinds of transmit-receive duplexers, using quarter-wave coax lines or parallel and serial reso-nance circuits are also used. These are not so suitable because of the resonance circuits, which cause ringing effects and affect the data in the first sample range gates. If circular polarization is applied (in IS radar operations) the duplexer can be replaced by a hybrid, which provides some 30 db decoupling between the transmitter and receiver port. The remaining RF signal leaking through the receiver port is usually attenuated by a so-called receiver protec-tor, which is a fast pin-diode switch disconnecting the receiver input from the hybrid receiver port during the transmission phase. In order to further protect the receiver during eventual malfunctions of the duplexer or the receiver pro-tector the status of these devices is monitored by proper hand-shake and inter-lock systems, which prevent the transmitter to be turned on in case of a fai-lure.
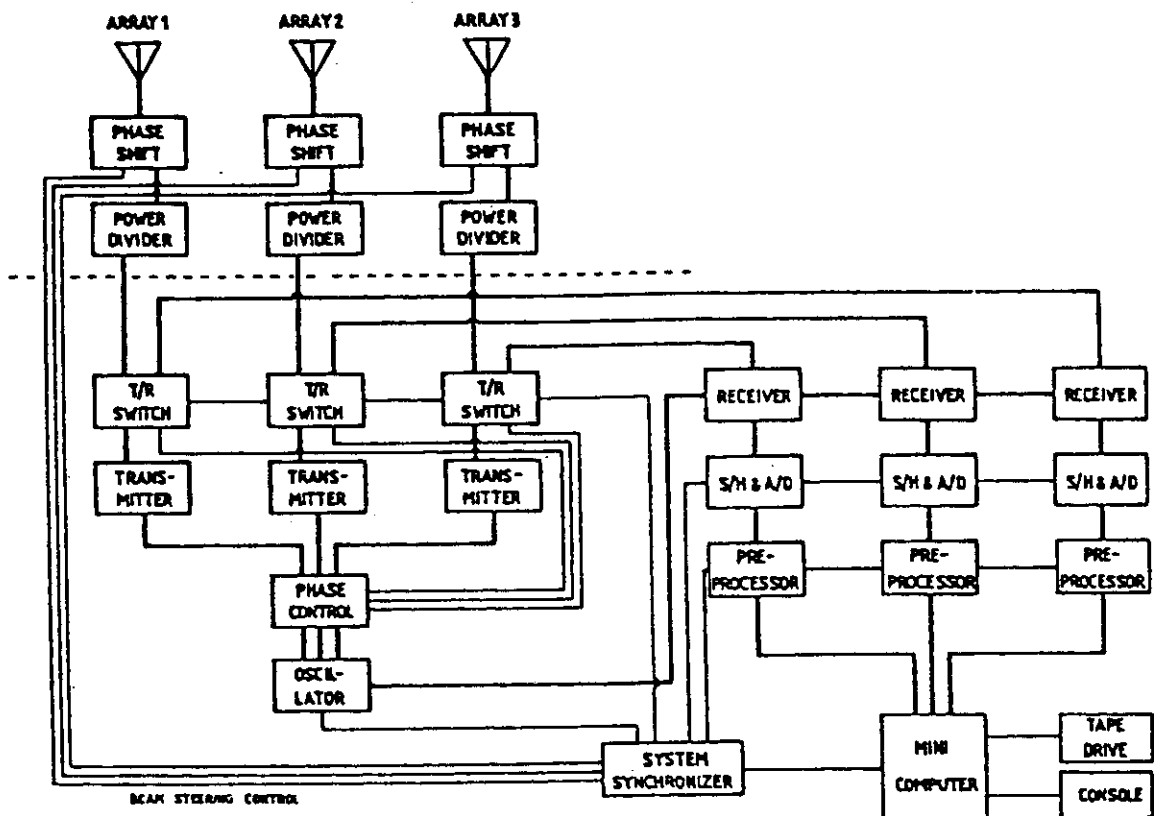
Figure 26. Block diagram of the Chung-Li VHF radar, which bases on the principal lay-out of Fig. 24 (from Brosnahan et al., 1983).

26

In Fig. 26 a block diagram of the Chung-Li VHF radar is shown, which is a dual-mode radar. Dual-mode means that the radar can be used in the Doppler as well as in the spaced antenna mode (for velocity and interferometer measurements). For the spaced antenna mode it has three separate antenna arrays for reception which are combined in phase for transmission. In the Doppler mode the antenna arrays can be either combined to point into the same direction during transmission and reception, or they can point at the same time into three different directions. The beam steering is done by phase shifters and the power distribution by power dividers, which are made from coaxial cables. The transmit-receive duplexer is called T/R switch (transmit-receive switch) in this diagram. Three transmitters are feeding the three antenna arrays. For providing the essential phase equality at the three antenna arrays, the transmitter drive RF signals are phase-controlled. In order to provide the phase-coherent radar system, the same oscillator controls the transmitters as well as the three receiver channels. Following the sample-and-hold (S/H) circuit and analog-digital converters (A/D) the data are preprocessed, i.e. coherently integrated, and transferred to the mini-computer. From there the data are dumped on tape. By the computer also the radar operation is controlled, particularly by loading the system synchronizer (radar controller) and starting the operation. The system synchronizer also steers the antenna beam directions. We now will briefly describe in more detail some typical sub-units of such a radar system.

3.1. Transmitters, Receivers and Oscillators

In Fig. 27 the principle block diagram of a transmitter is shown. The oscillator generates a continuous wave signal, which is pulse modulated (in amplitude and/or phase) by a fast switch controlled by pulse trains from the radar controller. The switching needs to be done with transition times, which are reasonably faster than the duration of the shortest pulse in single pulse applications or the pulse element in phase coding. Thus the switching of 1-μs pulse elements needs to be done within 100 ns or so. The pulsed RF signal, usually at a level of several mW, is amplified in driver stages up to peak power levels of several kW. The final amplifier of MST radars usually yields several ten kW peak RF output power. Most frequently vacuum tube amplifiers are applied in the high power stages, which need power supplies with at least 5-10 kV high voltage. Semi-conductor devices needing much lower voltages are now getting in more use,

TRANSMITTER

Figure 27. Principle block diagram of a typical MST or incoherent scatter radar transmitter.

C 27

particularly when distributed antenna modules are employed instead of one large antenna array. Because of the high output power requirements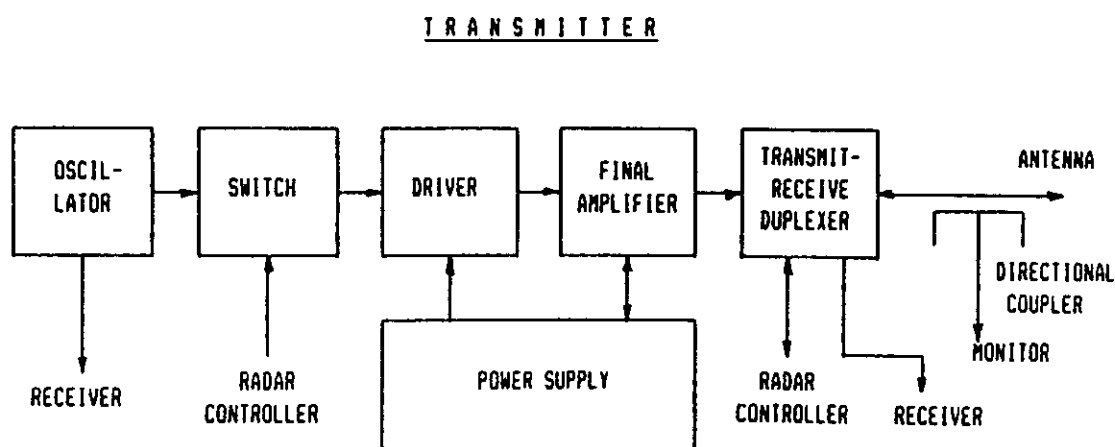 of more than 1 MW, the incoherent scatter radars apply klystron tubes in the final transmitter stage, which need pulsed power supplies with 50-100 kV high voltage. The high power - high voltage power supplies usually are equipped with a very fast protection switch (a so-called "crow bar"), which discharges the power supply within small fractions of a second in case of a transmitter malfunction to protect the final power amplifier tubes from damage.

Following the final amplifier the transmit-receive duplexer switches the antenna either to the transmitter or to the receiver as described in the last chapter. To allow a measurement of the output power a directional coupler is used after the duplexer output. By measuring the forward as well as the reflected power with two directional couplers the matching (i.e., the voltage-standing-wave-ratio: VSWR) of the antenna is usually monitored. If a phase controller is needed to provide exact phasing of separate antenna arrays, it usually is inserted in the low power stages of the transmitter. Such a device is principally described by the block diagram of Fig. 28. The signal from the transmitter output, measured with the directional coupler, is compared with the local oscillator (LO) reference signal with specified phase (for multiiple transmitter beam steering). The phase offset between both these signals is sampled and used to control the phase shifter, which changes the phase of the input signal (RFin). The RFout signal, available with the corrected phase at the output of the phase controller, is then fed to the next amplifier stage in the transmitter.

Usually the local oscillators are more complex because of necessary features, which are outlined in Figs. 29 and 30. For a super-heterodyne receiver, i.e. a multiple mixing of the receiver input signal to one or two intermediate frequencies with subsequent mixing to baseband, a main oscillator in any instance allows for the phase synchronization between these different frequencies (Fig. 29). In case of multi-frequency channel operation, also a set of phase-locked frequencies has to be generated. In practice the transmitter as well as the receiver oscillator signals have to be further processed as shown in Fig. 30. The main local oscillator signal is divided into two signals in the transmitter and the receiver path, respectively. In the transmitter path frequently a phase flip between 0° and 180° is implemented to allow phase coding (phase modulation), followed by the switch to turn on and off the transmitter signal (pulse amplitude modulation). In the receiver path a switch turns off the local oscillator signal during transmission to reduce any feed-through of leakage of the transmitter signal into the receiver. After power dividing of the local oscillator signal one path is phase shifted by 90° to allow baseband mixing to the quadrature components, i.e. real (Re) and imaginary (Im) part of the baseband signal. The control signals (FLP = flip, TXP = transmitter pulse, and LOP = local oscillator protect) are generated by the radar controller (see Chapter 5).

RF in
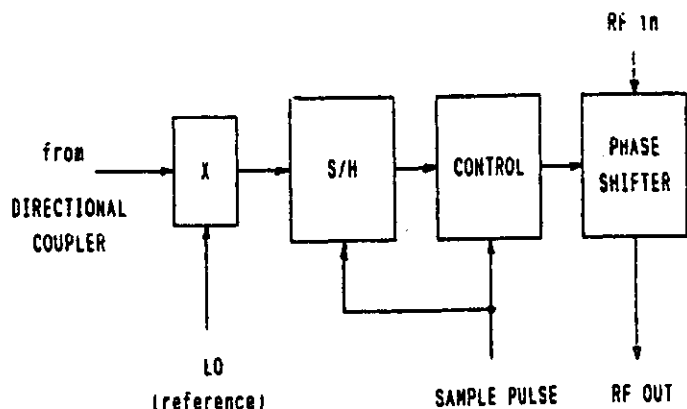
Figure 28. Block diagram of an automatic transmitter phase-controller, which is needed to phase-synchronize multiple transmitters feeding parts of an antenna.

28
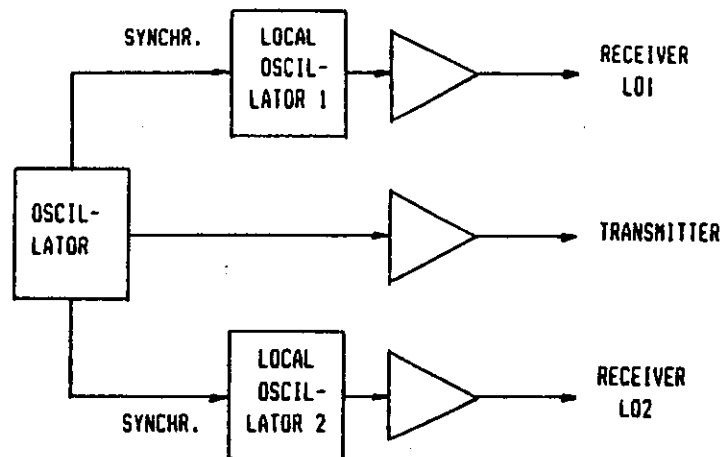
Figure 29. Block diagram of an oscillator circuit for super-heterodyne
receivers with two local oscillators LO1 and LO2 and the phase-
coherent transmitter oscillator control.

MASTER OSCILLATOR
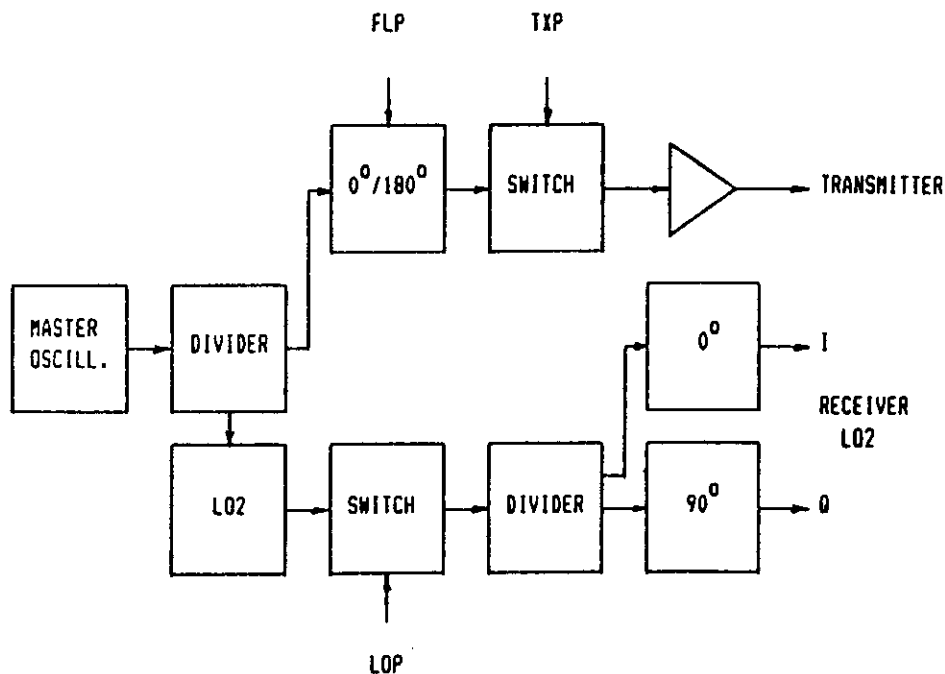
Figure 30. Block diagram of the master oscillator to control the
transmitter and the receiver, showing the particular phase
shifting and switching circuits for the transmitter and receiver
oscillator signals.

29
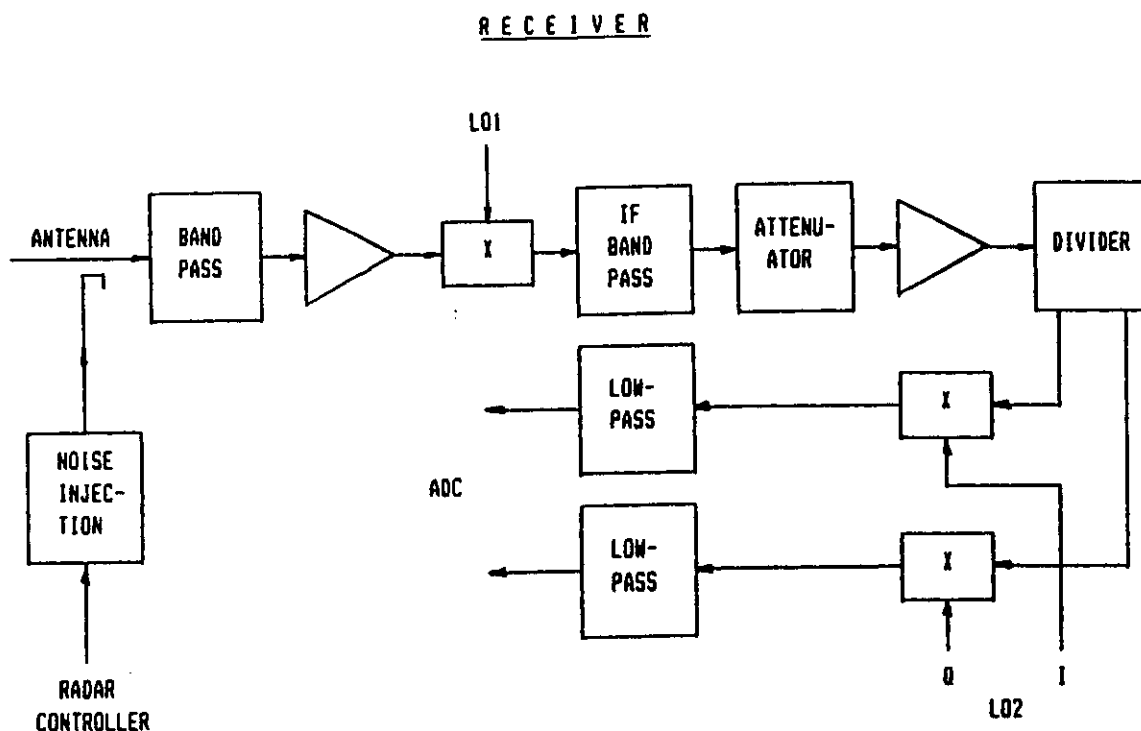
Figure 31.   Block diagram of the principle
receiver circuitry of MST and IS radars.

The receiver is principally described by the block diagram of Fig. 31. The
low-level signal from the antenna (either directly in case of separated trans-
mitter and receiver antennas or via the transmit-receive duplexer in case of a
common receiving-transmitting antenna) is fed to the low-noise preamplifier
through a band-pass. Frequently also a calibrated noise injection, which is
turned on and off by the radar controller, is directly fed into the receiver
front end. This is necessary to allow a well calibrated estimate of the receiver
amplification factor and thus a deduction of the system temperature and the
absolute power of the received signals. In the first mixer the receiver signal
is mixed with the signal from the first local oscillator (LO1) to the inter-
mediate frequency (IF). Again a pass-band filter separates the wanted IF from
the unwanted mixing products. Before further amplification usually a variable
attenuator is implemented to adjust the total amplification of the receiver and
thus the output levels for the final baseband mixer and the analog-digital con-
verters. Following the mixing to baseband with the LO2 signal, i.e. the qua-
drature detection (Re and Im), a lowpass filter is applied which usually should
match the signal bandwidth (given by the bandwidth of the transmitted pulse for
MST radars and by the bandwidth of the scattering process for IS radars). An
example of a low-noise receiver front-end of a UHF incoherent scatter radar,
which allows the calibrated noise injection, the reception of circular and
elliptical polarization as well as sideband conversion, is shown in Fig. 32. The
polarization adaption is achieved by phase changes of the horizontal (H) and the
vertical (V) signal components in the polarizer and the sideband conversion by
mixing from the upper side (1053.5 MHz) or the lower side (813.5 MHz). Depending
on the output from the last hybrid of the polarizer also the sense of rotation
of the polarization (left- or right-hand rotation) can be selected.
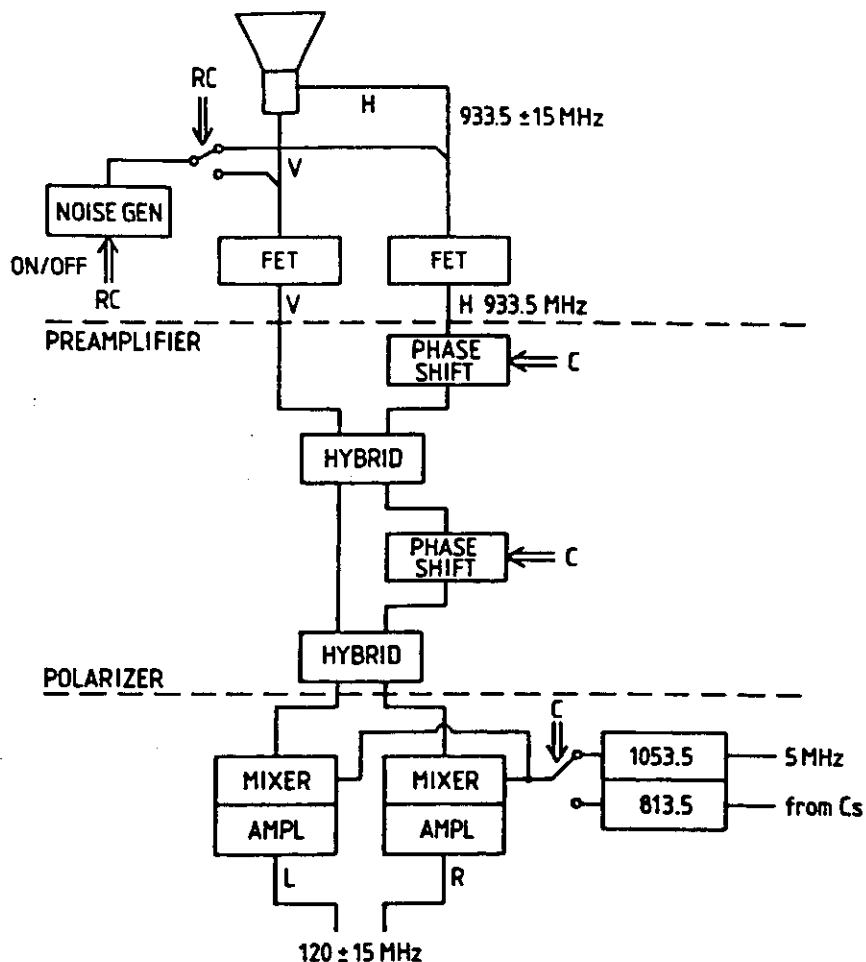
Figure 32. Block diagram of the 933-MHz receiver front-end of the EISCAT incoherent scatter radar receiving stations. The horizontal (H) and vertical (V) components of the signal from the feed horn of the dish antenna are combined by a polarizer (phase shift and hybrids) and mixed to the intermediate frequency 120 MHz. A noise generator, which is switched on and off by the radar controller, injects a calibration signal into the receiver front-ends.

3.2. Examples of Radar Systems

There are some technical system specifications, which principally apply for all atmospheric/ionospheric radar systems. A block diagram of a typical transmitter/receiver system of an MST radar is shown in Fig. 33. It depicts the design of the portable SOUSY Mini-VHF-Radar (46.8 MHz), which was operated at the Arecibo Observatory in 1980. According to individual requirements, many variations and modifications of such a system can be done, but Fig. 33 describes a generally basic design. The 120-MHz signal of the main or master oscillator (MO) is divided by four to obtain a 30-MHz intermediate frequency (IF) which can be modulated (MD) in amplitude (RFC = RF control) and phase (FLP = flip). This is to provide phase coding and DC-elimination (see Chapter 4 for more details). A similar divider generates the 0° and 90° signals, which are necessary for quadrature detection. The operational frequency 46.8 MHz is generated by mixing (X) with the local oscillator (LO) signal at 76.8 MHz. It is amplified in the transmitter (TX) and fed through the transmit-receive duplexer (TRX) to the antenna. The signal received at 46.8 MHz is gated (RGT = receiver gate), amplified in the
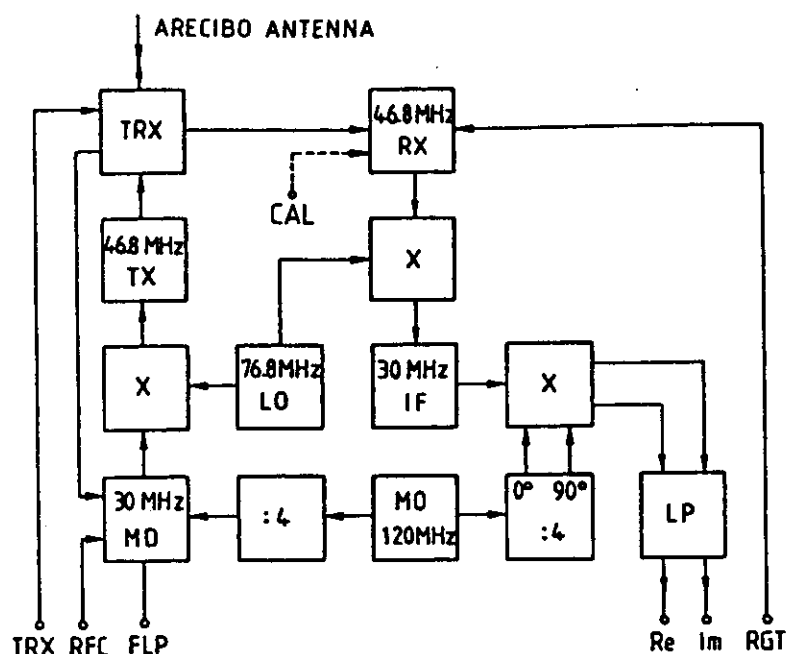
Figure 33. Block diagram of the transmitter-receiver system of
the portable Mini SOUSY-VHF-Radar, which was used with the
Arecibo Observatory dish antenna for MST studies.

receiver (RX), mixed with the LO-signal to an intermediate frequency (IF) of 30
MHz, and mixed down (X) to the baseband in the quadrature detector. The two
quadrature outputs, the real part (Re) and the imaginary part (Im), are low pass
filtered (LP) to match the receiver bandwidth to the bandwidth of the trans-
mitted pulse.

The transmitter peak power typically is between 1 kW and 1 MW for MST
radars with duty cycles up to several percent, while incoherent scatter radars
use duty cycles of some 10% and peak powers above 1 MW. The transmitter band-
width must cover the shortest pulse length of 1 us (≈2 MHz RF bandwidth). The
transmitter is normally operated in class-C mode to achieve an optimum effi-
ciency. Incoherent scatter radar transmitters use mostly high power klystrons.

The receiver linearity range usually exceeds 60 - 80 dB in order to avoid
saturation with strong clutter signals or in the case of large dynamic range
variations of the atmospheric signal. The phase flip and the quadrature detec-
tion must be within less than a few degrees accuracy, and the amplitude ratio of
the quadrature components must not deviate from unity by a few percent in order
not to distort the Doppler spectrum analysis. The stability and the phase noise
of the oscillators is usually better than 10^{-4} Hz/ms to allow a good accuracy of
coherent detection. The receiver base-bandwidth (postdetection) has to be about
1 MHz to provide the resolution of the shortest pulses of 1 μs. The intermediate
frequency bandwidth needs to be at least twice as large as the base-bandwidth.
Bessel filters are usually applied after the quadrature detector as low-pass or
post-detection filter in MST radars, but Butterworth filters in IS radars.

The receiver noise figure of an MST VHF radar need not be better than a few
dB (some 100 K), since the sky noise level (> 1000 K) determines the sensiti-
vity. A noise calibration signal of 1000 K, say, should be injected into the re-
ceiver frontend in order to provide an absolute power calibration (which also

32
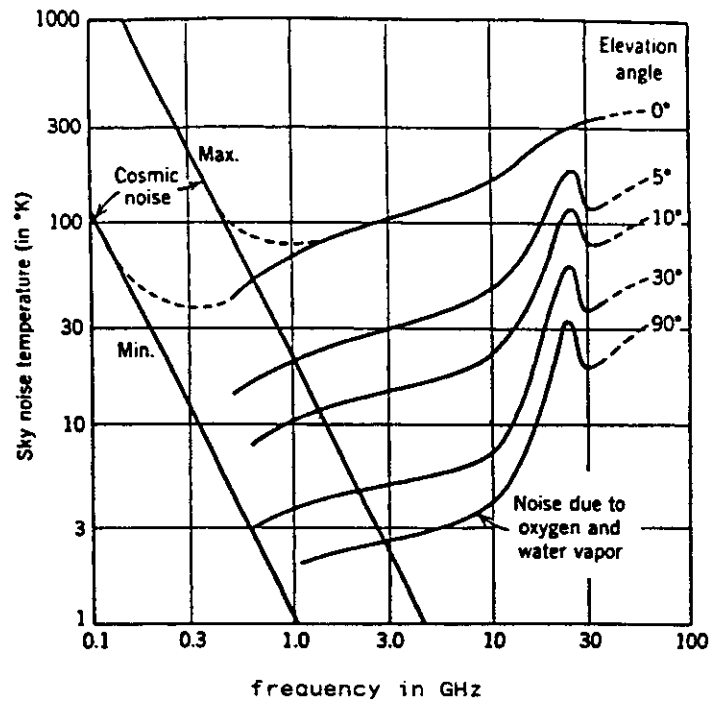
Figure 34. Sky noise temperature as function of frequency
and antenna elevation angle (from KRAUS, 1966).
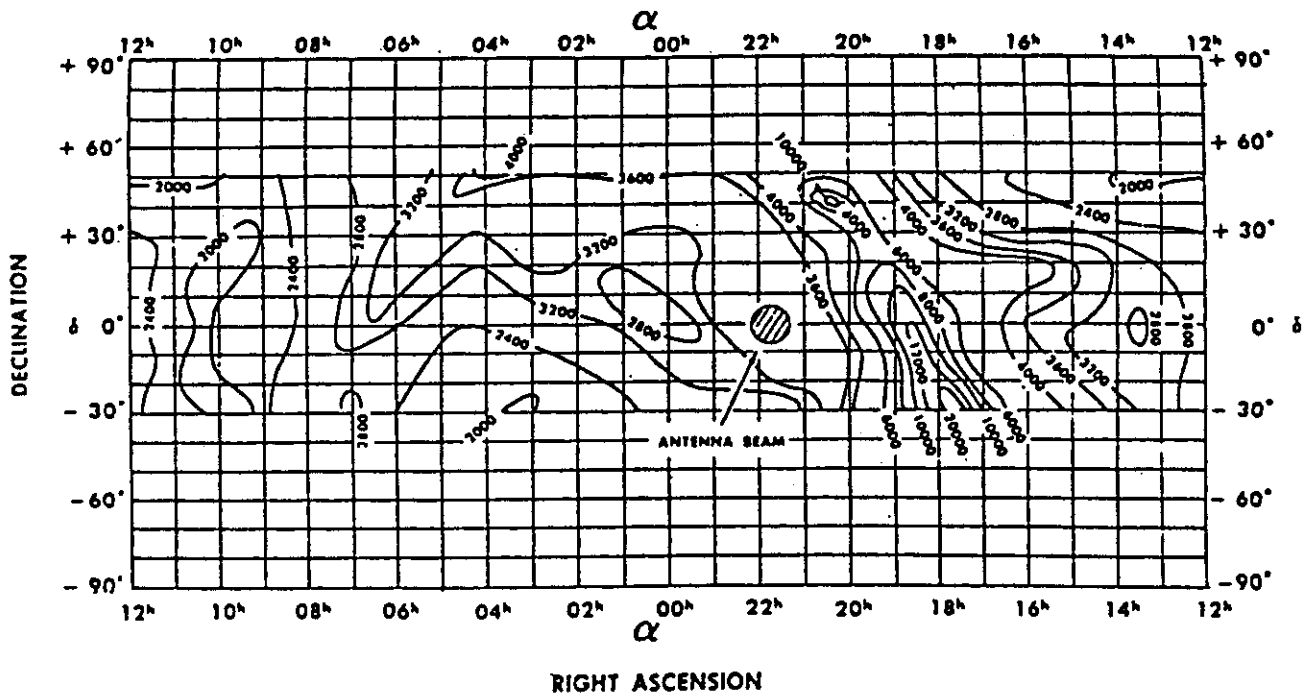
Figure 35. Sky noise map measured as function of declination and
right ascension on 64 MHz (after KO, 1958).

33

needs a continuous monitoring of the transmitter power). However at higher frequencies in the UHF band the sky noise is no more the determining factor as can be seen from Fig. 34. Therefore above several 100 MHz (e.g. in case of the incoherent scatter radars or for the UHF ST radars where the signal-to-noise ratio is usually very low) the receiver frontend has to be carefully designed for lowest equivalent noise temperatures. Usually system temperatures of several ten Kelvin can be achieved at some incoherent scatter UHF radars. The sky noise (from galactic radio sources) changes as function of time of the day and antenna pointing angle as depicted by Figs. 35 and 36 for frequencies of 64 MHz and 53.5 MHz, respectively. This changes the signal-to-noise ratio even if the reflectivity of the radar volumes would be constant. The known variation of sky noise and in particular the well known ephemeris and flux density of point-like radio sources (e.g. Cassiopeia or Cygnus) yield on the other hand a well suited means to calibrate antenna diagrams and antenna gains.
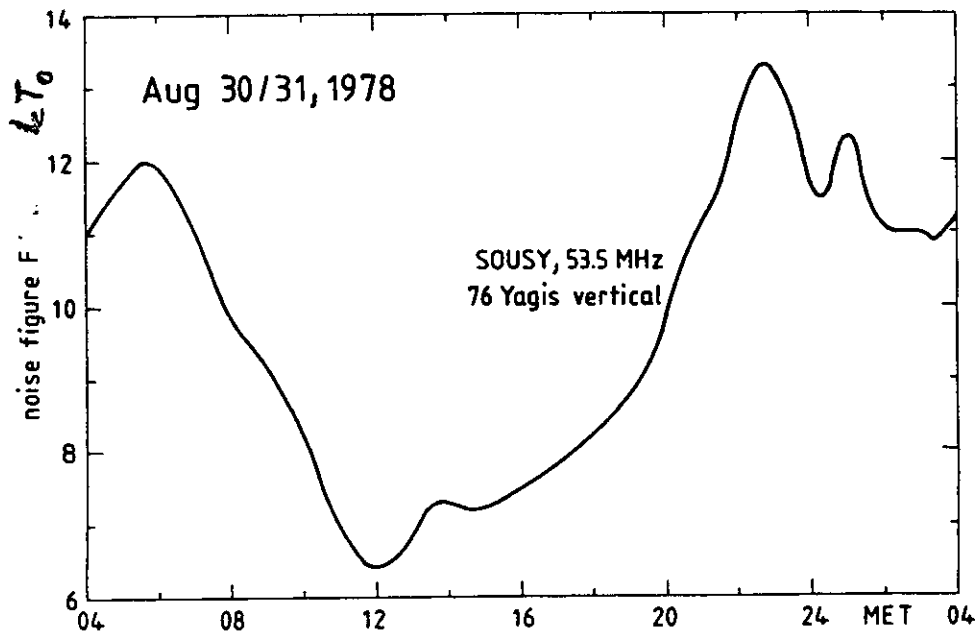
Figure 36. The diurnal variation of sky noise level on
30./31. August 1978 measured at the antenna of the
53.5-MHz SOUSY-VHF-Radar (52°N) in West Germany.
The equivalent noise figure of 0 dB corresponds to
a system temperature of 290 Kelvin.

In Figs. 37, 38 and 39 we show more block diagrams of three other radars, the Poker Flat MST Radar operating on 50 MHz, the MU radar operating on 46.5 MHz, which is used for MST as well as incoherent scatter observations, and the EISCAT radar systems, which operate as incoherent scatter radars in the 933 MHz and the 224 MHz bands. In Fig. 40 a block diagram of a 915 MHz wind profiler radar and in Fig. 41 the block diagram of the Arecibo bistatic S-band (2380 MHz) CW-radar is shown. The latter radar operates on 2380 MHz in phase-coded continuous wave (CW) mode. The experienced reader will notice several of the basic features in these schematic diagrams which we have mostly outlined in the foregoing chapter. More technical details of these radars should be found in the relevant literature.

POKER FLAT MST RADAR BLOCK DIAGRAM
(One Polarization Only)
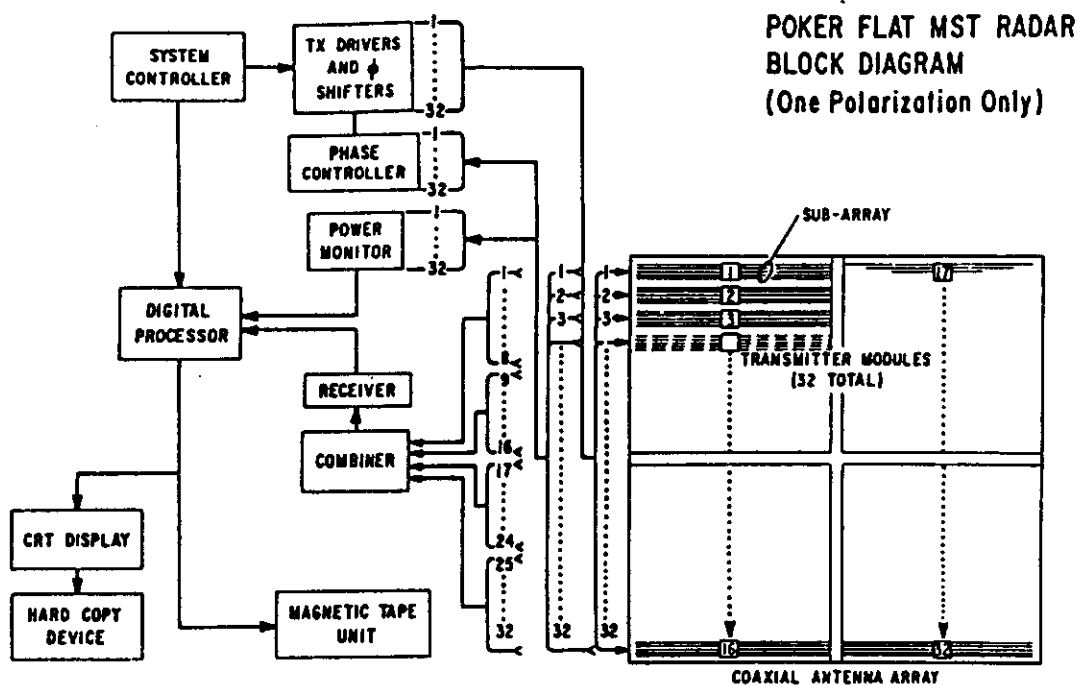
Figure 37. Block diagram of the Poker Flat
MST Radar (from BALSLEY et al., 1980).

MU RADAR BLOCK DIAGRAM
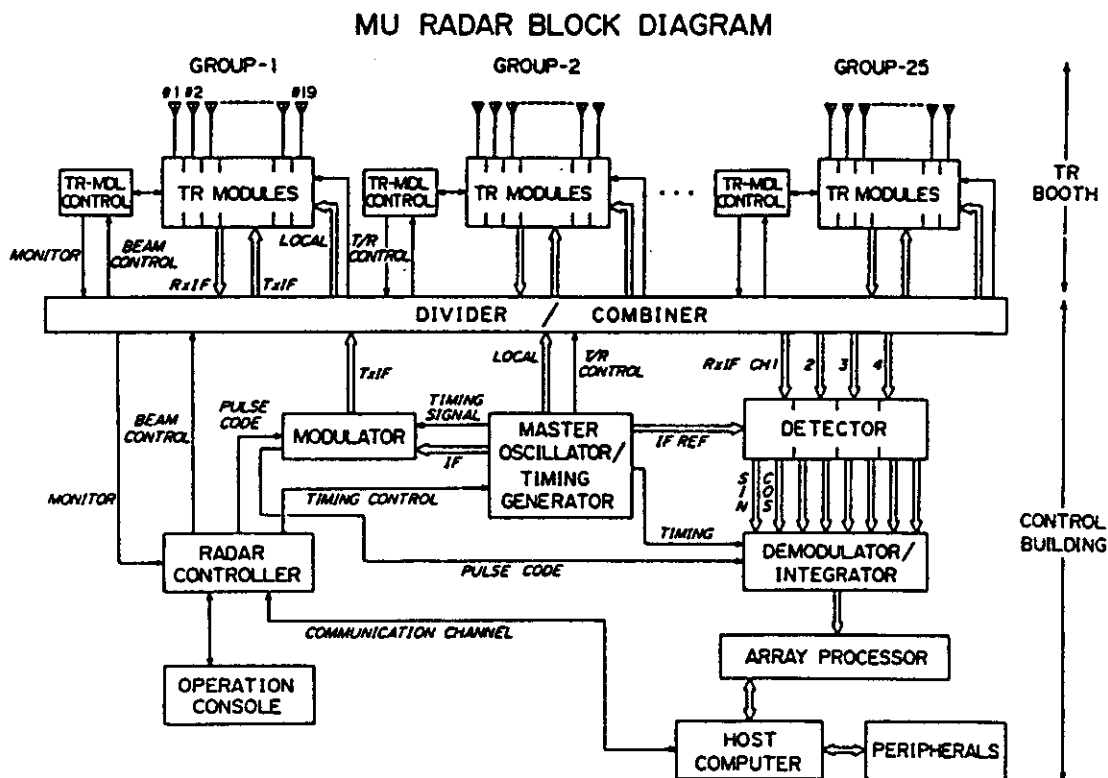
Figure 38. Block diagram of the MU radar
in Japan (from FUKAO et al., 1985a,b).

**ANTENNA
FULLY STEERABLE
DIAM. 32 M**

**STEERABLE IN MERIDIAN
30° ELEV. N. TO
60° ELEV. S.**

SOUTH

UHF 933.5 MHz

VHF 224 MHz

POL — T/R — UHF TRANS-MITTER — FREQUENCY SYNTHESIZ-ERS — VHF TRANS-MITTER — T/R

UHF PREAMPS — VHF PREAMPS

UHF RECEIVERS — RADAR CONTROLLER — Cs-STAND. CLOCK — RADAR CONTROLLER — VHF RECEIVERS

CORRELATOR — COMPUTER — CORRELATOR

TELEPHONE LINE TO KIRUNA
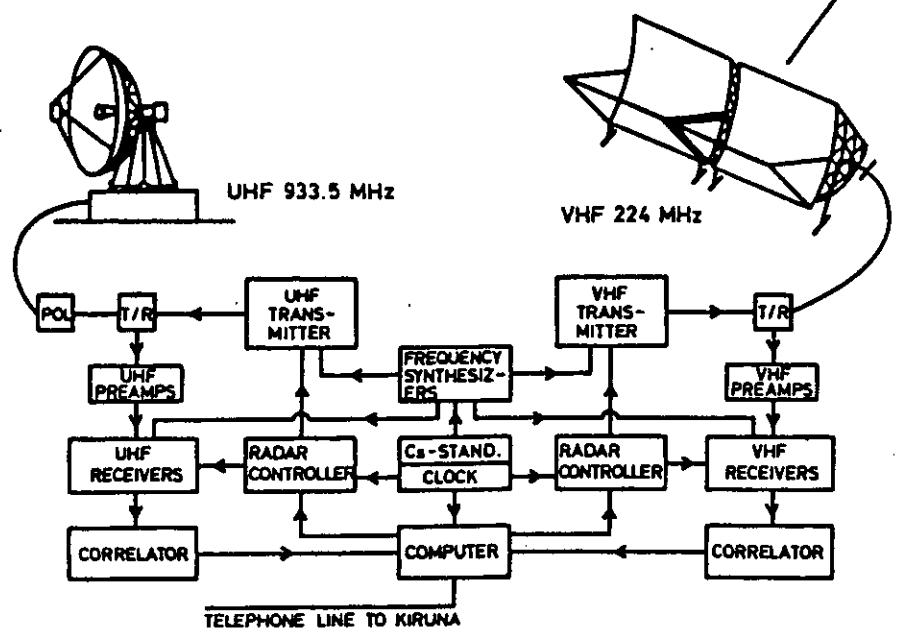
Figure 39. Schematic view and block diagram of the
EISCAT UHF and VHF radar system in Tromsö, Norway.

300-baud dedicated line
(data to S-250 computer)

Modem 1

S-120 Eclipse computer 2

Diskette 3

Disk 4

Surface data
Radiometer data

Switch 5

Terminal 6

Auto-answer modem 7

300-baud dial-up line (control)

Preprocessor and Radar controller 9

RF sources 10

TR   TX

Status readout 11

Antenna control 12

RF switch 18

Antenna 19

Pulsed 915-MHz   Driver 13   Power amp

Power supply 14

17

Limiter 16

Pre-amp 15

945-MHz LO

Receiver 8

30-MHz Reference

AC power to computer, RF sources, preprocessor, and receiver

Power conditioner 20

Figure 40. Block diagram of a 915-MHz Doppler radar
wind profiler (from FRISCH et al., 1986).

36
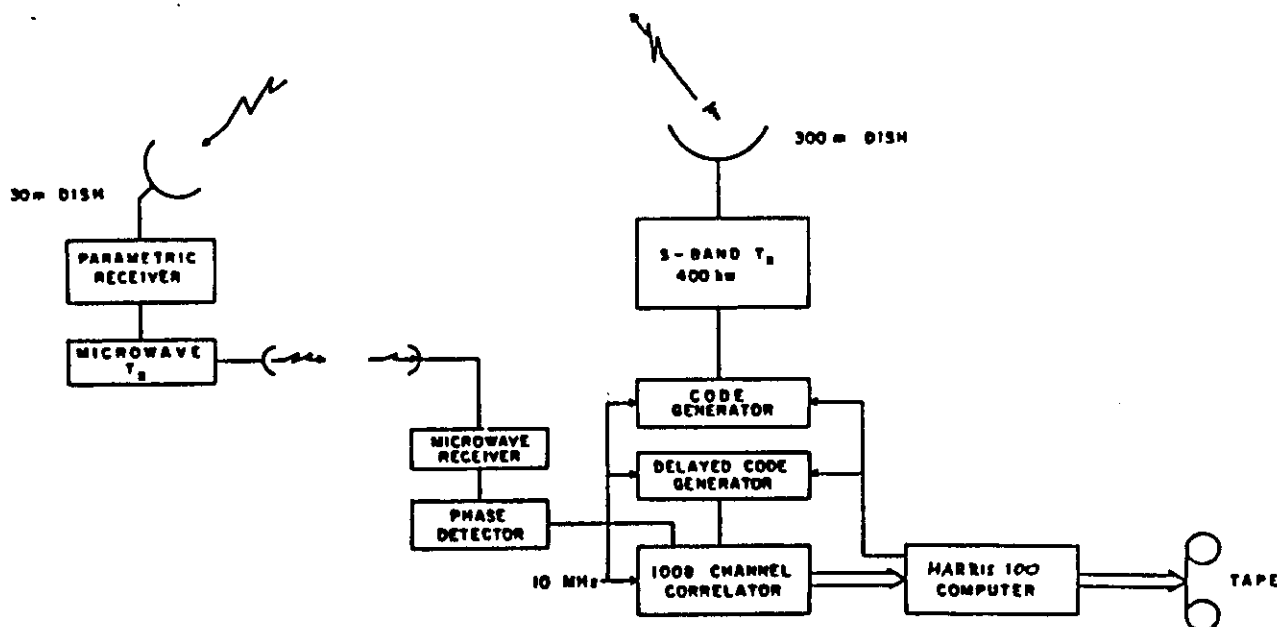
Figure 41. Block diagram of the bi-static S-band (2380 MHz),
phase-coded CW (continuous wave) radar system used at the
Arecibo Observatory in Puerto Rico for high resolution
stratospheric turbulence studies (from WOODMAN, 1980).

4. RADAR SIGNAL ACQUISITION AND PREPROCESSING

The simplified schematics of radar systems, shown in Figs. 6a and 6b, are
used for a basic explanation of the radar operation and data-acquisition proce-
dure. After we have briefly explained the lay-out of antennas, transmitters and
receivers, in the last chapters we will now explain the formalism of a basic
coherent system, the quadrature detection, the digital sampling as well as
subsequent data acquisition and phase decoding procedures. For more details see
WOODMAN and GUILLEN (1974), RÖTTGER and SCHMIDT (1979), SCHMIDT et al., (1979),
CARTER et al., (1980), CLARK and CARTER (1980), SATO and WOODMAN (1982), RASTOGI
(1983), for instance. Since these signal processing steps are mostly done in
specially designed hardware processors, we now briefly summarize the underlying
concepts.

4.1. Coherent Detection

The oscillator generates a signal s^0 at the angular frequency $\Omega_o = 2\pi f_o$
where $f_o = c/\Lambda_o$ is the center radar operation frequency. A pulse train, gener-
ated by the radar controller, imposes a modulation to this signal. After am-
plification in the transmitter (TX in Figs. 6a and 6b) the radar signal

$$s(t) = a(t) \exp(i(\Omega_o t + \phi(t))) \qquad (5)$$

is transmitted, where $a(t)$ determines an amplitude modulation (by the pulse
train) and $\phi(t)$ corresponds to a phase modulation (for coding), and $i = \sqrt{-1}$.
$a(t)$ and $\phi(t)$ are slowly varying as compared to $\Omega_o t$. The radar signal is scat-
tered/reflected from the radar volume and reaches the receiver (RX) via the same
or a separate antenna. Additionally, noise (sky noise and interference) is
received and adds to the radar echo.

37

For simplifying the explanation we will assume for a while that the transmitted signal s(t) is not modulated, i.e. $a(t)=const$ and $\emptyset(t)=const$, and the echo results only from a small radar volume at a given range. The echo signal s'(t) plus noise r(t), which are both band-limited because of the scattering process and/or the receiver bandwidth, can be represented by

$$c'(t) = s'(t) + r(t) = a_1(t)\cos \Omega_o t + i a_2(t)\sin \Omega_o t,$$

where $a_1(t)$ and $a_2(t)$ are independent Gaussian variables in a pure scattering process. The uncorrelated noise r(t) contributes only uncertainties to these estimates. After linear amplification in the receiver, c'(t) is coherently detected by multiplicative mixing with s^o. After low-pass or post-detection filtering (to eliminate high frequency components $2\Omega_o$, which are generated during the mixing procedure), this yields

$$c(t) = a^+(t)\cos \theta^+(t) + i a^+(t)\sin \theta^+(t),$$

where

$$a^+(t) = (a_1{}^2(t) + a_2{}^2(t))^{1/2}/2. \qquad (6a)$$

$$\theta^+(t) = \arctan (a_2(t)/a_1(t)).$$

The phase $\theta^+(t) = \Omega_o t - \theta'(t)$ is given by the Doppler frequency $\Omega_D = -4\pi V'/\Omega_o$, which is due to the bulk motion V' of the scatterers. The time variable phase $\theta'(t) = \theta(t) + \emptyset(t)$, where $\theta(t)$ is caused by the fluctuations of the scatterers-/reflectors in the radar volume. The amplitude $a^+(t)$ is a measure of the reflectivity of the scattering/reflection process. These latter statements are only valid if the noise contributions are separated from the signal. The coherently detected complex signal (+ noise) can be expressed in the form

$$c(t) = x(t) + iy(t), \qquad (6b)$$

where the real part $x(t) = a^+(t) \cos \theta^+(t)$ is called the in-phase component, and the imaginary part $y(t) = a^+(t) \sin \theta^+(t)$ is called the quadrature component. Both components, x and y, are called the quadrature components. The Fourier transform of c(t) is

$$\tilde{A}(\Omega) = \int c(t)\exp(-i\Omega t)dt = \tilde{X}(\Omega) + i\tilde{Y}(\Omega),$$

which yields the periodogram $P(\Omega) = \tilde{X}^2 + \tilde{Y}^2$; it is often also called power or Doppler spectrum. The measured $P(\Omega)$ is the convolution of the spectrum of the refractive index or the reflectivity fluctuations in the radar volume with the spectrum $P_T(\Omega)$ of the transmitted wave form (for the common case of pulsed transmissions), multiplied by the bandpass characteristics $P_R(\Omega)$ of the receiver. Since $P(\Omega)$ is much narrower than the envelope of $P_T(\Omega)$ and $P_R(\Omega)$ in MST radar investigations, these instrumental effects can mostly be disregarded. However, in incoherent scatter applications the spectrum of the scatter process $P_R(\Omega)$ is mostly wider than the envelope of $P_T(\Omega)$, which leads to the fact that the instrumental effects of receiver and transmitter pulse bandwidth have to be accounted for during the signal analysis.

4.2. Digital Sampling

We now take into account that the signal c(t) results from scattering and reflection in certain altitude ranges. Frequently these signals which originate from scatter or reflection of a transmitted radar signal are called "radar echoes". We now have to note that the transmitted signal is modulated in order to resolve the range from where the radar echoes arrive from. As sketched in Figs. 1 and 2, the echoes from different ranges then occur at different times at the analog receiver output. In order to allow adapted signal processing of
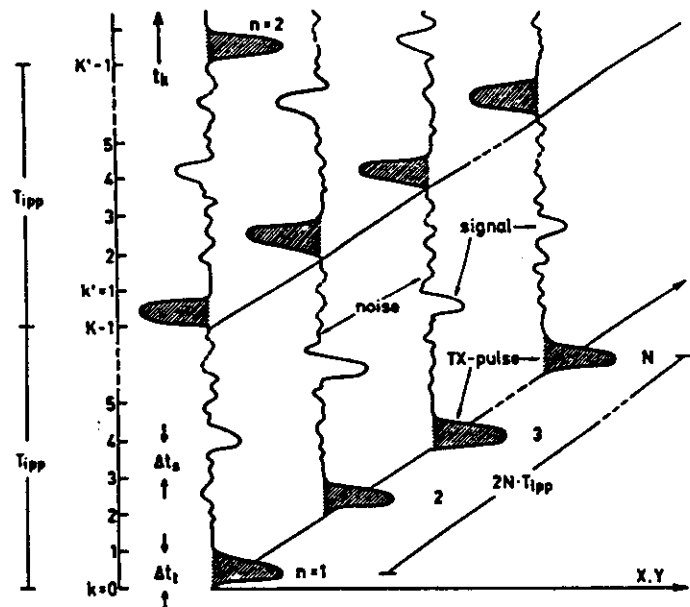
Figure 42. Range-time-amplitude diagram of single-pulse
transmitter modulation and coherent MST radar signals.

digitized data, the signal c(t) is sampled at discrete time intervals $t_k = k\delta t_s$ in the analog-digital converter (ADC). This is illustrated in Fig. 42, which shows the amplitude variations of one of the quadrature components of a coherent MST radar signal as they could be monitored with an oscilloscope connected to the output of the postdetection filters, which follow the quadrature detectors. The sequences $n = 1,2,...$ can be assumed to represent successive oscilloscope beam deflections (along the vertical axis), triggered by the leading edge of the transmitter pulse. This pulse is strongly attenuated by receiver gating, as was explained in the last chapter. It is flipped in phase by 180° from one pulse to the next (change from positive to negative amplitude), for the reason of DC-elimination (see details in the following Chapter 4.3). Corresponding to the transmitter-pulse phase $\emptyset$, the sign of the radar echo also changes from one to the next interpulse period. For convenience the phase of the radar echo is shown here to be similar to the transmitter-pulse phase. The echo phase can take any values, however, depending on the length of the phase path from the transmitter to the radar volume and depending on the relative changes of the scatterers within the radar volume.

On the vertical axis of Fig. 42 the time t_k is given, which directly can be converted to range by means of the definitions of Chapter 1.1. The sampling time interval δt_s should be equal to the radar transmitter pulse length δt_t, since this usually (in case of volume filling scatter) yields an optimum matching to the range gate width or resolution δr. However, in certain cases when narrow reflecting layers shall be resolved, shorter sampling intervals $\delta t^s < \delta t^t$ can be useful; this is called "range oversampling".

The signal and the noise had passed the receiver and postdetection filters and are therefore bandlimited. The response time of the receiver, which is approximately inversely proportional to the filter bandwidth, should also be equal to δt_s, respectively δt_t. The subscript k of t_k is the serial number of the range gate with $K = 0,1,...,$ K-1, where $k = 0$ corresponds to the beginning or a certain level of the transmitter pulse. Since the quadrature components are digitally sampled, we can write equation (6b) in the form $c_k = x_k + iy_k$. We also call c_k the complex raw data samples.

39

The number of sampling time steps between successive radar transmitter pulses is K, which is also the number of sampled range gates. The interpulse period is $T_{ipp} = K \, \delta t_s$. The cycle $k = 0, \ldots, K-1$ is repeated once with $k' = 0, \ldots, K'-1$ with a reversed phase of the transmitter pulse. Both cycles, denoted by k and k' (with $k' \triangleq k$ and $K' \triangleq K$), determine one radar cycle $2 \cdot T_{ipp}$ (note that here the radar cycle is two times the interpulse period, because of the introduced phase flip). The serial number of radar cycles is given by $n = 1,\ldots,N$. One radar burst is determined by N radar cycles, which last for $t_i = 2N \cdot T_{ipp}$. The generation of all pulse trains, needed to control these cycles of the transmitter and receiver-ADC-integrator system, is done in the radar controller, as described in Chapter 5.

4.3. Coherent Integration and Preprocessing

We will discuss here a standard preprocessing procedure of the pulse-to-pulse technique applied with MST radars. The spectrum which one would obtain for a coherent echo (MST radar) with the sampling rate T_{ipp} is very wide and mostly contains high frequency noise power. The signal power is confined to relatively low frequencies only ($f = 1/\tau_\epsilon \ll 1/2T_{ipp}$), where τ_ϵ is the signal coherence time. It is evident therefore that low pass filtering of a coherent signal, done before the spectrum analysis, will not change the signal characteristics but eliminates high frequency noise contributions. The simplest form of low pass filtering is just the complex addition of the signal + noise samples over an interval $t_i \ll \tau_\epsilon$. A readily noticed effect of such an averaging over N interpulse periods is the reduction of the number of total samples by a factor $1/N$. We have to note that this processing step of coherent integration cannot be applied for incoherent signal processing, because the signal coherence time is shorter than the interpulse period. This also means that the described DC- and clutter-elimination is not applicable for incoherent signals. The standard procedure of autocorrelation function and spectrum computation, however, is compatible in both applications.

Since the noise (r) and the signal (s) are independent of each other, their quadrature components add to $C_{kn} = C_{kn}^r + C_{kn}^s$, where C_{kn}^r ($= X_{kn}^r + iY_{kn}^r$) are the quadrature components of the noise and C_{kn}^s those of the signal. A DC-bias can result from a constant, instrumentally introduced voltage at the receiver output C_{kn}^i, or due to radar clutter C_{kn}^c (clutter = echo from a fixed target). All these contributions are additive:

$$C_{kn} = C_{kn}^r + C_{kn}^s + C_{kn}^i + C_{kn}^c.$$

We have to take into account that each radar cycle yields two samples per range gate, namely k and k'. The samples of signal and clutter are shifted by 180° from k to k', because the phase $\phi(t)$ of the transmitter was flipped by 180° (change $\phi(t)$ by 180° in equations (5) and (6)). This can be accounted for by changing the sign of $C_{k'n}$ when averaging

$$C_{k,k'} = \frac{1}{N} \sum_{n=1}^{N} (C_{kn} - C_{k'n})$$

$$= \frac{1}{N} \sum_{n=1}^{N} (C_{kn}^r - C_{k'n}^r + C_{kn}^s - C_{k'n}^s + C_{kn}^i - C_{k'n}^i + C_{kn}^c - C_{k'n}^c).$$

Since for the instrumental DC-bias $C_{kn}^i = C_{k'n}^i$, it is eliminated by averaging. This is called instrumental-DC elimination (DC = direct current, better to say: constant voltage contribution).

Because of the transmitter phase flip, we find that: $c_{kn}^s = -c_{k'n}^s$ and $c_{kn}^c = -c_{k'n}^c$. Since the noise is independent from one to the next interpulse period, a change in sign of c_{kn}^r does not change its statistical properties. We thus obtain, since $k' = k$:

$$c_k = \frac{2}{N} \sum_{n=1}^{N} (c_{kn}^r + c_{kn}^s + c_{kn}^c) \tag{7}$$

This averaging, commonly called "preintegration" or better "coherent integration", has become a standard process in MST radar operations. It yields coherently integrated data samples c_{kl} ($l=1, \ldots L$) at the time

$$t_l = 2 \cdot l \cdot N \cdot K \cdot \delta t_s$$

for the coherent integration period $t_i = 2 \cdot N \cdot K \cdot \delta t_s = 2 \cdot N \cdot T_{ipp}$.

If the summation in equation (7) extends over a time period $t_i = 2 \cdot N \cdot T_{ipp}$, which is much longer than δt_s, the high-frequency noise contribution vanishes. For a coherent integration period $t_L = 2 \cdot L \cdot N \cdot T_{ipp}$, with $(L >> N)$, which is much longer than τ_ϵ, the signal contribution approaches zero since it is fading in amplitude and phase. Only the clutter contribution

$$c_k^c = \frac{1}{L} \sum_{l=1}^{L} c_{kl}$$

remains, since it is constant in amplitude and phase. This can be used to eliminate the clutter component by means of a digital high pass filter operation: $c_{kl} = c_{kl} - c_k^c$. This operation is called clutter-DC elimination, and is done after the coherent integration.

For the coherent integration given by equation (7), the number N of added samples has to be selected carefully. It is evident that the integration period has to be much shorter than the typical time scale of signal variations due to the fluctuating scatter process as well as due to the frequency changes resulting from the bulk motions of the scattering or reflecting medium. The advantage is, however, that the processing can be made very efficient since only additions (subtractions) but no multiplication of the raw data series with a weighting function are necessary. It is also required that the real part x and the imaginary part y of the detected signal are correctly in quadrature (orthogonal). Ideally they must be phase-shifted by exactly 90° and must have equal amplitudes on the average, otherwise a distortion of the Doppler spectrum results. Accuracies of less than a few degrees phase difference and less than a few percent amplitude difference are tolerable, however, and can be obtained by proper hardware adjustment.

The coherent integration of the quadrature components, formulated by equation (7), is normally done in a digital preprocessor, called adder or integrator. Since this coherent integration is a low pass filter process it can be done also in an analogue filter, such as the clutter elimination which is a notch or high pass filter operation. Obviously the digital processing is much more versatile and flexible. Both analogue and digital preintegration reduce the number of data samples by some orders of magnitude, and compress the huge data flow from the ADCs to make it manageable for the host computer. This is the evident advantage of this preintegration process. We have to note, however, that this coherent integration process looses its advantages for higher frequency (>500-1000 MHz) radar applications. The reason is that the signal coherence time is inversely proportional to the radar operating frequency and consequently the coherent integration time has to be reduced. It is often thought that this

41

process of coherent integration also increases the signal-to-noise ratio since the voltages of the coherent signal but the power of the incoherent noise add. This leads to an improvement of the signal-to-noise (power) ratio by the factor N, since the noise bandwidth is reduced by the factor 1/N, whereas the signal bandwidth remains unchanged. If one reasonably defines the noise in such a way that its bandwidth is equal to the signal bandwidth (e.g., RÖTTGER and LARSEN, 1989), the coherent integration process only reduces the wide noise bandwidth to the acceptable limit close to the signal bandwidth. and the signal-to-noise ratio does not change by this coherent integration. The advantage of the coherent integration process is still the essential reduction of the number of raw data samples, without giving away information on the signal.
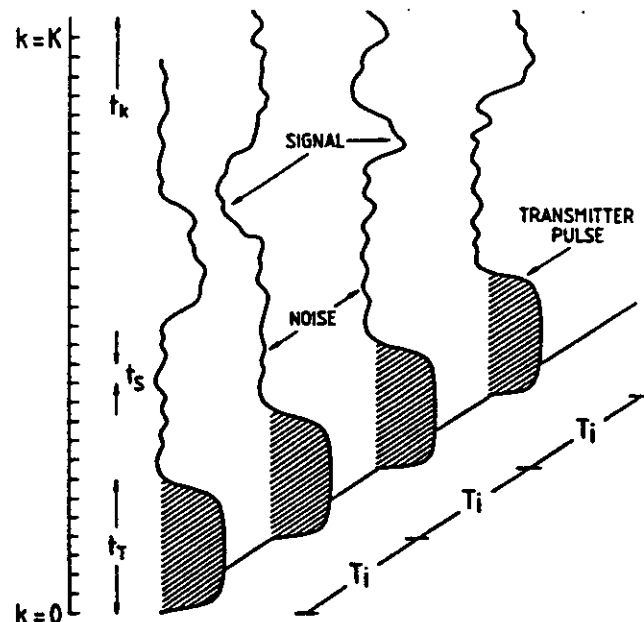
Figure 43.   Range-time-amplitude diagram of a long-pulse
IS radar modulation and incoherent signals.

    This kind of coherent integration used in the pulse-to-pulse technique cannot be applied for incoherent scatter signals, because the signal coherence time is shorter than the interpulse period, and thus the preprocessing needs to be done differently as was principally explained already in Fig. 3. For clearness the same example of an incoherent signal (Fig. 43) is drawn in the same manner as for the coherent MST radar signal (Fig. 42). We notice in Fig. 43 the "incoherence" from one to the next interpulse period, which leads to the fact that the correlation-function and spectrum analysis has to be done within one interpulse period and the ACFs and spectra then are integrated subsequently. The Fig. 43 shows that a fairly long pulse is still needed to obtain samples for the longest lag of the autocorrelation function (ACF) in order to achieve the necessary frequency resolution. This obviously deteriorates the range/altitude resolution. To overcome this problem, so-called multi-pulse modulation is applied, and is explained in Fig. 44. This modulation is most efficiently applied by modulating different frequency channels F1-F6 (within the passband of the transmitter and receiver) in order to fill the gaps between the sub-pulses of this pulse pattern. This increases the average power to the maximum allowable level, but needs a particular multi-frequency channel design of transmitter and receiver. To improve the range resolution further the subpulses can be Barker-coded. Such a multi-pulse multi-frequency Barker-code scheme is successfully used in the EISCAT incoherent scatter radar systems (e.g., TURUNEN, 1986).
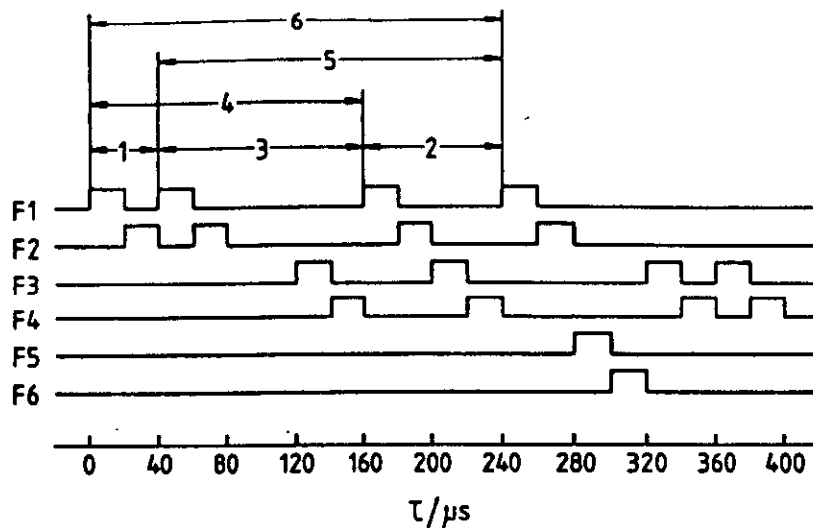
Figure 44. Multi-pulse multi-frequency-channel pulse pattern used
in incoherent scatter applications to improve the range reso-
lution and allow measurements of the lag products of the signal
autocorrelation function for the temporal lag indices j = 1 to 6
(after TURUNEN, 1986).

The application of this modulation scheme as well as the successing "alter-
nating code scheme" has become standard praxis in incoherent scatter work as has
the "complementary code scheme" in the MST radar work. We will explain the
latter coding scheme after we have briefly outlined some basic formulations of
the correlation analysis, which is applied in principle also in the decoding
procedures. Again we have to consider that most of the described preprocessing
can be done by specially designed digital hardware.

4.4. Correlation and Spectrum Analysis

After the preprocessing by appropriate coherent integration (for coherent
signals) or immediate correlation function processing (for incoherent signals)
one usually deducts specific signal parameters, such as signal power, Doppler
shift and spectrum width. Usually these are the standard parameters in MST
applications, whereas in incoherent scatter applications more information is
extracted from the spectral shape (see BARON, 1977) by special fitting routines.
Before doing this, one has to eliminate the noise which is remaining within the
bandwidth given by the signal. The elimination of the noise and further signal
processing can be done in the time domain by correlation (covariance) function
analysis or in the frequency domain by spectrum analysis. These data processing
steps, which follow the hardware preprocessing, can be suitably done by speci-
ally designed software in real time in the host computer or off line in separate
computers by reading the data from tape. In incoherent scatter applications
usually the correlation function computations are done in a special purpose
hardware correlator, whereas in MST radar applications the essential preprocess-
ing procedures, which need special hardware. are the coherent integration and
decoding. In the latter case further processing to obtain the ACFs or spectra
need to be done after the preprocessing.

Since the covariance function and the power spectrum are Fourier transforms
of each other, both contain the same relevant information. Depending on the
purpose and the feasibility of the analysis, either of both approaches, is used
in practice (RASTOGI and WOODMAN, 1974; WOODMAN and GUILLEN, 1974; Hagfors,
1977; RÖTTGER and SCHMIDT, 1979; SCHMIDT et al., 1979; CARTER et al., 1980;
CLARK and CARTER, 1980; SATO and WOODMAN, 1980; RASTOGI, 1983).

43

/\ (\ 2

The complex autovariance function of the quadrature components $c(t)$ is

$$\varrho(\tau) = \int c(t) \cdot c^*(t + \tau)dt,$$

where τ is the temporal displacement, and the $*$ denotes the complex conjugate. In digital form

$$R_k(\tau_j) = \frac{1}{L-j} \sum_{l=1}^{L-j} c_{kl} \cdot c^*_{kl+j} = c_{kl} \cdot c^*_{kl+j}, \quad \text{with } j=0,\ldots,J-1 \text{ and } J \le L,$$

where j is the lag index defining the lag τ_j. For a fixed range k, we find $c_l = x_l + iy_l$, and the covariance function becomes

$$R(\tau_j) = (x_l x_{l+j} + y_l y_{l+j}) + i(x_{l+j} y_l - x_l y_{l+j})$$

$$= R_r(\tau_j) + i R_i(\tau_j),$$

or $\quad R(\tau_j) = |R(\tau_j)| \exp(i\phi(\tau_j))$,

with $\quad |R| = (R_r^2 + R_i^2)^{\frac{1}{2}} \quad$ and $\quad \phi = \arctan(R_i/R_r)$.

In radar applications the term correlation function is often used for $R(\tau_j)$ instead of covariance function. The correct definition of the correlation function $\varsigma(\tau_j)$ is given by the normalized covariance function:

$$\varsigma(\tau_j) = R(\tau_j)/ R(0).$$

As well as the autocorrelation function of the series $c(t)$ we also compute cross-correlation functions for two different series, $c_1(t)$ and $c_2(t)$, in the spaced antenna applications and use their modulus in the drift analysis and their phase and amplitude in the interferometer analysis. In a principally similar way also cross spectra are computed from two time series.

The power spectrum is the Fourier transform of $\varsigma(T)$, weighted by $W(T)$:

$$P(\Omega) = \int W(\tau) \cdot \varsigma(\tau) \exp(-i\Omega\tau)d\tau$$

or in digital form:

$$P_k(\Omega_m) = \frac{1}{J} \sum_{j=0}^{J-1} W_j \cdot R_{kj} \exp(-i\Omega_m j t_i),$$

where W_j is an arbitrary weighting function (e.g., $W_j = J^{-1}$ for all j, etc.) and $\Omega_m = m \pi/J \cdot t_i$; $m = 0,\ldots, J$. The length of the integration time interval is $t_i = 2 \cdot N \cdot T_{ipp}$ in the case of a coherent signal. For an incoherent signal, t_i corresponds to the time interval over which lag samples of the ACF are collected.

4.5. Phase Coding

Another preprocessing step which is generally similar to preintegration is the decoding procedure. The principal reason for applying coding/decoding (pulse compression) is to achieve a maximum average power at optimum resolution and maximum unambiguous range. A fairly low duty cycle of 0.1% and hence a low sensitivity would for instance result from using a single pulse of 1 µs duration

44

(δr = 150 m) and an interpulse period of 1000 µs (r_{max} = 150 km). Increasing the pulse length to 32 µs would increase the duty cycle to 3.2%, but deteriorate the range resolution to 4.8 km. The range resolution of 150 m can still be achieved by phase-coding the transmitter pulse in time (lag) increments of, say 1 µs. The decoding has to be done by cross correlating the received complex time series c_k (separately for real and imaginary part) with the transmitted code s_m:

$$C_{k*}' = \sum_{m=0}^{M-1} C_{k*+m} \cdot S_m \qquad (8)$$

where M is the length of the code and k* corresponds to the range gate k at lag zero where the correlation function C_{k*}' has a maximum. Thus, the decoding is nothing else but an integration of the signal amplitudes over several range gate samples, which are multiplied by the weighting factor s_m.

The simplest and most versatile phase coding scheme is the binary code, where the phase is flipped between the two states -1($=0°$) and +1($=180°$). Since here the weights s_m are +1 or -1, the multiplication needed in the decoding process reduces to an addition/subtraction operation. For this reason the decoding can be done in a preprocessor similar to a hardware preintegrator, or the integrator/decoder can even be one unit, as we will outline in Chapter 5. Note that the decoding has to be done for the amplitudes, since these contain the phase information An advantage in MST radar applications is also that the decoding/integration processes are interchangeable, which reduces the number of operations by about two orders of magnitude (e.g., WOODMAN et al., 1980).

The best codes for radar applications obviously are those where the range sidelobes of the correlation function (8) at k* $\neq$ k are a minimum. Reasonable sidelobe suppression is achieved with Barker codes, where the phases are flipped in a sequence (e.g., +++++--++-+-+ for the 13-baud Barker code). The correlation function is 13,0,1,0,1,0,1,0,1,0,1,0,1. The best range sidelobe suppression, achievable with a Barker code, is M^{-1}. The reason is that these sidelobes contain power from other range gates k* $\neq$ k, which cause ambiguities. The sidelobes of the code extend out to ranges $M \cdot \delta t_m$ on both sides of the center peak. Since the codes cannot be infinitely long, because the minimum range is extended with the length of the code (which obviously increases the minimum range from where echoes can be received), the sidelobe suppression of Barker codes is limited. A good sidelobe suppression is for instance needed if strong echoes occur only in a limited number of range gates.

A better sidelobe suppression can be gained by application of quasi-random codes, which however need decoding before the preintegration as well as to transmit a long series of different code sequences. Also alternating codes appear useful in incoherent scatter applications (e.g., LEHTINEN and HÄGGSTRÖM, 1987). The most suitable codes for MST radar work are the complementary codes (e.g., SCHMIDT et al., 1979), which theoretically have no sidelobes. A complementary code consists of a pair of two code sequences s_1 and s_2. These have the property that their correlation function sidelobes are exactly equal, but opposite in sign. Normally both code sequences are transmitted at one and the next interpulse period, and the range samples of these two periods are preintegrated and decoded separately. The coherent addition of the decoded sequences then yields the total elimination of the sidelobes (k* $\neq$ k) if the signal is coherent from one to the next interpulse period. The zero lag value k* = k contains the total signal amplitude. As an example the 8-baud complementary code pair A,B:

$$s_1 = A = +++-++-+ \quad \text{and} \quad s_2 = B = +++---+-$$

45

yield the correlation functions:

$$c_1 = 8,-1,0,3,0,1,0,1 \quad \text{and} \quad c_2 = 8,1,0,-3,0,-1,0,-1$$

and the addition yields:

$$c_1 + c_2 = 16,0,0,0,0,0,0,0.$$

The peak value of this decoded function at $k* = k$ is 2M. There is still the shortcoming of a long code, that it extends the shortest observable range. This can be overcome by transmitting a sequence of a complementary code and a short single pulse in one radar cycle. In Fig. 45 the range-time-amplitude diagram for the simplest 2-baud complementary code with additional phase-flip for instrumental DC-elimination is shown. All these decoding preprocessing steps are most suitably done in a special purpose hardware integrator-decoder. For coding purposes, the hardware radar controller needs to generate the necessary amplitude and phase control pulse trains for the transmitter.
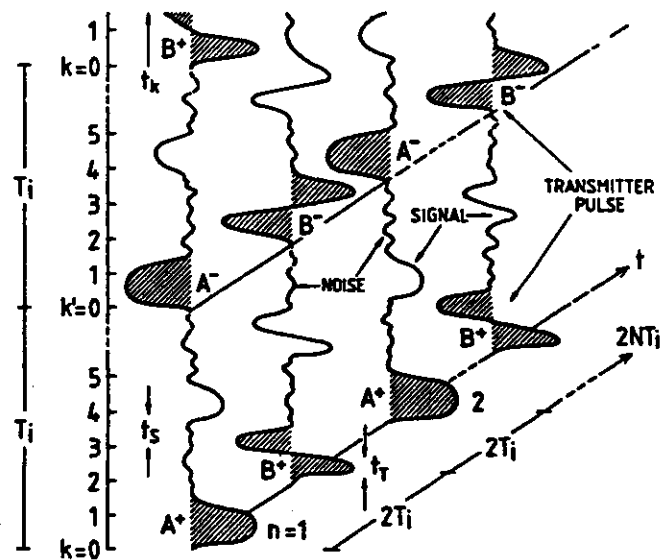
Figure 45. Range-time-amplitude diagram of a two-baud
complementary code modulation with DC-phase flip
used in MST radar applications.

5. RADAR CONTROL AND DATA ACQUISITION

We will here briefly describe the basic system units which are needed to process the digitized data in terms of coherent integration, correlation function computation and decoding as well as the principle lay-out of a radar controller.

We first describe in Fig. 46 the basic lay-out of an integrator or adder. The data from the ADC are range-gate by range-gate stored into memory. According to equation (7), the data from one interpulse periods are added onto the corresponding data from the successive interpulse period in the arithmetic-logic-unit (ALU). This is recurrently done as long as the integration period is chosen, i.e. the number of interpulse periods preselected for the coherent integration (controlled through the host computer). After the completion of the integration cycle, the coherently integrated data are dumped via the direct-memory-access (DMA) to the host computer.

46
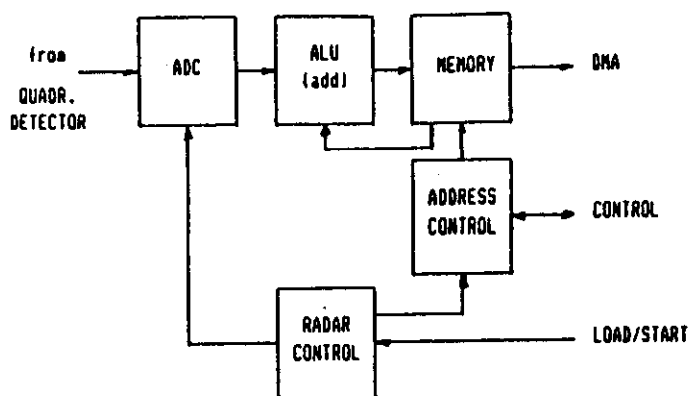
Figure 46. Block diagram of an
integrator/adder preprocessor
for coherent signal acquisition.

The coherent integration can also be done in the same unit as is used for decoding and the correlation function computation is done. Both the correlation and the decoding operation consist of a multiplication and an addition cycle, where the former needs complex processing and the latter needs to be done for the quadrature components separately. In Table 3 we have outlined the principles of the computation of correlation function, decoding and coherent integration in a graphic form, which should allow better understanding of the hardware configuration sketched in the diagram of Fig. 47.

TABLE 3

COMPUTATION OF CORRELATION FUNCTION, DECODING, COHERENT INTEGRATION

Data Series C_l

(range (k) or time (l))

(A) Correlation Function:

$$R_j = \sum_l C_l \cdot C_{l+j} \quad \text{(lag j)}$$

(B) Decoding:

$$C_l = \sum_m C_{l+m} S_m \quad (l=k)$$

5-baud Barker code

(C) Integration:

$$C_l = \sum_n C_{l\,n} \quad (l=k)$$

The square blocks in Table 3 indicate data samples at range or time gates. The samples in the first row are supposed to be the original data. The hatched part of the diagram indicates data samples which are accessible at a register through which the original data are shifted. The correlation function is computed according to the formula A in Table 3. To compute the zero lag, the range (time) samples of the first (unhatched) row with indices j=J and its replica in the last row j=0 are multiplied for each range or time label l, and then all products are summed up over l. To obtain the first lag, the last but one series, which is delayed by one sample with respect to the last row, is multiplied and added in the same way. According to this algorithm all the following lags are computed. In praxis, the last lag is computed first, since the data sample at j=J-1 is available first after the original data series had been shifted by one in a shift register (see explanation of Fig. 47 on the next page).

In a very similar way the decoding is performed (formula B in Table 3), since it comprises a cross-correlation function computation which can be performed by the same hardware setup. The only difference to the correlation function computation is, that instead of the data time series the code is used in the delayed data series. In the example of Table 3 a 5-baud Barker code is shown. It is to be noted, that the first completely decoded data point is available only after 5 steps of j at J-5, when the 5 bauds of the code are completely existent in the shift register (for longer codes of course the corresponding longer delays have to be considered). The combination (i.e., multiplication and addition according to the formula B) of series j=J-5 with j=J yields the decoded value at l=0. As another example for instance j=0 with j=J yields the decoded sample at l=3. Note that a further shift than given by l=0 does not allow the

CORRELATOR - DECODER - INTEGRATOR
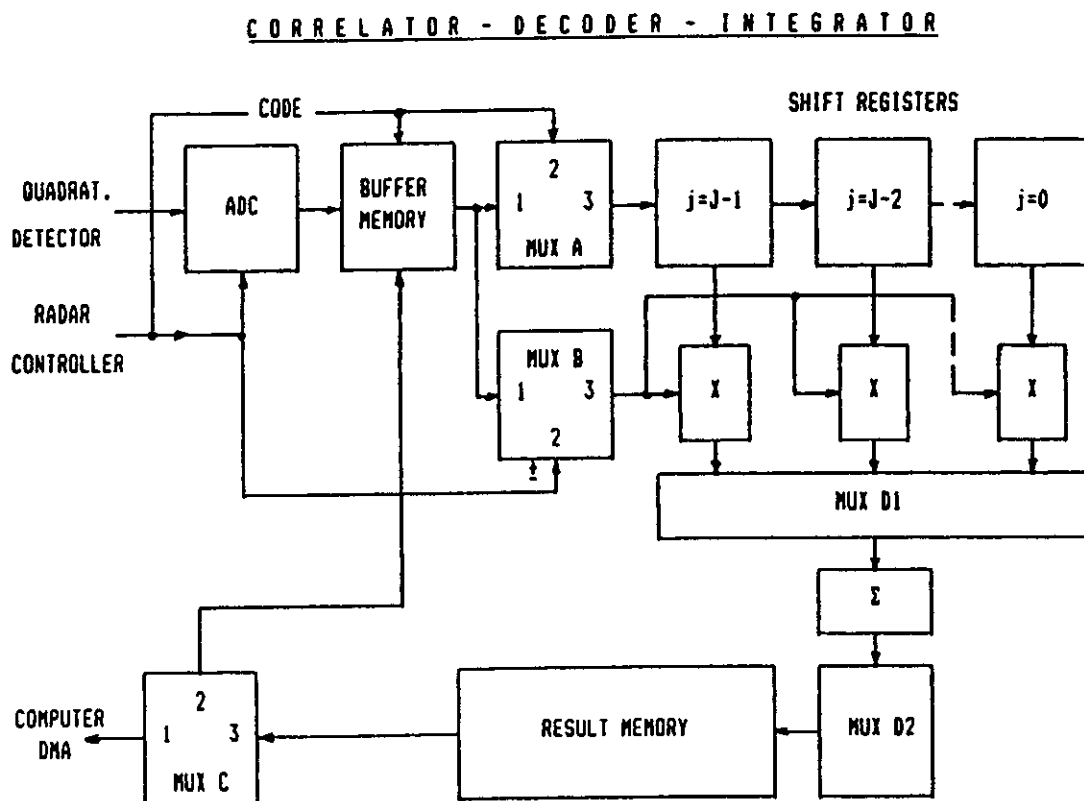
Figure 47. Block diagram of a hybrid version of a correlator-decoder-integrator.

48

complete decoding unless the data time series j=J is further extended beyond 8 samples in this example. In praxis this means that always a data set has to be available which is longer than a single data series by number L_c, where L_c is the number of bauds in a code minus one. Decoding of complementary codes is done in principally the same way, but as a final step the two cross-correlation functions resulting from the decoding of code s_1 and its complement s_2 have to be added. The coherent integration is simply done, according to formula C in Table 3, in the same hardware processor by just adding the samples for each 1 (or k) separately over a preselected number of interpulse periods.

We have to note that all these procedures have to be done separately for the real part as well as for the imaginary part of the quadrature components. For convenience we explain only the integration, decoding and correlation function computation for a single component.

In Fig. 47 we show a block diagram of such a described hybrid "correlator-decoder-integrator". We admit that other realizations may be more practicable, but this layout should show that such a hybrid processor is feasible in principle. The different modes can be understood by following the paths which are selected by different multiplexer positions. In the integrator mode the multiplexer A (MUX A) is connecting ports 1 and 3, multiplexer B ports 2 and 3, multiplexer C ports 1 and 3 and multiplexers D1 and D2 provide that each multiplier is connected to the correct range gate. The data are transferred from the buffer memory to the multipliers, where the sign is changed according to the corresponding phase flip of the transmitter pulse. The multiplier of course could be eliminated if provision would be made to allow also subtractions in the adder. For each range gate the data are added in the accumulator, from where they are multiplexed into the result memory after the specified number of coherent integrations. Depending on the size of the result memory several sets of coherently integrated data are stored and afterwards dumped to the main computer.

For correlation function computations the multiplexers have to be in the positions A: 1-3, B: 1-3 and C: 1-3. The main part of the correlator is the shift register by which the data series is shifted according to the lag indices of the decoding or correlation function. Each data sample of the shifted series is then multiplied with the data sample of the non-shifted data series. For decoding the shifted data series is the code, and for auto-correlation computation the shifted series is the same unshifted data series. After this multiplication the data are accumulated, i.e. summed up, and after completion of the correlation analysis dumped into the result memory from where they are transferred into the host computer. The correct selection of the lag products and their redistribution to the result memory is again provided by multiplexers D1 and D2.

For decoding of the original data series, the multiplexer A is in position 2-3, multiplexer B in position 1-3, and multiplexer C in position 1-3. The original data are existent at the multipliers and according to the position of the code in the shift register, the decoding is performed by multiplication. If the multiplexer A is in position 2-3, B in 1-3 and C in 2-3 a coherently integrated sample set could be also decoded in the same processor and afterwards dumped to the computer. It is noted that also a correlation function computation of decoded as well as coherently integrated data could be possible if the pre-processed data are fed back by multiplexer C in position 2-3 to the result memory. Although the described layout of a multi-purpose integrator-decoder correlator explains the three main processing procedures of MST and IS radars and the solution looks feasible, it may in praxis be more realistic to use three separate units for integration, decoding and correlation function / spectrum analysis.

49

TABLE 4

R A D A R   C O N T R O L

cycle 1   cycle 2

```
PRP  ____|‾|_____|‾|_____

TRX  ___|‾‾‾‾|_____|‾‾‾‾|_____

TXP  ____|‾‾|_____ __|‾‾|_____

FLP  ___|‾|_|‾|_|‾|_____ __|‾|_|‾|_____

FRI  ___|‾‾‾‾|_____ _____

FR2  _____|‾‾‾‾‾|_____

RGT  ___|‾‾‾‾‾|_____|‾‾‾‾‾|_____

LOP  ___|‾‾‾‾‾|_____|‾‾‾‾‾|_____

RIA  _____|‾|_____|‾|_____

ADC  _____|||||||||||||||||||||_____|||||||||||||||||||||_____

SGN  ___|‾‾‾‾‾‾‾‾‾‾‾‾‾‾‾‾‾‾‾‾‾‾‾‾‾‾‾‾‾|_____

CAL  _____|‾|_____|‾‾

ANT  __|‾‾‾‾‾‾‾‾‾‾‾‾‾‾‾‾‾‾‾‾‾‾‾‾‾‾‾‾‾‾‾‾‾‾‾‾‾‾‾‾‾‾‾‾‾‾‾‾‾‾‾‾‾‾‾‾‾‾‾‾‾‾‾‾‾‾

AUX  _____|‾|_____|‾|_____
```
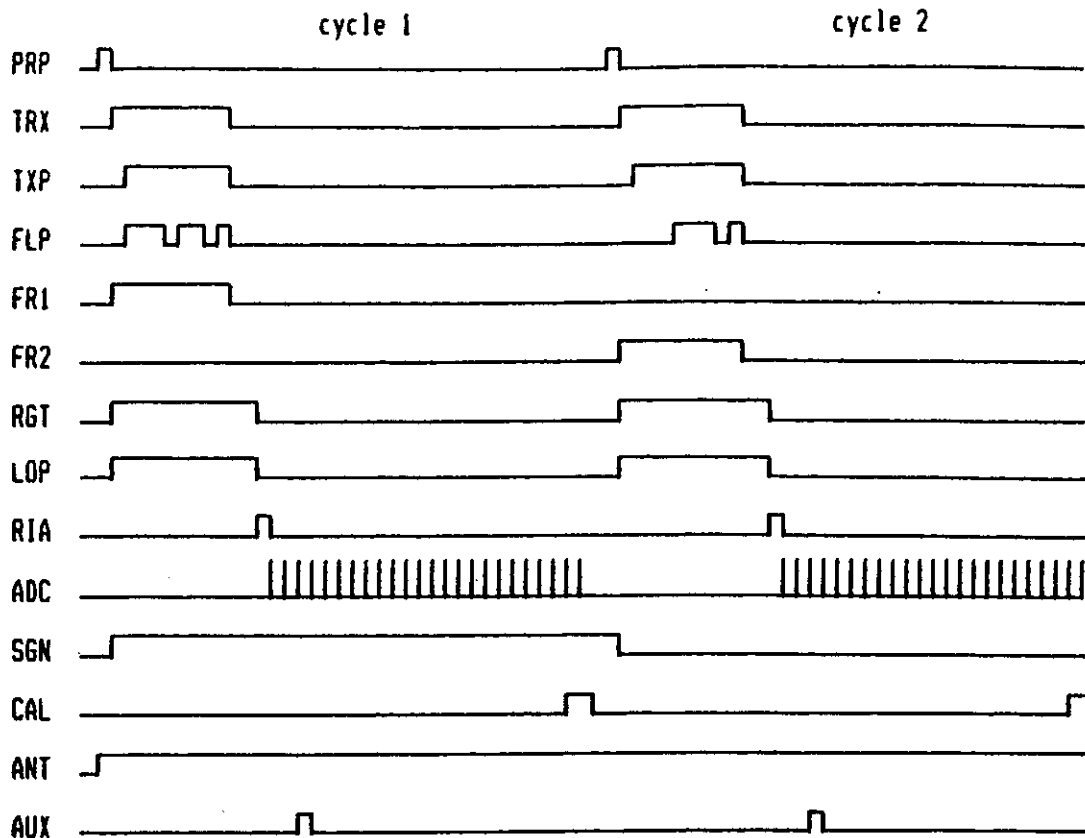
PRP = prepulse (trigger)
TRX = transmitter-receiver duplexer
TXP = transmitter on
FLP = phase flip (coding)
FRI = frequency 1
FR2 = frequency 2
ANT = antenna control

RGT = receiver gating on
LOP = local oscillator protect on
RIA = reset integrator address
ADC = analog-digital conversion
SGN = sign for integration
CAL = calibration (noise injection)
AUX = auxiliary

All the timing control of the outlined procedure results from the radar controller or system synchronizer, which of course also generates the control pulses for the transmitter, the receiver and the ADC. A typical example of pulse trains of control pulses, which are generated by the digital radar controller, is demonstrated in the example of Table 4. Following a pre-pulse (PRP), which is used to to trigger external control or monitor devices, the transmit-receive duplexer (TRX) is switched on, followed by a receiver gate pulse (RGT) and the pulse to turn off the local oscillator (LOP). Then the switch on of the transmitter radio frequency is controlled (RFC), which is phase flipped (FLP) between 0° to 180° for coding. The analogue-digital-converter starts sampling (ADC) after RFC off and the TRX, RGT and LOP have opened the receiver and after the reset of the integrator address (RIA) has taken place. At certain range gates a calibration signal (CAL) is injected. The whole sequence is repeated after one interpulse period when only the phase flip is inverted (for DC-elimination). For application of the complementary coding scheme a second double pulse code (con--sisting of the complementary pattern) is transmitted, and this radar cycle is repeated N times to yield one radar burst. Additionally, different frequencies

(FR.) and pulses for antenna control (ANT) and other purposes can be generated, which can change from one to the next interpulse period or radar burst. In more advanced systems multichannel receivers and ADCs are used (e.g. spaced antenna parallel processing (e.g. RÖTTGER, 1981)).

The MST radar operation, which is synchronized and which is usually started and stopped by external clock control (in the host computer), takes place in several nested sequences : (1) the radar cycle, i.e. the transmission of one code unit of radar pulses with preselected duration and the sampling of the real and imaginary signal at preselected range gates (e.g. 128). (2) the integration cycle (burst), i.e. the repetition and coherent integration of an externally selected number of radar cycles. (3) record cycle, i.e. the repetition of a preselected number of integration cycles (e.g. 64) to form one total record which is stored in memory. Together with the time and other system parameter information (such as the radar controller program etc.) the data record is then dumped via the computer to file or magnetic tape.

All the control sequences for the radar system are generated by the radar controller, of which a basic block diagram is shown in Fig. 48. The computer loads the instructions, which pulses should be generated and for how long these should be switched on (duration) as well as how many interpulse periods should be coherently integrated, into the radar controller memory. The computer can via the real-time clock start and stop the radar controller. Further interlocks, either via the computer or other fast hardware devices, inhibit under certain failure conditions radar controller pulses in order to protect the radar system from malfunctions or damage if transmitter pulsing would be during the receiving phase.

RADAR CONTROLLER/SYSTEM SYNCHRONIZER
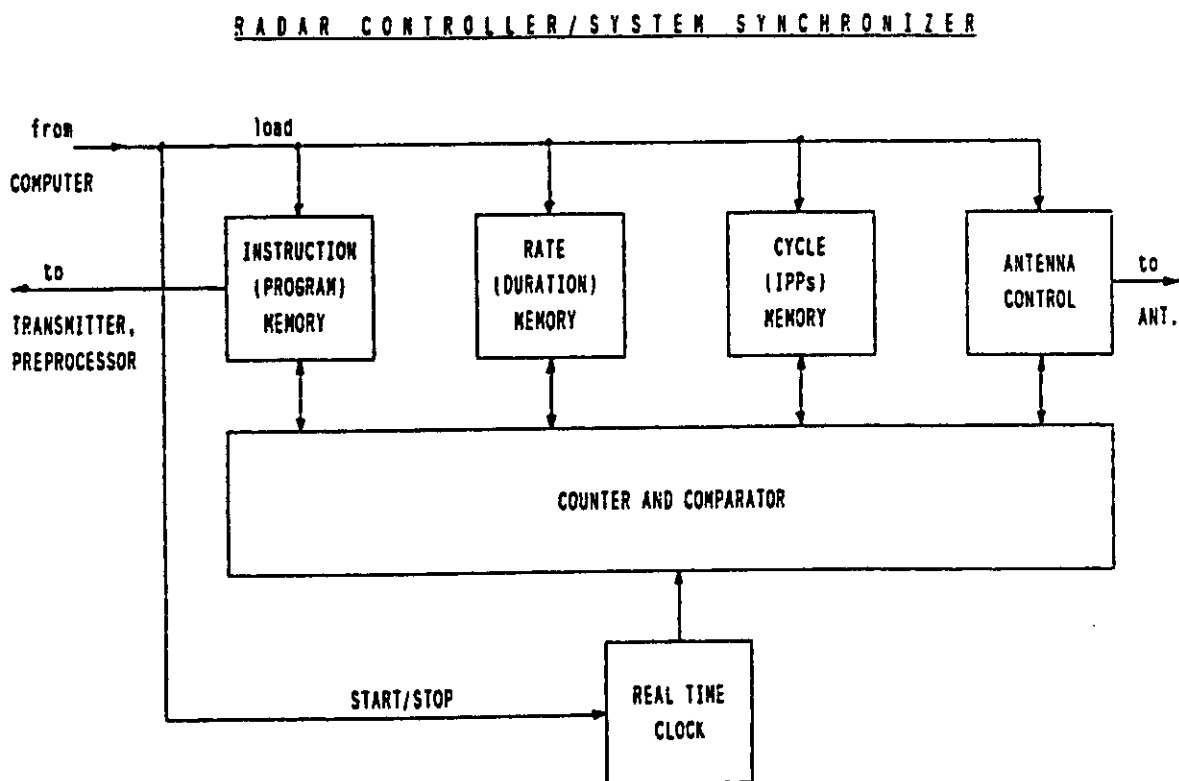
Figure 48. Block diagram of a radar controller or system synchronizer.

51

r\ ⊽(

It is generally found that 8-bit ADCs are sufficiently matched to the linearity range of the receivers (> 60 dB). If strong clutter signals are present the capacity must eventually be extended to >12 bit or a range-dependent attenuation has to be used. Applying an 8-bit ADC and a 16-bit integrator allows tc add samples from at least N = 256 radar cycles in one channel. If more samples would have to be added, the adder and result memory word length would have to be extended. The dump could still be at 16-bit word length if a scaler would be used to scale down the result data according to the number of integrations. The preintegration time for 256 integrations would be $t_i = 2N \cdot T_{ipp} = 128$ ms for $T_{IPP} = 250$ µs, corresponding to a maximum unambiguous range of 37.5 km and a maximum resolvable radial velocity of 12 ms^{-1} ($f_{Dmax} = 4$ Hz). Applying a 4-bit complementary code and a 300-m range resolution would result in a transmitter duty cycle of about 3%.

MUFFIN FUNCTIONAL BLOCK DIAGRAM
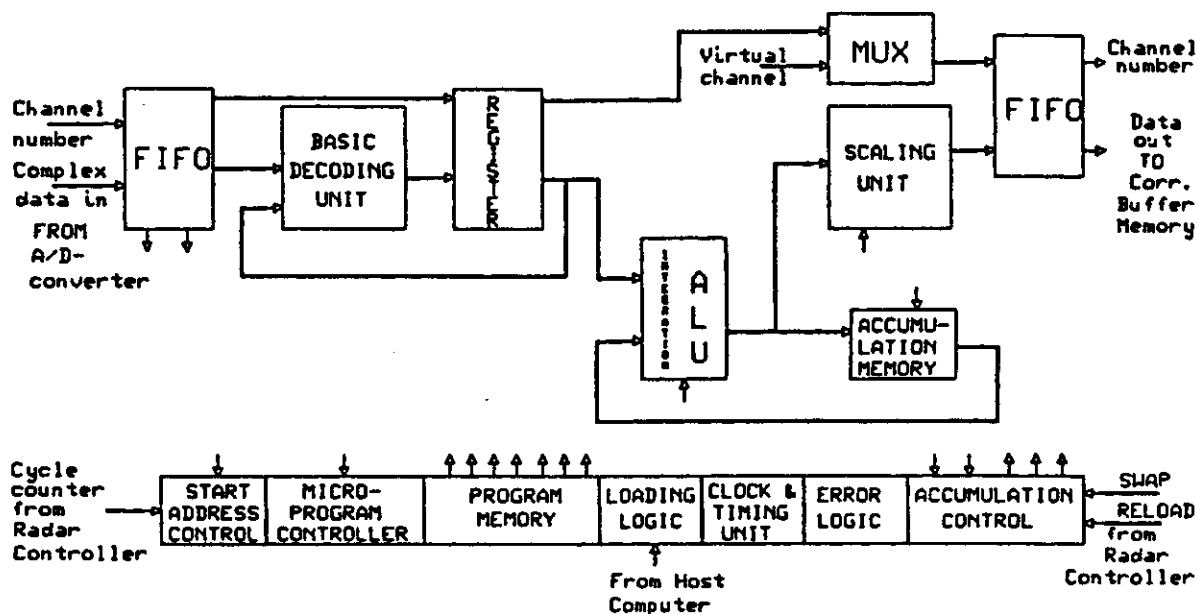
Figure 49. Block diagram of a multi-channel finite-impulse response filter and integrator (MUFFIN) under development as preprocessor for particular coding schemes applied at the EISCAT radars.

There exist many more sophisticated data preprocessing units at several radars and it cannot be in the scope of this lecture to describe those in detail, as it was not possible to line-out all the different variations of the transmitter-receiver-antenna systems. We finally would only like to add the block diagram (in Fig. 49) of a multi-channel finite-impulse-response filter and integrator which is presently under design at the EISCAT radar facilities and shall be used for on-line preprocessing (integration, decoding, correlation computation and radar control) of incoherent scatter and coherent scatter data (POSTILA, 1988, personal communication).

C52

6.   AN OVERVIEW ON SOME RADAR SYSTEMS AND THEIR TECHNICAL PARAMETERS

Descriptions of the early VHF radar systems were given by WOODMAN and GUILLEN (1974), GREEN et al. (1975), CZECHOWSKY et al. (1976), RÖTTGER et al. (1978), BALSLEY et al. (1980), and design considerations were summarized by BALSLEY (1978a,b), GAGE and BALSLEY (1978) and BALSLEY and GAGE (1982). More recent developments and technical details were described for instance by CZECHOWSKY et al. (1984), KATO et al. (1984), RÖTTGER (1984), STRAUCH et al. (1984), FUKAO et al. (1985a,b), FRISCH et al. (1986), ECKLUND et al. (1988) and RÖTTGER and LARSEN (1989).

We present in Table 5 the technical parameters of the MU radar (Middle and Upper atmosphere radar) of the Radio Atmospheric Science Center of the Kyoto University (from FUKAO et al., 1985a,b), in Table 6 the basic parameters of a 405 MHz wind profiler radar (from FRISCH et al., 1986), in Table 7 the primary system specifications for an operational wind profiler (from UNISYS, 1987) are repeated, which is supposed to be used in meteorological routine applications. In Table 8 the basic parameters of the EISCAT incoherent scatter radar systems operating in the 933 MHz and 224 MHz bands are summarised. We then display in Table 9 a most complete list of all the MST, ST and incoherent scatter radars as well as some wind profiler systems. Finally we show in Fig. 50 photos of a few well known research radar facilities.

TABLE 5

Basic Parameters of the MU (Middle and Upper Atmosphere) Radar
Operated by the Radio Atmosphere Science Center of the Kyoto University
(from FUKAO et al., 1985a,b)

LOCATION	Shigaraki, Shiga, Japan
	(34.85°N, 136.10°E)
RADAR SYSTEM	monostatic pulse radar;
	active phased array system
OPERATIONAL FREQUENCY	46.5 MHz
ANTENNA	circular array of 475 crossed Yagis
	aperture 8330 m² (103 m diameter)
Beam width	3.6° (one way; half power for full array)
Steerability	steering is completed in each IPP
Beam directions	1657; 0°-30° off-zenith angle
Polarizations	linear and circular
TRANSMITTER	475 solid state amplifiers
	(TR modules: each with output power
	of 2.4 kW peak and 120 W average)
Peak power	1 MW (maximum)
Average power	50 kW (duty cycle of 5%) (maximum)
Bandwidth	1.65 MHz (maximum)
	(pulse width: 1-512 μs variable)
IPP	400 μs to 65 ms (variable)
RECEIVER	
Bandwidth	1.65 MHz (maximum)
Dynamic range	70 dB
IF	5 MHz
A/D converter	12 bits x 8 channels
PULSE COMPRESSION	binary phase coding up to 32 elements,
	Barker and complementary codes

CS3

TABLE 7

System specifications for an operational Wind Profiler Radar
(after UNISYS, 1987)

Maximum height	16.25 km
Minimum height	0.5 km
Vertical range cell spacing	250 m
Maximum horizontal wind	200 mph
Maximum vertical wind	50 mph
Frequency band	400-435 MHz (404.37 std)
Peak power	16 kW
Average power	2200 W
Pulse width (compressed)	2/6.67 μs
Pulse repetition period	100/153 μs (nom)
Antenna type	coaxial collinear array
Antenna gain	>32 dB
Sequential beams	vertical, east and north
Sidelobe suppression	-20 to -40 dB
Receiver noise figure	0.5 dB
Signal processor	Digital I and Q
Data processor	MicroVax II
Operating software	higher order language
Fault monitoring	microprocessor control
Two-way data modem	RS-232C landline
Satellite telecom	GOES transmission (401 MHz)
Prime electrical power	115/230 VAC, 50-60 Hz
MTBF (mean time between failure)	>4400 hours
MTTR (mean time to repair)	60 minutes
Operational conditions	
Temperature	-40°C to +50°C
Humidity	0-100%
Wind speed	140 mph (185 mph gusts)
Rain	3 inches/hour
Snow	4 feet
Ice	3 inches radial

TABLE 6

Basic Parameters of a 405-MHz Wind Profiler Radar
(from FRISCH et al., 1986)

RADAR

Frequency	405.25 MHz
Authorized bandwidth	1.00 MHz
Peak power	30 kW
Average power	0.4 kW maximum
Pulse width	1, 3, 9 μs
Pulse repetition period	100, 150, 300 μs
Antenna aperture	9 m x 9 m
Antenna pointing	15° off-zenith to north and east

ANTENNA TYPE — phased array of Yagi-Uda elements

Two-way beamwidth	4.3°

DATA PROCESSING

	1 μs pulse	3 μs pulse	9 μs pulse
Time domain averaging	120 pulses	75 pulses	35 pulses
Spectral average	8	16	24
Maximum radial velocity	±15.41 ms^{-1}	±16.44 ms^{-1}	±17.62 ms^{-1}
Spectral resolution (64 points)	0.48 ms^{-1}	0.51 ms^{-1}	0.55 ms^{-1}

HEIGHT SAMPLING

	1 μs pulse	3 μs pulse	9 μs pulse
First height	0.4 km AGL	2.4 km AGL	4.0 km AGL
Height spacing	100 m	290 m	870 m
Number of heights	24	24	14

54

C54

TABLE 8   The EISCAT Radar Facilities (Jan. 1989)

Parameters of the EISCAT UHF system:

Transmitter (Tromsø only):

Peak transmitted power	1.6 MW
Maximum duty cycle	12.5%
Operating frequencies	(929.5±0.5n) MHz, (n(15) n=0-10)
Pulse widths	1-19999 μs
Risetime	0.1 μs
Maximum waveform repetition rate	1000 Hz
Modulations	on-off, phase-flip (0°/180°), frequency-step

Antennas at all sites (Tromsø, Kiruna, Sodankylä):
Location and height of the UHF antennas above sea level (MSL),(Datum ED-1950):

Tromsø site (Ramfjordmoen): (transmitter-receiver)	69°35'11.239" N 19°13'38.746" E h = 86.3 m
Kiruna site: (receiver)	67°51'38.373" N 20°26'06.800" E h = 417.9 m
Sodankylä site: (receiver)	67°21'49.286" N 26°37'37.697" E h = 197.3 m
Frequency band	933 ± 10 MHz
Rotation axes	Azimuth/Elevation
Azimuth angle range	540°
Elevation angle range	95° (0°-95°)
Lowest elevation permitted (transm.)	10° (5° within certain limited azimuth sectors)
Maximum rate of angular motion	1.3°/sec (each axis)
Diameter of main reflector	32.00 m
Feed system	Cassegrain
Diameter of subreflector	4.58 m
Focal length	11.01 m
Polarization	arbitrarily selectable, circular usually transmitted
Gain (calculated)	48.1 dB
Aperture efficiency (calculated)	0.651
Noise contribution (measured)	20-21 K
Half-power beamwidth	0.6°
Speed of mechanical movement, azimuth and elevation	80°/min
Fresnel zone limit	8.37 km
Rayleigh distance	1.59 km

Receivers:

Type of frontend	Cooled GaAsFET amplifier (Kiruna and Sodankylä) Uncooled GaAsFET (Tromsø)
System temperature	~35 K (Kir., Sod.) ~95 K (Tromsø)
Number of IF channels	8 at each site
IF filter bandwidths	1.2 and 8.0 MHz
Detector	phase-coherent demodulator yielding quadrature components
Post-detection filters	12.5,25,50,0,100.0,250.0 kHz 1MHz, 2MHz (all selectable)

Parameters of the EISCAT VHF system (Tromsø only):

Transmitter:

Peak transmitted power	1.5 MW
Maximum duty cycle	4.5%
Operating frequencies	(222.4±0.2n) MHz, (n=5,6,7,8)
Pulse widths	1-1000 μs
Risetime	0.1 μs
Maximum waveform repetition rate	1000 Hz
Modulations	on-off, phase-flip, frequency_step

Antenna:

Location	69°35'11.9408" N 19°13'13.2300" E h = 85.3 m (reference point centre of elevation axis)
Frequency band	224 ±1.25 MHz
Parabolic cylinder	2 panels for transmission, independently movable
Height of each panel	40 m
Width of each panel	30 m
Total width	120 m
Feed system	128 crossed dipoles (32 per panel)
Plane of mechanical motion	8.5° west of north
Speed of motion	5.0° min^{-1}
Mechanical motion limits	30°-45° north to 70°-90° south of zenith
Effective aperture (on-axis)	3250 m²
Beamwidth (on-axis)-vertical	1.7°
-transverse	0.6°
Gain	43 dBi
Off-axis phase steerability	21.3° in steps of 1.25°
Polarization	circular

Plane of mechanical movement	0.5°, measured 0.55° ±0.05° west of north
Operational modes	I: Combined mode, all elements aligned, physical area 5520 m². II: Split beam mode. element 1+2 and 3+4 pairwise aligned, structure behaves as two independent antennae, each of physical area 2400 m².
Effective area, broadside, mode 1 circular polarization:	3250 m²
horizontal polarization:	3330 ±240 m²
vertical polarization:	2930 ±210 m²
Polarization	Mode I: (i) Right- and left hand circular, possibility for polarization flipping from pulse to pulse (ii) Linear at ±45° with respect to vertical Mode II: Lefthand circular (transmission)
Beamwidths, broadside (calculated)	Mode I: 0.6° east/west 1.7° north/south Mode II: 1.2° east/west 1.7° north/south
Beam steering by phasing	21.3° east and west of transit plane, steps approximately 1.2°
Range of mechanical movement	30° south to 60° north of zenith
Speed of mechanical movement	5°/min

Receiver:

Frontend amplifiers	solid state (gain >50 dB)
System temperature	~250K
Number of frequency channels	8
IF filter bandwidths	1.2, 8.0, 18.0 MHz
Detector	phase-coherent demodulator
Post-detection filters	selectable from 12.5 to 100 kHz in octave steps.

55

TABLE 9   INCOHERENT SCATTER, MST AND WIND PROFILER RADARS (DEC. 1988)

Radar	Location	Frequency (MHz)	Antenna Gain (dB)	Average Power-Aperture Product ($W \cdot m^2$)	Altitude Coverage	Beam Directions
Arecibo *)	Puerto Rico	2380	75*)	$1 \cdot 10^{10}(x)$	ST	bistatic
Arecibo *)	.	430	61	$6 \cdot 10^8(x)$	I(M)ST	multi
Arecibo	.	46.8	42	$5 \cdot 10^7$	MST	multi
Buckland Park	Australia	54.1	35*)	$3 \cdot 10^6$	ST	5, SA
Chung-Li	Taiwan/R.O.C.	52	29	$1 \cdot 10^7$	ST	5, SA
EISCAT *)	N.Scandinavia	933	48	$9 \cdot 10^7$	I(M)ST	multi
EISCAT *)	,Norway	224	43	$2 \cdot 10^8(x)$	I(M)MST	multi N-S
Equatorial Radar *)	Indonesia	47	44	$4 \cdot 10^9(x)$	IMST	1441
Fairbanks *)	AL/U.S.A.	≈220	40	$1 \cdot 10^8$	ST	5
Flatland	IL/U.S.A.	40.5	27	$4 \cdot 10^8$	ST	6
India *)	India	53	38	$7 \cdot 10^8$	MST	several
Jicamarca	Peru	49.9	44	$1 \cdot 10^{10}(x)$	IMST	several, SA
Millstone Hill *)	MA/U.S.A.	440	46	$5 \cdot 10^7$	I(M)ST	several
MU Radar	Japan	46.5	34	$4 \cdot 10^8$	IMST	1657, SA
Penn State	PA/U.S.A.	49.9	27	$9 \cdot 10^3$	ST	2
Penn State	.	405	30	$3 \cdot 10^4$	ST	1
Poker Flat -)	AL/U.S.A.	49.9	40	$3 \cdot 10^8$	MST	3
Ponape, Christmas	Pacific	49.8	32	$5 \cdot 10^8$	ST	1, 3
PROUST	France	935	51*)	$7 \cdot 10^6$	ST	1; bistatic
Provence	.	45-49	30	$5 \cdot 10^8$	ST	several
Sondrestrom *)	Greenland	1290	50	$4 \cdot 10^7$	I(M)ST	multi
SOUSY	W.Germany	53.5	31	$7 \cdot 10^7$	MST	multi, SA
SOUSY mobile	Norway, etc.	53.5	35	$7 \cdot 10^7$	MST	4
Sunset -)	CO/U.S.A.	40.5	24	$6 \cdot 10^6$	ST	5
United Kingdom *)	Wales/U.K.	≈50	28	$6 \cdot 10^7$	MST	several
Urbana	IL/U.S.A.	40.9	28	$2 \cdot 10^7$	MST	several
Wind Profilers	CO, OK/U.S.A.	49.8	27	$8 \cdot 10^5$	ST	2
.	.	405	30	$3 \cdot 10^4$	ST	2
.	.	915	40	$2 \cdot 10^4$	ST	3
Wind Profilers (30) *)	Central U.S.A., etc.	≈404	32	$1 \cdot 10^5$	ST	3

-) operation discontinued   *) in planning or construction phase   M = mesosphere, S = stratosphere, T= troposphere
s) mostly ionospheric radar   ') TX antenna gain in bistatic mode   (M) = D-region in incoherent scatter mode
x) mostly for radar astronomy   SA = spaced antenna capability   I = ionosphere-thermosphere incoherent scatter
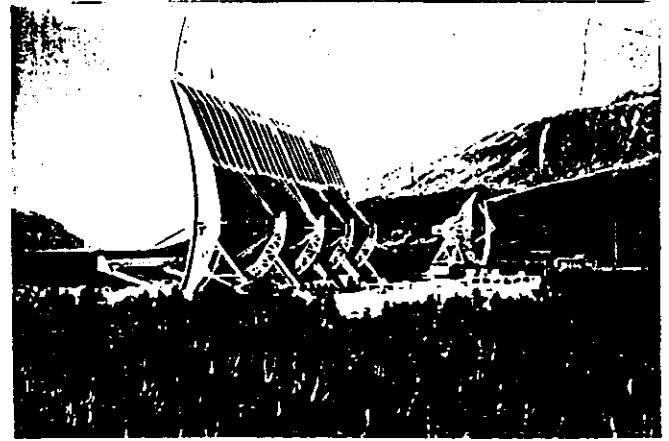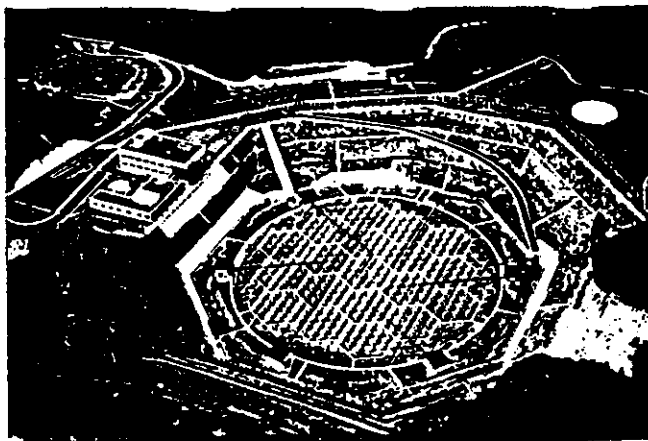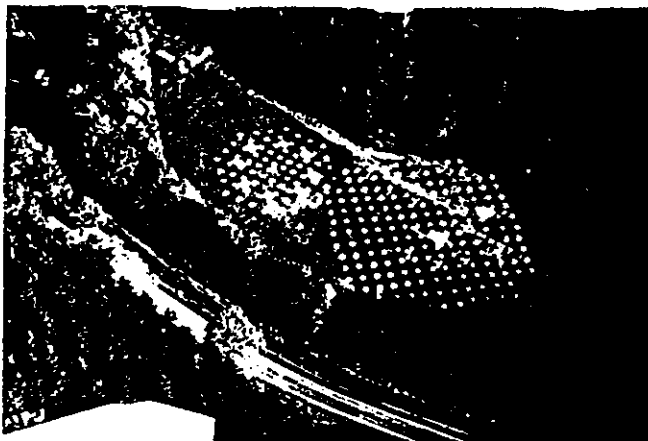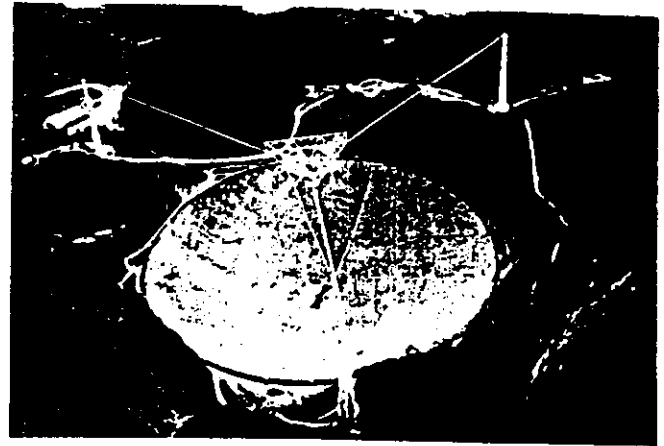
56

C 56

Figure 50. Photos of radar observatories:
Jicamarca/Peru, Arecibo/Puerto Rico,
SOUSY/West Germany, Poker Flat/Alaska,
MU Radar/Japan, EISCAT/Norway.

C57

REFERENCES

Balsley, B.B. (1978a), The use of sensitive coherent radars to examine atmospheric parameters in the height range 1-100 km, Preprint Vol. 18th Conf. on Radar Meteorology, 190-193 (publ. by Amer. Meteor. Soc., Boston, MA).

Balsley, B.B. (1978b), Design considerations for coherent radar systems for probing the troposphere, stratosphere, and mesosphere, Preprint Vol. 18th Conf. on Radar Meteorology, 387-390 (publ. by Amer. Meteor. Soc., Boston, MA).

Balsley, B.B. and K.S. Gage (1982), On the use of radars for operational wind profiling, Bull. Amer. Meteor. Soc., 63, 1009-1018.

Balsley, B.B., W.L. Ecklund, D.A. Carter and P.E. Johnston (1980), The MST radar at Poker Flat, Alaska, Radio Sci., 15, 213-223.

Baron, M.J. (1977), The Chatanika radar system, in: Radar Probing of the Auroral Plasma (Proc. of the EISCAT Summer School, 1975; A. Brekke, ed.), 103-141 (publ. by Scandinavian University Books, Oslo).

Battan, L.J. (1973), Radar Observation of the Atmosphere, The University of Chicago Press.

Bowhill, S.A. and B. Edwards (Eds.) (1983, 1984, 1986), Handbook for MAP, 9, 14, 20 (publ. by SCOSTEP Secretariat, Dept. Elec. Engin., University of Illinois, Urbana, IL).

Brosnahan, J.W., J.K. Chao and J. Röttger (1983), Chung-Li, Taiwan dual mode (Doppler and spaced antenna) VHF radar: preliminary specifications, Handbook for MAP, 9 (S.A. Bowhill and B. Edwards, eds.), 383-386 (publ. by SCOSTEP Secretariat, Dept. Elec. Engin., University of Illinois, Urbana, IL).

Carter, D.A., B.B. Balsley and W.L. Ecklund (1980), The Poker Flat MST radar: signal analysis and data processing techniques with examples, Preprint Vol. 19th Conf. on Radar Meteorology, 563-567 (publ. by Amer. Meteor. Soc., Boston, MA).

Clark, W.L. and D.A. Carter (1980), Real-time scaling of atmospheric parameters from radars using the MST technique, Preprint Vol. 19th Conf. on Radar Meteorology, 599-604 (publ. by Amer. Meteor. Soc., Boston, MA).

Czechowsky, P., J. Klostermeyer, J. Röttger, R. Rüster, G. Schmidt and R.F. Woodman (1976), The SOUSY-VHF-Radar for tropospheric, stratospheric and mesospheric sounding, Preprint Vol. 17th Conf. on Radar Meteorology, 349-353 (publ. by Amer. Meteor. Soc., Boston, MA).

Czechowsky, P., G. Schmidt and R. Rüster (1984), The mobile SOUSY Doppler radar - technical design and first results, Radio Sci., 19, 441-450.

Doviak, R.J. and D.S. Zrnic (1984), Doppler Radar and Weather Observations, Academic Press, Inc., Orlando, FL.

Ecklund, W.L., D.A. Carter and B.B. Balsley (1988), A UHF wind profiler for the boundary layer: brief description and initial results, J. Atmos. Ocean. Techn., 5 (in press).

Evans, J.V. (1969), Theory and practice of ionosphere study by Thomson scatter radar, Proc. IEEE, 57, 496-500.

Frisch, A.S., B.L. Weber, R.G. Strauch, D.A. Merritt and K.P. Moran (1986), The altitude coverage of the Colorado wind profilers at 50, 405, and 915 MHz, J. Atmos. Ocean. Techn., 3, 680-692.

Fukao, S., S. Kato, T. Aso, M. Sasada and T. Makihira (1980), Middle and upper atmosphere radar (MUR) under design in Japan, Radio Sci., 15, 225-231.

Fukao, S., T. Sato, T. Tsuda, S. Kato, K. Wakasugi and T. Makihira (1985a), The MU radar with an active phased array system: 1. antenna and power amplifiers, Radio Sci., 20, 1155-1168.

Fukao, S., T. Tsuda, T. Sato, S. Kato, K. Wakasugi and T. Makihira (1985b), The MU radar with an active phased array system: in-house equipment, Radio Sci., 20, 1169-1176.

Gage, K.S. and B.B. Balsley (1978), Doppler radar probing of the clear atmosphere, Bull. Amer. Meteor. Soc., 59, 1074-1093.

Gossard, E.E. and R.G. Strauch (1983), Radar Observation of Clear Air and Clouds, Elsevier Publ. Comp., Amsterdam.

Green, J.L., J.M. Warnock, R.H. Winkler and T.E. VanZandt (1975), A sensitive VHF radar for the study of winds, waves and turbulence in the troposphere, stratosphere and mesosphere, Preprint Vol. 16th Conf. on Radar Meteorology, 313-315 (publ. by Amer. Meteor. Soc., Boston, MA).

Hagfors, T. (1977), Incoherent scatter radar observations, in: Radar Probing of the Auroral Plasma (Proc. of the EISCAT Summer School, 1975; A. Brekke, ed.), 75-101 (publ. by Scandinavian University Books, Oslo).

Hagfors, T., P.S. Kildal, H.J. Kärcher, B. Liesenkotter and G. Schroer (1982), VHF parabolic cylinder antenna for incoherent scatter radar research, Radio Sci., 17, 1607-1621.

Hardy, K.R. (1972), Studies of the clear atmosphere using high power radar, in: Remote Sensing of the Troposphere (V.E. Derr, ed.), chapter 14 (publ. by Wave Propag. Lab., NOAA/ERL, Boulder, CO).

Hocking, W.K. (1989), Target parameter estimation, Handbook for MAP (this issue).

Kato, S., T. Ogawa, T. Tsuda, T. Sato, I. Kumura and S. Fukao (1984), The middle and upper atmosphere radar: first results using partial system, Radio Sci., 19, 1475-1484.

Ko, H.C. (1958), The distribution of cosmic radio background radiation, Proc. IRE, 46, 208-215.

Kraus, J.D. (1966), Radio Astronomy, McGraw-Hill Book Comp., New York.

Lehtinen, M.S. and I. Häggström (1987), A new modulation principle for incoherent scatter measurements, Radio Sci., 22, 625-634.

C 59

Ochs, G.R. (1965), The large 50 Mc/s dipole array at Jicamarca radar observatory, <u>NBS Rep. 8772</u> (publ. by National Bureau of Standards, U.S. Dept. of Commerce, Boulder, CO).

Rastogi, P.K. (1983), Data processing techniques used with MST radars – a review, <u>Handbook for MAP</u>, <u>9</u> (S.A. Bowhill and B. Edwards, eds.), 477-488 (publ. by SCOSTEP Secretariat, Dept. Elec. Engin., Univ. of Illinois, Urbana, IL).

Rastogi, P.K. and R.F. Woodman (1974), Mesospheric studies using the Jicamarca incoherent-scatter radar, <u>J. Atmos. Terr. Phys.</u>, <u>36</u>, 1217-1231.

Röttger, J. (1981), The capabilities of VHF radars for meteorological observations, <u>ESA SP-165</u> (Nowcasting: Mesoscale Observations and Short-Range Prediction), 143-148 (publ. by European Space Agency, Paris).

Röttger, J. (1984), The MST radar technique, <u>Handbook for MAP</u>, <u>13</u> (R.A. Vincent, ed.), 187-232 (publ. by SCOSTEP Secretariat, Dept. Elec. Engin., Univ. of Illinois, Urbana, IL).

Röttger, J. and M.F. Larsen (1989), UHF/VHF radar techniques for atmospheric research and wind profiler applications, in: <u>Radar in Meteorology</u> (D. Atlas, ed.) (to be publ. by Amer. Meteor. Soc., Boston, MA).

Röttger, J. and G. Schmidt (1979), High-resolution VHF radar sounding of the troposphere and stratosphere, <u>IEEE Trans. Geosci. Electr.</u>, <u>GE-17</u>, 182-189.

Röttger, J., J. Klostermeyer, P. Czechowsky, R. Rüster and G. Schmidt (1978), Remote sensing of the atmosphere by VHF radar experiments, <u>Naturwissenschaften</u>, <u>65</u>, 285-296.

Sato, T. and R.F. Woodman (1982), Spectral parameter estimation of CAT radar echoes in the presence of fading clutter, <u>Radio Sci.</u>, <u>17</u>, 817-826.

Schmidt, G., R. Rüster and P. Czechowsky (1979), Complementary code and digital filtering for detection of weak VHF radar signals from the mesosphere, <u>IEEE Trans. Geosci. Electr.</u>, <u>GE-17</u>, 154-161.

Skolnik, M.I. (1970) (ed.), <u>Radar Handbook</u>, McGraw-Hill, Inc., New York.

Strauch, R.G., D.A. Merritt, K.P. Moran, K.B. Earnshaw and D. van de Kamp (1984), The Colorado wind-profiling network, <u>J. Atmos. Ocean. Techn.</u>, <u>1</u>, 37-49.

Turunen, T. (1986), GEN-SYSTEM – a new experimental philosophy for EISCAT radars, <u>J. Atmos. Terr. Phys.</u>, <u>48</u>, 777-785.

Wilson, D.A. and L.J. Miller (1972), Atmospheric motion by Doppler radar, in: <u>Remote Sensing of the Troposphere</u> (V.E. Derr, ed.), chapter 13 (publ. by Wave Propag. Lab., NOAA/ERL, Boulder, CO).

Woodman, R.F. (1980), High-altitude resolution stratospheric measurements with the Arecibo 2380-MHz radar, <u>Radio Sci.</u>, <u>15</u>, 423-430.

Woodman, R.F. and A. Guillen (1974), Radar observations of winds and turbulence in the stratosphere and mesosphere, <u>J. Atmos. Sci.</u>, <u>31</u>, 493-505.

Woodman, R.F., R.P. Kugel and J. Röttger (1980), A coherent integrator-decoder preprocessor for the SOUSY-VHF-Radar, <u>Radio Sci.</u>, <u>15</u>, 233-242.